Universitat Autònoma de Barcelona

Pedestrian Tracking in Wireless Networks: an Experimental Approach

Alejandro Correa Vila

Pedestrian Tracking in Wireless Networks: an Experimental Approach

Universitat Autònoma de Barcelona

Ph.D. Dissertation by
Alejandro Correa Vila

Thesis Advisors:
Prof. Antoni Morell Pérez and Prof. José López Vicario

Doctorat en Telecomunicació i Enginyeria de Sistemes
Department de Telecomunicacions i Enginyeria de Sistemes
Escola d'Enginyeria
Universitat Autònoma de Barcelona

January, 2017

To my beloved parents and sister.

Abstract

Humans spend a large part of its lives in indoor environments and yet there is not a positioning system that can be deployed in any indoor environment of the world and accurately estimate the position of the people inside this environment. For this reason, in the last decade there has been an increasing interest in the research of indoor positioning systems. This PhD dissertation aims to contribute to the study of indoor positioning systems with the design of new systems from an experimental point of view, that is, we aim to design systems that can be implemented using nowadays commercial technologies.

First, we have considered the design of an hybrid positioning system that combines the inertial measurements from a hip mounted inertial measurement unit with the RSS measurements from a wireless sensor network. Particularly, we design two methods for exploiting the statistics of the RSS measurements in order to extend in time the short term accuracy of the inertial sensors.

Afterwards, we continue the study of indoor positioning systems based on WSN by extending the problem to the multiple receiver case. We deploy multiple receivers on the body of the user and take advantage of the different attenuations suffered due to the effect of the human body on the wireless signals in order to estimate the position, velocity and heading of the user without the need of using inertial sensors.

Finally, with the aim of applying our designs to mass market applications, we move to a WiFI network and commercial devices, smartphones and smartwatches. The smartphone cooperates with the smartwatch in order to circumvent the problems produced for the use of third party WiFi networks. Specifically, we design an hybrid indoor positioning system that combines the inertial measurements from a smartphone placed in the pocket of the user with the RSS measurements received from the smartphone and the smartwatch.

Acknowledgements

Now that I see near the end of my PhD I would like to thank those who have made this journey easier with their support over the years. First, I would like to thank my directors Dr. Antoni Morell Pérez and Dr. José López Vicario for their help, their constant support and, especially, for all the useful advice received during these years. I would also like to thank Dr. Stephan Sand for the opportunity to do the research stay in his group at DLR, for his useful advice and for the kind treatment I received during the months that I lived in Germany. I would like to extend this acknowledgement to the Department of Telecommunications and Systems Engineering of UAB and the Institute of Communications and Navigation of DLR.

I cannot forget about Marc (office mate and flatmate for many years), and all the people that I have met over the years: Albert, Enric, Ricard, Moi, Mercedes, Alfred and other PhD students and postdocs with whom I have shared these years, both from UAB and DLR. With them I experienced great moments and I shared a lot of time in front of a coffee (perhaps too much). I cannot forget about those friends who helped me at all times, both my flatmates and my friends from Vila-real, especially Vicent and Ana for their direct involvement in this dissertation, helping me with the English grammar and the design of the cover.

Finally, I would like to express my eternal gratitude to all my family, especially my parents and my sister, because without them this thesis would never have been possible.

Alejandro Correa Vila

29/01/2017

Contents

Acronyms

AoA	Angle of Arrival.
CDF	Cumulative Density Function.
DoF	Degrees of Freedom.
DS-CMT	Distance Statistics Covariance Matrix Tunning.
EKF	Extended Kalman Filter.
FIR	Finite Impulse Response.
GPS	Global Positioning System.
GSM	Global System for Mobile communications.
HMM	Hidden Markov Model.
IMU	Inertial Measurement Unit.
IoT	Internet of Things.
IPS	Indoor Positioning Systems.
KF	Kalman Filter.
KL	Kullback-Leibler.
kNN	k Nearest Neighbors.
LOS	Line Of Sight.
LS	Least Squares.
LTE	Long Term Evolution.
MEMS	MicroElectroMechanical Systems.
ML	Machine Learning.
MLE	Maximum Likelihood Estimator.
NLOS	Non Line Of Sight.
NN	Neural Network.

PDF Probability Density Function.

PF Particle Filter.

PT-CMT Power Threshold Covariance Matrix Tunning.

QoS Quality of Service.

RFID Radio Frequency IDentification.

RMSE Root Mean Square Error.

RSS Received Signal Strength.

SHS Step and Heading System.

SLAM Simultaneous Localization And Mapping.

SNR Signal to Noise Ratio.

SVM Support Vector Machine.

TDoA Time Difference of Arrival.

ToA Time of Arrival.

ToF Time of Flight.

UKF Unscented Kalman Filter.

UWB Ultra Wide Band.

WLS Weighted Least Squares.

WSN Wireless Sensor Network.

ZUPT Zero velocity UPTdate.

Notation

In general, boldface upper-case letters denote matrices ($\mathbf{A}$), boldface lower-case letters denote column vectors ($\mathbf{a}$), and italics denote scalars (a).

$\log_a(\cdot)$	Base a logarithm.
$\ln(\cdot)$	Natural logarithm.
$\exp(\cdot)$	Exponential function.
$a \ll b$	a is much less than b.
$a \approx b$	a is approximately equal to b.
$\mathbf{A}^T$	Transpose of matrix $\mathbf{A}$.
$\mathbf{A}^{-1}$	Inverse of matrix $\mathbf{A}$.
$diag(\mathbf{A})$	Main diagonal of matrix $\mathbf{A}$.
$\mathbf{I}$	Identity matrix.
$\hat{\mathbf{a}}$	Estimation of the vector $\mathbf{a}$.
$\bar{\mathbf{a}}$	Mean of the values of the vector $\mathbf{a}$.
$\|\mathbf{a}\|$	Euclidean norm of $\mathbf{a}$.
$\mathbf{x}_k$	Value of vector $\mathbf{x}$ at the k-th time instant.
$\mathbf{x}_{0:k}$	Values of vector $\mathbf{x}$ from time instant 0 to time instant k.
$p(\mathbf{x}, \mathbf{y})$	Joint probability distribution of $\mathbf{x}$ and $\mathbf{y}$.
$p(\mathbf{x}\|\mathbf{y})$	Probability distribution of $\mathbf{x}$ conditioned on $\mathbf{y}$.
$p(\mathbf{x}; a, b)$	Probability distribution of $\mathbf{x}$ with parameters a and b.
$\hat{\mathbf{x}}_{k\|k}$	Estimated mean of the posterior distribution of the state at time k given the measurements up to time k.
$\mathbf{P}_{k\|k-1}$	Estimated prediction of the covariance matrix of the state at time k based on the state at time $k-1$.

$\mathbf{P}_{k\|k}$	Estimated covariance matrix of the posterior distribution of the state at time k given the measurements up to time k.
$\mathcal{N}(\mu,\sigma^2)$	Gaussian distribution with mean μ and variance σ^2.
$\mathcal{N}(\mathbf{x};\mu,\sigma^2)$	Gaussian distribution of variable $\mathbf{x}$ with mean μ and variance σ^2.
$\sim$	Distributed as. Used to make equivalences between random variables and the PDFs that generate them.
$E[\cdot]$	Statistical expectation.
$Var[\cdot]$	Statistical variance.

Chapter 1

Introduction

1.1 Motivation

The human being has always wanted to determine its own position in order to be able to find important places like for example sources of water or food. The expansion of human communities around the Earth, with the consequent establishment of trade routes, boosted the need to know the position in a more general context. Originally, the recognition of natural landmarks as mountains and rivers was employed for positioning. Later on, it was the man who started building its own landmarks as the lighthouses. The celestial navigation that has been used for centuries is another example of landmark based positioning. For many years, the research community developed new methods for positioning but it was not until the 1960s, with the development of the first satellite navigation systems and its evolutions, that we were able to compute our position anywhere in the Earth with accuracies in the range of meters. Notwithstanding, the positioning problem is not already solved as there are still places where the satellite navigation systems cannot be employed like urban canyons or indoor scenarios. For this reason, the research efforts of scientists have been now focused in the development of indoor positioning systems (IPS).

Recently, the evolution of IPS facilitates the creation of indoor location based services which build applications on top of the knowledge of the position. Examples of this kind of services are the location of products stored in a warehouse, the tracking of equipment inside a hospital, the guidance of firemen inside buildings with reduced visibility due to smoke, among others like the guidance of people inside airports or the development of assisted living systems for elderly care. In fact, the predicted market value of indoor location services for 2020 is US$10 billion [1]. Therefore, there is a special interest in developing IPS that can be easily scaled to mass market applications and deployed in millions of buildings in the world. The current trend to reduce the cost of the systems is to use the

wireless infrastructures already deployed for communications as landmarks for positioning. Among the multitude of available technologies for communications (LTE, WiFi, Bluetooth, wireless sensor networks (WSN), ultra wide band (UWB), ...) the WiFI technology is the most commonly employed because it is already worldwide deployed. Although WSNs are also commonly used due to its key role in the internet of the things (IoT) and the future of smart cities. Similarly, the development of the microelectromechanical systems (MEMS) provide us with low cost inertial sensors that can also estimate the position of a pedestrian without the need of any infrastructure in the building. Note that most of these technologies are already available in nowadays commercial smartphones converting the smartphone in the perfect device for mass market positioning systems.

Within this framework, this PhD dissertation provides a contribution to the study of indoor positioning systems for pedestrians from an experimental perspective. More precisely, we designed IPS based on the received signal strength (RSS) of the signals received from wireless networks that can be implemented with the current commercial technologies. Our study begins with the indoor positioning systems based on the combination of inertial measurements and the RSS of a WSN. Then, we deploy multiple receivers in the body of the user and we study the multiple receiver case where the inertial measurements are substituted for multiple RSS measurements from different receivers. Moreover, we also study IPS based on the current smartphone technologies, based on the RSS of a WiFi network and the inertial sensors embedded in the smartphone, with the aim of obtaining positioning systems that can be easily scaled to mass market applications.

1.2 Outline

The objective of this PhD dissertation is the design of indoor positioning systems from an experimental point of view, that is, the systems will be implemented using nowadays commercial technologies and the metric used for measuring the goodness of our system will be the error committed during a series of experimental tests.

Chapter 2 presents a review of the state of the art of indoor positioning systems with special attention to the methods based on the RSS and hybrid systems involving inertial and RSS measurements.

Chapter 3 presents an overview of the Bayesian estimation theory focusing on the analytical solution provided by the Kalman filter (KF) and detailing the conditions of optimality of the KF solution. Besides, the suboptimal approach provided by the extended Kalman filter (EKF) is also detailed.

Chapter 4 is devoted to the study of the statistical characteristics of RSS based position measurements and its contribution to the improvement of the performance of hybrid systems combining RSS and inertial measurements. In particular, an IPS is designed based on the RSS of a WSN and the inertial measurements of a hip mounted inertial measurement unit (IMU). The combination of the measurements is done using an EKF with two novel methods for automatically configuring the measurement noise covariance matrix, taking into account the statistics of the RSS measurements in contrast with other works where this matrix is ad-hoc adjusted without considering the statistics of the measurements. The designed methods allow the EKF to benefit from the goodness of the inertial sensors in the short term and, assisted by the RSS measurements, extend their accuracy also in the long term.

Chapter 5 continues with the study of indoor positioning systems based on WSN extending the positioning problem to the multiple receiver case, that is, the user carries multiple receivers on the body. In that situation, we present a solution that exploits the different attenuation suffered by the receivers, depending on its position on the body of the user, to estimate the position, velocity and heading of the user without the need of employing inertial sensors. Particularly, machine learning (ML) techniques are employed to classify the measurements into groups with similar statistics and then obtain the relative distance and angle from the user to an anchor node of a WSN. This information is then converted to position and velocity measurements and combined using an EKF in order to improve the position estimation. The designed system is able to accurately track the position of the user with time invariant position errors.

Chapter 6 is dedicated to smartphone based IPS with the aim of designing a system with easy scalability to mass market applications. We take advantage of the increasing popularity of smartphones and smartwatches and use them as positioning devices. To do so, we use the integrated WiFi transceiver and inertial sensors as the measurement sources of our positioning system. First, we evaluate the typical problem of the RSS positioning systems when they are applied to external WiFi networks and then, we extend the idea of multiple receivers to the smartphone and smartwatch case by designing a method based on Gaussian mixture models (GMM) that overcomes the main issues identified thanks to the combination of measurements from different receivers. The enhanced position estimation based on the GMM is combined with the inertial measurements from a smartphone placed on the pocket of the user through an extended Kalman filter. The result is an IPS that can be implemented in commercial smartphones and smartwatches and so it can be easily scaled to mass market applications.

Chapter 7 concludes this PhD dissertation with a summary and discussion of the obtained results. Some suggestions for future work in the field are also outlined.

1.3 Research contributions

The main contribution of this thesis is the study of indoor positioning systems for pedestrians from an experimental point of view based on the implementation of all the systems designed with nowadays commercial technologies. Next, the details of research contributions in each chapter are presented.

Chapter 4

The main results of this chapter addressing the design of covariance matrix tuning methods for the EKF applied to pedestrian indoor navigation have been published in one journal paper and two conference papers:

- A. Correa, M. Barcelo, A. Morell and J. L. Vicario, "Enhanced Inertial-Aided Indoor Tracking System for Wireless Sensor Networks: A Review," in IEEE Sensors Journal, vol. 14, no. 9, pp. 2921-2929, Sept. 2014.
- A. Correa, M. Barcelo, A. Morell and J. L. Vicario, "Distance-based tuning of the EKF for indoor positioning in WSNs," 2014 22nd European Signal Processing Conference (EUSIPCO), Lisbon, 2014, pp. 1512-1516.
- A. Correa, A. Morell, M. Barcelo and J. L. Vicario, "Navigation system for elderly care applications based on wireless sensor networks," 2012 Proceedings of the 20th European Signal Processing Conference (EUSIPCO), Bucharest, 2012, pp. 210-214.

Chapter 5

The main results of this chapter are related to the design of algorithms for combining RSS from multiple receivers deployed around the body of the user and have been published in one journal paper and one conference paper:

- A. Correa, M. Barcelo , A. Morell and J. L. Vicario, "Indoor Pedestrian Tracking by On-Body Multiple Receivers," in IEEE Sensors Journal, vol. 16, no. 8, pp. 2545-2553, April 15, 2016.
- A. Correa, M. Barcelo, A. Morell and J. L. Vicario, "Indoor pedestrian tracking system exploiting multiple receivers on the body," 2014 International Conference on Indoor Positioning and Indoor Navigation (IPIN), Busan, 2014, pp. 518-525.

Chapter 6

The main results of this chapter consist on the application of the indoor positioning problem to smartphones and smartwatches and have been published in one journal paper:

- A. Correa, E. Munoz Diaz, D. Bousdar, A. Morell and J. L. Vicario, "Advanced Pedestrian Positioning System to Smartphones and Smartwatches," in Sensors Journal, vol. 16, no. 11, pp. 1903-1921, Nov. 2016.

Other research contributions

During the PhD period, several collaborations have been carried out resulting in one patent, five journal papers and four conference papers:

- A. Correa, S. Sand, "Verfahren zum Ermitteln des Zustands eines drahtlosen Übertragungskanals", Deutsch patent, DE102016202739, 2016.
- A. Morell, A. Correa, M. Barcelo and J. L. Vicario, "Data Aggregation and Principal Component Analysis in WSNs," in IEEE Transactions on Wireless Communications, vol. 15, no. 6, pp. 3908-3919, June 2016.
- M. Barcelo, A. Correa, J. L. Vicario, A. Morell and X. Vilajosana, "Addressing Mobility in RPL With Position Assisted Metrics," in IEEE Sensors Journal, vol. 16, no. 7, pp. 2151-2161, April, 2016.
- M. Barcelo, A. Correa, J. L. Vicario, A. Morell, "Cooperative interaction among multiple RPL instances in wireless sensor networks", Computer Communications, vol. 81, no. 1, pp. 61-71, May 2016.
- M. Barcelo, A. Correa, J.L. Vicario, and A. Morell. "Joint routing, channel allocation and power control for real-life wireless sensor networks", in Trans. Emerg. Telecommun. Technol., vol. 26, no. 5, pp. 945-956, May 2015.
- M. Barcelo; A. Correa; J. Llorca; A. Tulino; J. Lopez Vicario; A. Morell, "IoT-Cloud Service Optimization in Next Generation Smart Environments," in IEEE Journal on Selected Areas in Communications , vol.PP, no.99, pp.1-1, Oct. 2016.
- M. Barcelo, A. Correa, X. Vilajosana, J. L. Vicario and A. Morell, "Novel Routing Approach for the TSCH Mode of IEEE 802.15.14e in Wireless Sensor Networks with Mobile Nodes," 2014 IEEE 80th Vehicular Technology Conference (VTC2014-Fall), Vancouver, BC, 2014, pp. 1-5.

- M. Barcelo, A. Correa, J. L. Vicario and A. Morell, "Cooperative Multi-tree Sleep Scheduling for Surveillance in Wireless Sensor Networks," MILCOM 2013 - 2013 IEEE Military Communications Conference, San Diego, CA, 2013, pp. 200-205.

- M. Barcelo, A. Correa, J. L. Vicario and A. Morell, "Joint routing and transmission power control for Collection Tree Protocol in WSN," 2013 IEEE 24th Annual International Symposium on Personal, Indoor, and Mobile Radio Communications (PIMRC), London, 2013, pp. 1989-1993.

- M. Barcelo, A. Correa, J. L. Vicario and A. Morell, "Multi-tree routing for heterogeneous data traffic in wireless sensor networks," 2013 IEEE International Conference on Communications (ICC), Budapest, 2013, pp. 1899-1903.

Chapter 2

State of the Art

It is widely accepted that GPS has become the *de facto* standard for outdoor positioning and tracking applications. However, there is no equivalent system for indoor scenarios. Therefore, considerable research effort has been focused on this topic recently. Indoor positioning systems have been designed for providing information about the position of a person or object inside a building. Traditionally these systems can be classified into three groups:

- **Network based systems:** these systems are build on the top of a wireless network deployed in the scenario and use the information of the wireless signals to estimate the position of the user carrying a wireless device.

- **Inertial based systems:** these systems use self-contained sensors that measure the motion of the user and estimate its position relative to the starting point without the need of any physical infrastructure deployed in the building.

- **Hybrid systems:** these systems jointly combine two or more different methods in order to enhance the estimation of position.

A complete classification of IPS is shown in Figure 2.1 including references to remarkable works. Note that hybrid systems are not subclassified. There are lots of possible combinations of IPS that can form an hybrid system and a general classification of these systems is not feasible. In this chapter, we only focus on those hybrid systems related to the IPS designed in this PhD dissertation. In the rest of the chapter we will review each class of IPS following this classification.

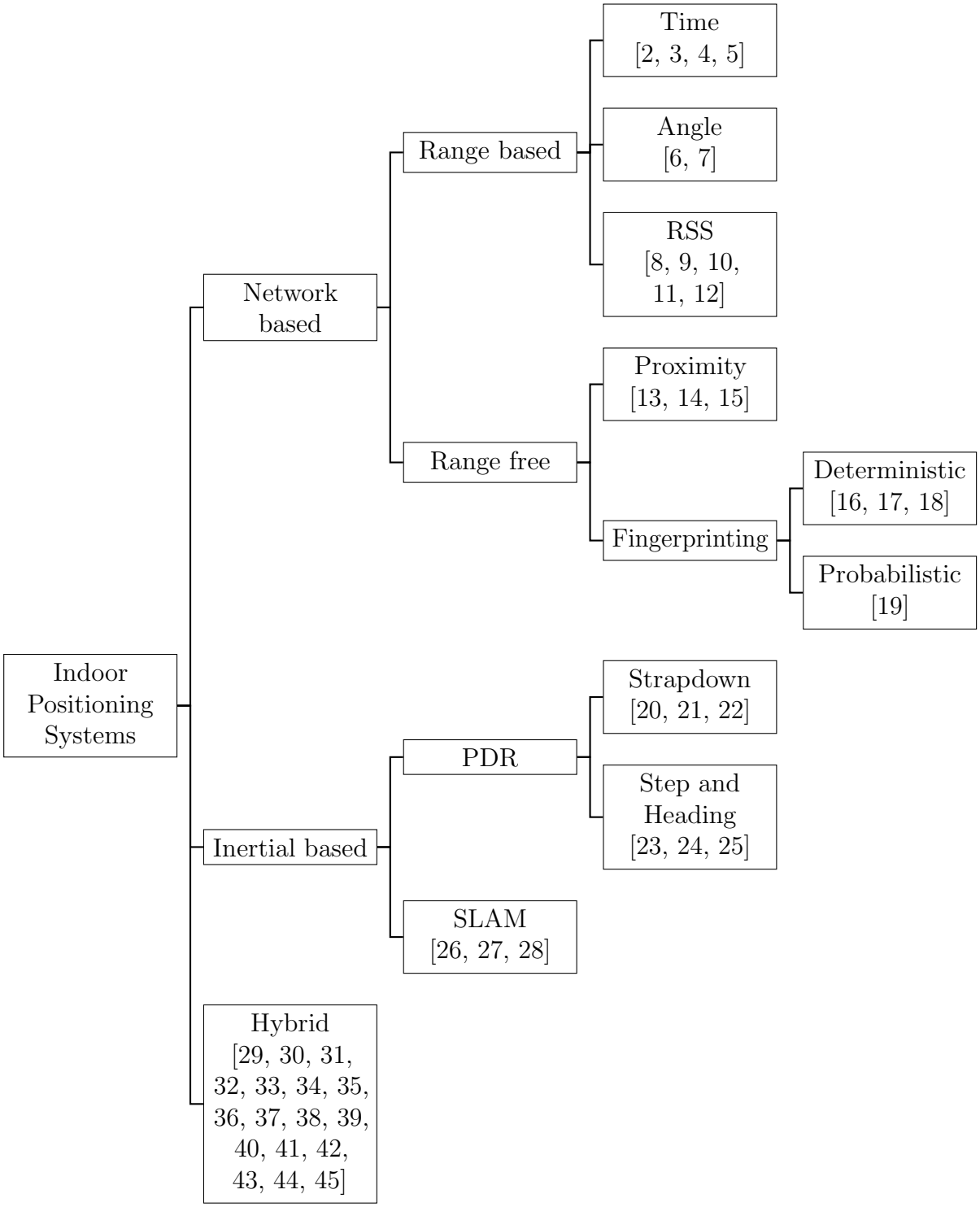

Figure 2.1: Classification of Indoor Positioning Systems

2.1 Network based systems

There are many different wireless networks that can be deployed in an indoor environment. From the typical WiFi networks that are deployed in millions of buildings around the world for providing internet access to the wireless sensor networks (WSN) designed for the IoT or the popular Bluetooth beacons among other alternatives such as the ultra wide band networks. Leaving aside the election of the wireless network, which obviously will determine the accuracy and precision of the IPS, we can classify the network based IPS systems according to the information obtained from the wireless signals into two groups: *i*) range based methods and *ii*) range free methods.

Range based methods extract geometric information (distance or angle) from the signals of different anchor nodes in the wireless network and then combine the geometric constraints of each anchor to obtain the position of the user. Alternatively, the range free methods are based on the inter-node connectivity information or in the identification of signal features patterns that are location dependent.

2.1.1 Range based

There are different ways for extracting geometric information from wireless signals, the most common ones are the methods based on the propagation time of the signal, between the transmitter and the receiver, the angle of arrival (AoA) or the received signal strength. In the following, we briefly detail the fundamentals of each class of methods analyzing its advantages and disadvantages.

Time

Time based localization algorithms measure the propagation time of a signal between the transmitter and the receiver, also known as time of flight (ToF), and compute the distance between the user and the anchor node d as follows,

$$d = \Delta t \; v, \tag{2.1}$$

where$\Delta\ t$ is the ToF and v is the propagation speed. The simplest approach is known as time of arrival (ToA). In this case the transmitter includes in the radio packet the time when the signal is transmitted and the receiver computes the reception time. In this way, the receiver has all the information for computing the distance. The position of the user can be obtained, if the distance to multiple anchors nodes is known, using a lateration method. Lateration methods compute the position of a user as the intersection of different

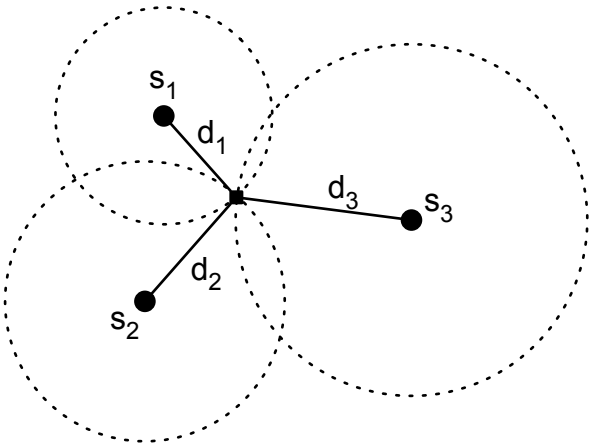

Figure 2.2: Lateration method concept.

circles with center the anchors position and radius the estimated distance as depicted in Figure 2.2. For a two dimensional position estimation it is necessary to estimate the distance to at least three anchor nodes.

It is fundamental in a ToA method to take into account that ToA methods require synchronization between all nodes, as the time of reference must be the same in all cases. This can be a problem for certain kind of wireless networks with simple low power devices and high restrictions in the algorithm complexity, as it is the case of WSN. An alternative method that relaxes the synchronization constraints is the time difference of arrival (TDoA). There are two main implementations of TDoA:

- The first TDoA method computes the difference in the ToA of a signal transmitted to two different receivers. For each TDoA measurement the transmitter must be in a hyperboloid with a constant range difference between the two receiver positions [46]. This method relaxes the synchronization constraint to the receivers.

- The second TDoA method is based on the difference in the ToA of two different signals with different propagation times. Usually, the first signal is the radio packet and the second one is a kind of sound signal due to the difference in the propagation speed between the electromagnetic waves (propagate at the speed of light $\approx 300000\,\mathrm{km/s}$) and the acoustic waves (propagation speed $\approx 340\,\mathrm{m/s}$) [47]. This method does not need synchronization but the nodes must include additional hardware in order to send two kind of signals simultaneously.

One example of a time based positioning system is the Active Bat system [2]. This system is based on the TDoA of ultrasound signals. The user carries a transmitter and the

signals are received by a grid of ceiling mounted receivers, which are synchronized using a wired connection. The system reports accuracies within 9 cm for the 95% of measurements. The main disadvantages of the system are related to the placement of the receivers in the ceiling which increases the cost and reduces the scalability.

Another example based also in ultrasound signals is the Cricket system [3]. The working principle of the Cricket system is similar to the Active Bat system but in this case the computation of the position is performed by the user which carries an ultrasound receiver. A set of ultrasound transmitters are deployed around the building, which also transmit radio frequency signals for synchronization.

More recent works are based on the UWB technology, this technology improves the ranging accuracy due to the large bandwidth used [4]. The use of a large bandwidth allows to implement shorter pulses which increase the time resolution and accuracy of the ToF estimations. Therefore the accuracy of the positioning system is also improved. The fundamental limits of wide band localization methods are determined in [48] and in [49] where the problem is extended to cooperative networks. More information about UWB systems can be found in [4, 5].

Time based localization methods are susceptible to errors produced for inaccuracies in the clocks or errors in the time estimation. Take into account that for a signal traveling at light speed 1 μs of error corresponds to an approximate distance error of 300 m. Furthermore, NLOS conditions produce a positive bias in the distance estimation. Therefore, time based systems must include methods for detecting NLOS conditions, increasing in this way the complexity of the algorithms.

Angle

Angle based localization methods use the angle of arrival of a signal to compute the position of the receiver. The working principle is similar to time based methods but instead of using the distances to the anchor nodes the angles are used. There are typically two main methods of obtaining the AoA of a signal [8]:

- Use an array of sensors (for ultrasound systems) whose location relative to the node center are known and use the difference in the ToA of the signal at each sensor to compute the AoA of the anchor node. In the case of using radio signals the array of sensors is replaced by an antenna array.
- Use two or more directional antennas pointing to different directions and with overlapping main beams. Then compute the AoA as a function of the ratio of the

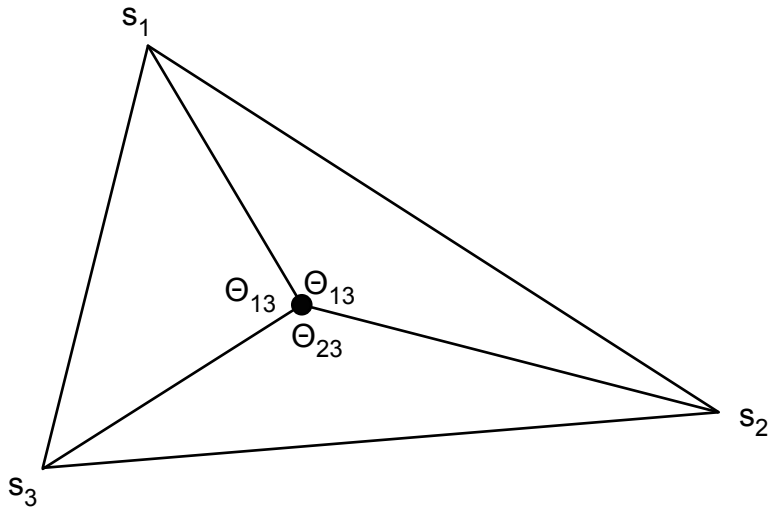

Figure 2.3: Triangulation method concept.

RSS of the individual antennas.

Once the AoA of multiple anchor nodes is estimated, the computation of the position is done using triangulation. The basic idea is shown in Figure 2.3. If the position of the vertices of a triangle are known, it is possible to compute the position of any node inside the triangle knowing the angle at which the interior point sees the vertices [6]. There are many different ways of solving the triangulation problem, in [7] the most common methods are reviewed and a new method that does not take into account the ordering of the anchor nodes is presented.

The main disadvantage of AoA based methods is the increase in the cost of the system due to the additional hardware, as these systems need arrays of sensors or antennas. Furthermore, if the AoA is computed based on the ToF of the wireless signals, inaccuracies in the clocks of the devices impinge in the accuracy of the position estimations.

RSS

RSS based localization methods estimate the distance between the user and an anchor node using the received signal strength. These methods are based on the concept that the attenuation suffered by a signal travelling from a transmitter to a receiver depends on the distance travelled. In order to estimate the distance it is necessary to model the wireless environment using a propagation model. Traditionally, the log-distance path loss model is employed, where it is considered that the attenuation (in dB) is proportional to the

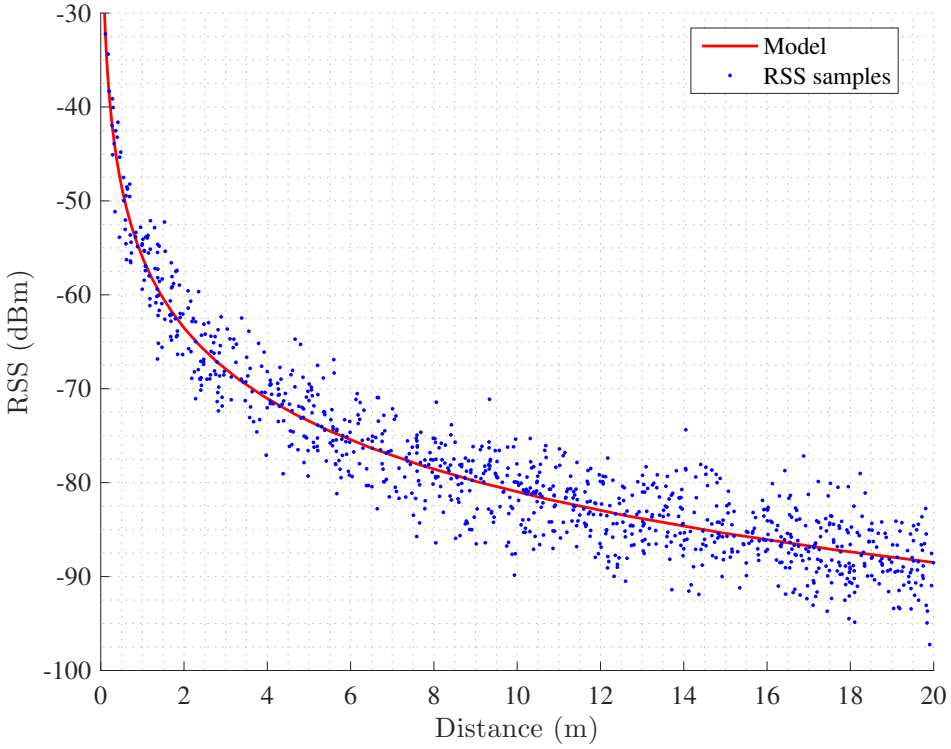

Figure 2.4: Calibration of a propagation model.

logarithm of the distance travelled [8], that is,

$$RSS = P_{1m} - 10\alpha \log_{10} d - \gamma, \tag{2.2}$$

where d is the distance to the anchor node, P_{1m} is the received power at 1 meter from the transmitter in dBmW, α is the path loss exponent and $\gamma \sim \mathcal{N}\left(0, \sigma_\gamma^2\right)$ is a zero mean Gaussian noise that models the shadowing effects. Note that the parameters of the model, i.e. P_{1m} and α, have to be experimentally obtained for each scenario, which requires a measurement campaign to adjust the model to the scenario. The calibration process consists in the collection of the RSS in predefined positions with known distance to anchors and the computation of the model parameters, which is usually done using regression methods. Figure 2.4 shows the calibration process with the collected samples and the computed log-distance path loss model.

Once calibrated, distance is estimated according to the path loss model using the maximum likelihood estimator (MLE), which for the case of the distance estimation is [9]:

$$\hat{d} = 10^{\frac{RSS - P_{1m}}{10\alpha}}. \tag{2.3}$$

As in the case of time based localization algorithms the position of the user is estimated combining the distance information of multiple anchor nodes using a lateration method

[10]. RSS based methods are attractive due to its inherent simplicity, as far as the RSS measurements are natively supported by most transceivers. Unfortunately, the variability of the wireless channel jointly with the attenuation of the signal due to walls, objects or the human body introduce errors in the distance estimation and makes the RSS based localization algorithms less accurate than time or angle based algorithms. A review of the main sources of error of RSS based algorithms can be found in [11] where the authors also include a list of recommendations for the appropriate implementation of RSS based algorithms.

An example of a RSS based localization system can be found in [10], where authors use the correlation between the RSS samples in nearby locations to fit different path loss models depending on the position of the user and therefore adapt to changes of the propagation model between areas of the same building. In [9] a cooperative method for the localization of the nodes in a WSN is presented. A comparison of the accuracy of the RSS based methods versus the time based methods is presented in [12] where the authors compute the Cramér-Rao bound under Gaussian and log-normal models.

2.1.2 Range free

Range free methods are based on the connectivity information of a wireless network, which can be used to estimate the position without computing any range measurement to an anchor node. There are mainly two kind of range free algorithms:

- **Proximity methods:** these methods use the connectivity information to infer directly the position of the user based on the number of anchors in the neighborhood.
- **Fingerprinting methods:** these methods are based on location dependent characteristics of the signals received from the wireless network. First a database of the characteristics and the real location where they were measured is collected. Then, the position is estimated by selecting the position of the database sample that best matches the real data.

Proximity

The proximity algorithms are based on the following simple idea: if a user is receiving a signal from an anchor node, the position of the user must be near the position of the anchor node. The operation mode is as follows: first, the user scans the channel looking for the radio signals from the anchors nodes. Once an anchor node is detected, the position of

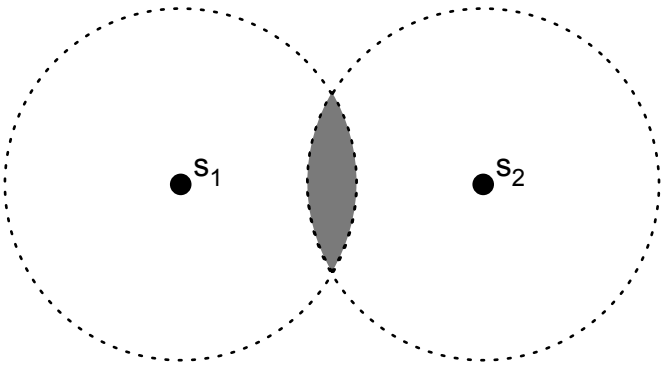

Figure 2.5: Proximity method concept.

the user is estimated as the position of the anchor node. In the case of detecting more than one radio signal, the anchor node with the strongest received signal is selected.

Figure 2.5 describes the method, where the circles represent the coverage area of the anchor nodes. Any user located in the circle of node s_1 will estimate its own position as the position of the anchor node s_1 whereas if the object is located in the circle of anchor s_2 it will estimate the position as the position of the anchor node s_2. In the intersection of both circles the selection of the anchor node will be done in terms of the RSS.

One of the first system to employ the proximity method was the Active Badge system [13]. This system uses a network of infrared sensors that detect the signals transmitted by the active badge an provide a localization algorithm with room accuracy.

The error committed by the proximity methods is directly related to the size of the coverage areas. Furthermore, if the coverage area of the anchor nodes is reduced, the number of anchor nodes needed for a total coverage of an indoor area increases. For this reason, proximity methods are particularly suited for low cost wireless devices such as RFID, where the deployment of a large number of tags in a building does not escalate the cost of the system [14]. Moreover, the use of passive RFID tags reduces the maintenance cost of the network as the battery of the anchor nodes must not be regularly replaced.

A more general way of using connectivity information is employed in the centroid algorithm, where the estimation of position is computed as the centroid of the position of the anchor nodes received [15], that is,

$$\hat{\mathbf{m}} = \left[\frac{1}{N} \sum_{i=1}^{N} x_i, \frac{1}{N} \sum_{i=1}^{N} y_i \right], \tag{2.4}$$

where $\hat{\mathbf{m}}$ is the estimated position of the mobile node and x_i, y_i are respectively the x

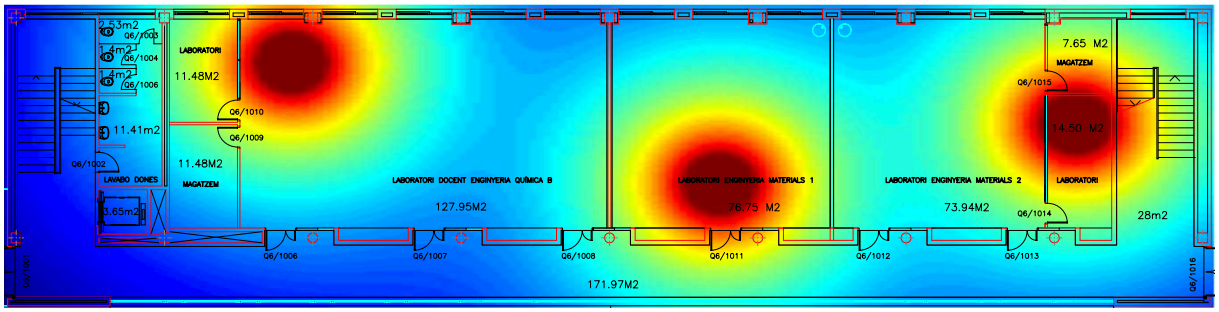

Figure 2.6: Simulated distribution of RSS in an indoor scenario.

and y coordinates of the i-th anchor node. In the centroid method the accuracy of the position estimation is also dependent on the number of nodes. In general, proximity based methods cannot obtain highly accurate position estimations, the obtained accuracy is in the order of the average distance between the anchors deployed in the building. However, the simplicity of these methods offers a good solution for room accuracy systems based on low complex wireless networks.

Examples of proximity methods based on RFID can be found in [50, 51, 52] where the authors review the RFID based localization methods available in the literature.

Fingerprinting

Fingerprinting methods are based on the uniqueness of radio signals received at different positions, which is due to the propagation issues in the complex indoor environment. It is common the presence of radio signals in most of the indoor environments, such as the ones received from WiFi, WSN or Bluetooth networks deployed in the buildings among other signals as for example GSM or LTE signals. The complexity of the indoor environment produces big differences between the signals received at different locations due to multipath, shadowing or the propagation in NLOS environments. Figure 2.6 shows the distribution of the RSS in an indoor environment with three deployed anchor nodes under ideal propagation conditions. The color change from blue to red as a function of the aggregated received power of the three anchors. It can be shown the different areas created by the received power. Note that this effect can be magnified by including the multipath and NLOS to the propagation model considered.

The main idea behind the fingerprinting method is to generate a database of the characteristics of the signals at different positions (fingerprints) and then compare the signals received by the user with the database and estimate the position of the user as the position of the fingerprint that best matches the received signals. The creation of the database samples requires an intensive campaign of measurements in order to collect

the fingerprints of the radio signals, typically the RSS, and create a radio map of the indoor environment. This process is time consuming and vulnerable to environmental changes. Furthermore, the accuracy of the system depends on the assumption of similar wireless conditions between the collection of the fingerprints and the current signals [53]. The movement of humans or objects inside the building will produce differences between the database and the online collected measurements that will cause an increase in the positioning error.

There are two kind of fingerprinting methods: *i*) deterministic and *ii*) probabilistic. One of the first deterministic fingerprinting system was the RADAR system developed at Microsoft [16]. The system collects the RSS and SNR as fingerprints from a WiFi network and reports an accuracy of 3 m. The position is estimated as the position of the fingerprint that minimizes the Euclidian distance between the online measurements and the fingerprints. The search methodology employed is the k nearest neighbors (kNN) approach. Similarly, in [17] authors present a fingerprinting method based an the weighted extension of the kNN algorithm. The advantage of the kNN approaches is the reduced computational complexity of these algorithms. There are other systems that increase the accuracy of the position estimation at the expense of a higher computational cost, such as systems based on support vector machines (SVM) [54] or linear discriminant analysis [18].

In the group of the probabilistic approaches the aim is to find the location with maximum likelihood. The Horus system [19] uses a probabilistic model of the signal distribution in the environment and computes the position with maximum posterior probability. There are other systems based on Bayesian networks [55] or on the Kullback-Leibler divergence [56].

The collection of fingerprints is not reduced to the measurement of the characteristics of radio signals, recent works proved that it is also possible use the geomagnetic field [57]. An study of the feasibility of magnetic fingerprints is performed in [58]. Independently of the source of fingerprints the main disadvantage of fingerprinting methods is the effort needed for the collection of the database samples. These methods cannot be easily extrapolated from one building to another without doing a new calibration campaign. For this reason, recently researchers have shown an increasing interest in reducing the effort of the calibration process [53]. More information about fingerprinting methods can be found in [59].

2.2 Inertial based systems

Contrarily to the network based systems, where the position of the user is estimated measuring the features from the signals received from a wireless network, inertial based systems compute their own position without any help from a physical infrastructure. The inertial sensors measure physical quantities related to the motion of the object or user where the sensors are mounted. Typically inertial sensors are grouped into an IMU, which is formed by a 3 axis accelerometer that measures the linear acceleration, a 3 axis gyroscope that measures the angular velocity and a 3 axis magnetometer that measures the magnetic field[1]. There are two main kinds of inertial navigation systems [60]:

- **Strapdown systems:** these systems estimate the position of the user by the double integration of the acceleration.
- **Step and heading systems (SHS):** these systems estimate the position by adding to the initial position estimation vectors representing the step length and the step heading of the user.

Regardless of the approach used the first step of an inertial navigation system is the computation of the relative orientation of the sensor and the body of the user. The measurements of an IMU are expressed in the sensor coordinate frame, whenever we attach the IMU to the body of the user, the axes of the sensor coordinate frame may not coincide with the axes of the navigation frame. Any misalignment in the axes produces errors in the measurements, therefore the estimation of the relative orientation is a crucial part of an inertial navigation system. The relative transformation between two coordinate frames can be obtained by sequentially rotating around three axis, where the angles of rotation are expressed as Euler angles, that is, the roll (ϕ_x), pitch (θ_y) and yaw (ψ_z). The definition of the Euler angles is shown in Figure 2.7.

The transformation between coordinate frames is done using the following rotation matrices [61]:

$$\mathbf{O}_{\phi_x} = \begin{bmatrix} 1 & 0 & 0 \\ 0 & -\cos(\phi_x) & \sin(\phi_x) \\ 0 & \sin(\phi_x) & \cos(\phi_x) \end{bmatrix}, \tag{2.5}$$

$$\mathbf{O}_{\theta_y} = \begin{bmatrix} \cos(\theta_y) & 0 & \sin(\theta_y) \\ 0 & 1 & 0 \\ -\sin(\theta_y) & 0 & \cos(\theta_y) \end{bmatrix}, \tag{2.6}$$

[1]The magnetometer is not an inertial sensor, however in this work we group it into the inertial measurement unit as this is the typical term used in the literature.

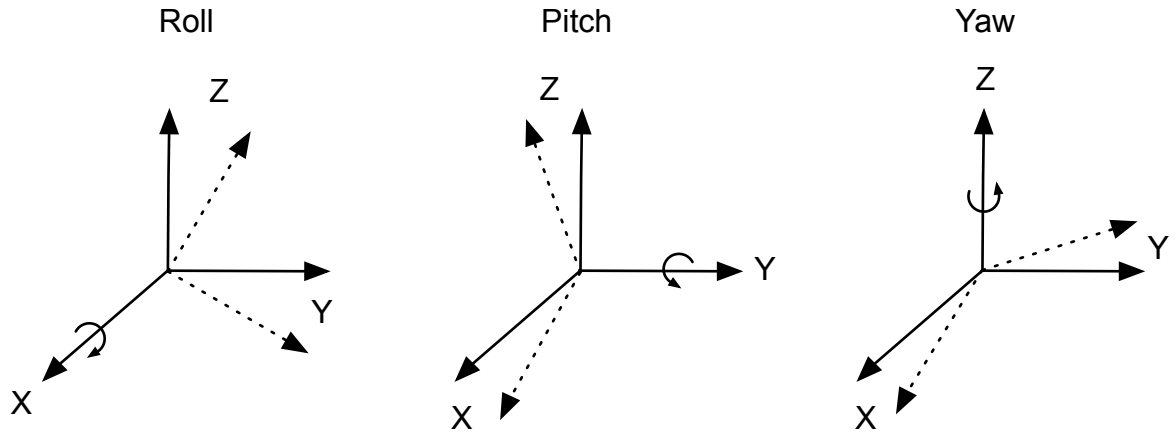

Figure 2.7: Roll, pitch and yaw angles.

$$\mathbf{O}_{\psi_z} = \begin{bmatrix} \cos(\psi_z) & \sin(\psi_z) & 0 \\ -\sin(\psi_z) & \cos(\psi_z) & 0 \\ 0 & 0 & 1 \end{bmatrix}, \tag{2.7}$$

where $\mathbf{O}$ represents the rotation matrix. The rotations are applied in the following order:

$$\mathbf{O}_T = \mathbf{O}_{\phi_x}\mathbf{O}_{\theta_y}\mathbf{O}_{\psi_z}, \tag{2.8}$$

and the measurements of the IMU in the navigation frame $\mathbf{z}_{IMU}^{NF}$ are obtained by multiplying the IMU measurements in the sensor frame $\mathbf{z}_{IMU}^{SF}$ by the rotation matrix $\mathbf{O}_T$, that is,

$$\mathbf{z}_{IMU}^{NF} = \mathbf{O}_T \ \mathbf{z}_{IMU}^{SF}. \tag{2.9}$$

In order to estimate the rotation angles the earth gravitational field, measured by the accelerometers, is typically employed. In the absence of any external acceleration, the output of an accelerometer corresponds to the earth gravitational field. Therefore it is possible to estimate the roll and pitch angles knowing that if the sensor coordinate frame is aligned with the earth coordinate frame the gravitation vector must fall in the z axis [61], that is,

$$\tan\phi_x = \frac{a_y}{a_z}, \tag{2.10}$$

$$\tan\theta_y = \frac{-a_x}{\sqrt{a_y^2 + a_z^2}}, \tag{2.11}$$

where a_x, a_y and a_z are the outputs of the accelerometer in the x, y and z axis, respectively. Unfortunately the gravitational field is invariant to the rotation of the yaw angle and

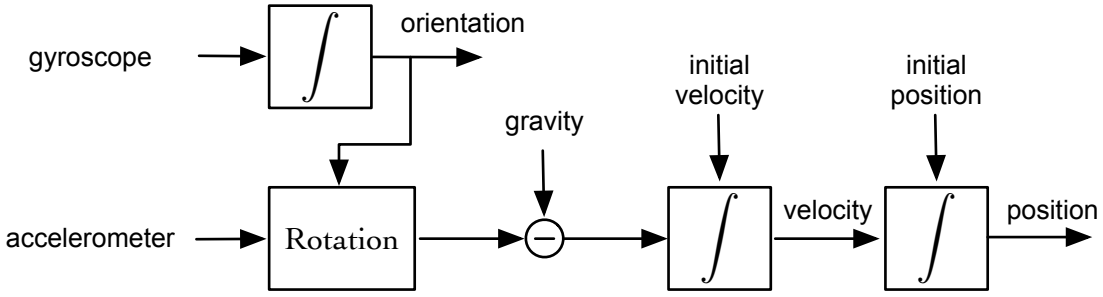

Figure 2.8: Strapdown navigation system.

therefore the yaw angle remains unknown using this method. This fact is circumvented in indoor positioning systems by assuming knowledge about the initial orientation of the user or by computing the initial orientation using the earth magnetic field.

2.2.1 Strapdown systems

The idea beyond the strapdown inertial navigation systems is to estimate the position of the user by the double integration of the acceleration signal $\mathbf{a}(t) = \left[a_x(t), a_y(t), a_z(t)\right]$. Thereby, the integration of the accelerometer signal results in the velocity and in turn the integration of the velocity results in the position [62], that is,

$$\mathbf{v}\,(t) = \mathbf{v}\,(0) + \int_0^t \mathbf{a}\,(t) - \mathbf{g}\,dt, \tag{2.12}$$

$$\mathbf{m}\,(t) = \mathbf{m}\,(0) + \int_0^t \mathbf{v}\,(t)\;dt, \tag{2.13}$$

where $\mathbf{v}$ is the velocity, $\mathbf{g}$ the gravity and $\mathbf{m}$ the position, all of them related to the navigation frame. Figure 2.8 shows the block diagram of a strapdown navigation system. First, the angular velocity measured by the gyroscope is integrated in order to track the orientation of the sensor frame with respect to the navigation frame. Note that once the initial orientation is known, the orientation at any time can be known by accumulating the rotation done in each axis, which is measured by the gyroscope. Once the orientation is known, the signal from the accelerometer is rotated to the navigation frame and the gravitation force is subtracted before the integration of the acceleration signal to obtain the velocity and the position.

The errors in the measurements of the sensors affect differently to the estimation of position. On the one hand, the errors of the accelerometer produce a drift in the

position because the integration procedure accumulates the errors over time. On the other hand, the errors of the gyroscope result in an erroneous rotation matrix and therefore the measurements of the accelerometer are incorrectly projected into the navigation frame. Furthermore, the strapdown navigation systems subtract the value of the earth gravitational field before the integration. Any error in the alignment of the frames will produce a bias due to a gravitational component projected to the horizontal plane. This source of error cannot be neglected as the magnitude of the acceleration caused by the gravity is usually greater than the acceleration produced by the movement of the user. In fact, the errors in the gyroscope measurements are the ones limiting the accuracy of the inertial strapdown systems. In general, the error in the estimation of position grows cubically with time due to the integration of the accelerometer and gyroscope signals. Using the current MEMS technology, the estimation of position will deviate over the meter in seconds making the estimation of the trajectory of a human in the long term unfeasible [63].

Recently, Foxlin et. al. [20] demonstrated that using a foot mounted IMU the time dependency of the position estimation errors in strapdown systems, which typically grows cubically with time, can be reduced to a linear growth if the zero velocity update (ZUPT) is applied. The idea beyond ZUPT is to detect the stance phases of the human walking, when the foot is firmly planted on the ground and the velocity is zero, and apply these zero velocity measurements to an extended Kalman filter that estimates the errors of the inertial measurements. However, the ZUPT strategy cannot correct the errors in the yaw angle. In order to amend this, several authors proposed techniques for reducing the gyroscope bias, such as the zero angular rate update [64] or the heuristic heading reduction [65]. An example of a inertial strapdown system using these techniques can be found in [21]. Similarly, the authors in [22] applied these updates using an unscented Kalman filter (UKF) for the estimation of the inertial measurement errors.

2.2.2 Step and heading systems

Contrarily to the strapdown navigation systems, the step and heading systems do not use the integration of the acceleration signal to compute the position of the user. Instead, these systems detect the steps and estimate the length and heading of each step from the accelerometer and gyroscope signals. Then recursively estimate the position of the user by accumulating vectors that represent the movement of the user at each step, that is,

$$m_x(k) = m_x(k-1) + l_{step}(k)\cos(\theta(k)), \tag{2.14}$$

$$m_y(k) = m_y(k-1) + l_{step}(k)\sin(\theta(k)), \tag{2.15}$$

where m_x and m_y are respectively the x, y components of the position, k is the time index, l_{step} the step length and θ the heading. The fundamental cycle for a step and heading system is [60]:

- Identification of the subset of data of an individual step.
- Estimation of the step length.
- Estimation of the heading.

Typically, the step of a pedestrian is divided into two phases: *i*) the stance phase where the foot is firmly planted on the ground and *ii*) the swing phase where the foot is in the air. Most of the algorithms designed to identify step events are based on the detection of the stance phase. Usually, threshold based methods are used to identify the lack of activity measured by the IMU during the stance phase. Traditionally these methods are based on the magnitude of the acceleration but the angular velocity has also been employed [60]. Alternatively there are methods that detect repetitive events on the walking data. Figure 2.9 shows the module of the acceleration during a walk of a pedestrian, the raw data and the filtered data are shown as many methods filter the data to eliminate high frequencial noise components of the accelerometer measurements. The detection of the steps can be done by counting the number of peaks produced by the strike of the heel in the floor [66]. Other methods compute the zero crossings of the acceleration signal after subtracting the gravity [67]. More complex methods correlate the received signal with a pre-stored template of the acceleration during a step [68]. Due to the repetitive behavior of the acceleration during the steps, spectral analysis is also employed to detect peaks in the typical stepping frequencies [69]. Recently, in [23] authors present a step detection method based on the pitch angle measured by the gyroscope of a smartphone placed in the pocket of the user.

The estimation of the step length can be obtained from the vertical displacement of the pelvis as shown by Weingberg et. al. in [70]. Following this procedure the step length is estimated as,

$$l_{step} = K \sqrt[4]{a_{z_{max}} - a_{z_{min}}}, \tag{2.16}$$

where K is a user-specific constant and $a_{z_{max}}$, $a_{z_{min}}$ are respectively the maximum and minimum of the acceleration in the vertical axis. The step length can also be estimated as a linear function of the step frequency considering that the step length and frequency increase with the speed of the user [69].

Finally, the last point of the fundamental cycle of step and heading systems is the estimation of the heading of each step. The heading estimation of these systems is equal

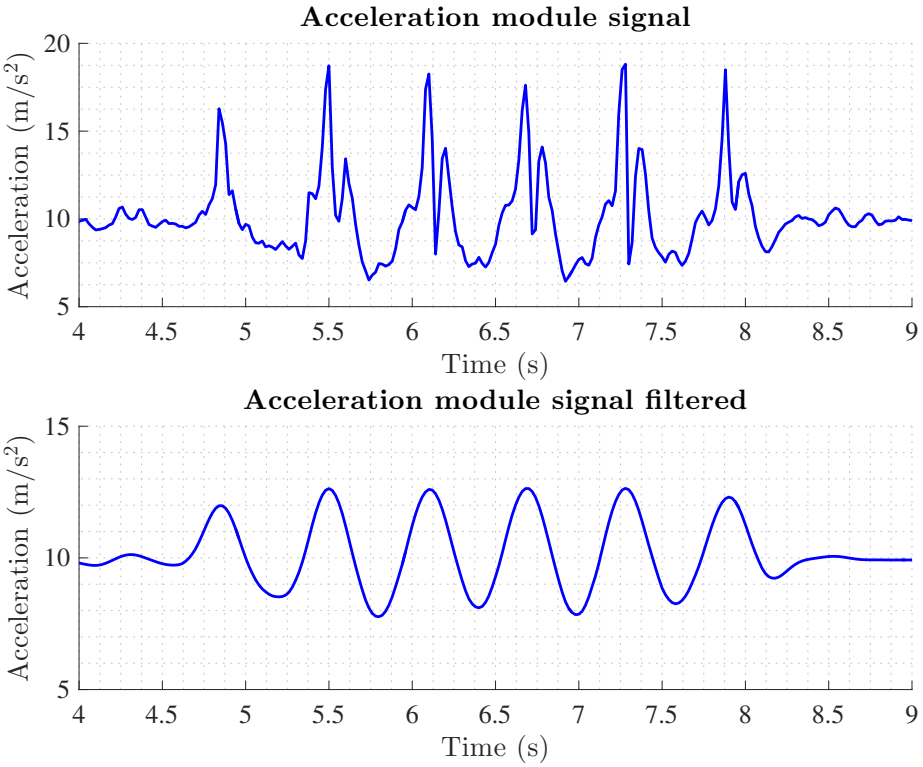

Figure 2.9: Acceleration signal measured on the hip of a pedestrian during a walk.

to the strapdown systems, that is, the heading is obtained by the integration of the gyroscope signal. Thus, the final position estimation is drifted by the errors accumulated during the integration. Fortunately, in the step and heading systems the growth of the error is linear with time instead of the cubic error present in strapdown systems. The heading can be obtained also using a magnetometer but in indoor environments that include ferromagnetic materials, the heading estimation is compromised. The fusion of both measurements has shown relatively good accuracy [36] as both measurement errors are complementary, that is, the gyroscope produce high accurate measurements in the short term and the magnetometer gives low accurate measurements but stable in time.

An example of a step and heading system is found in [24], where the authors design a system for hand held smartphones. Similarly, in [23] a step and heading system for smartphones placed in the pocket of the user is designed where the steps are detected using the gyroscope signal. A comparison of the performance of different systems using low cost sensors is presented in [25].

Despite the improvements of the step and heading systems in the reduction of the drift, it exists and therefore these kind of systems cannot be applied for a long period of time without any correcting strategy.

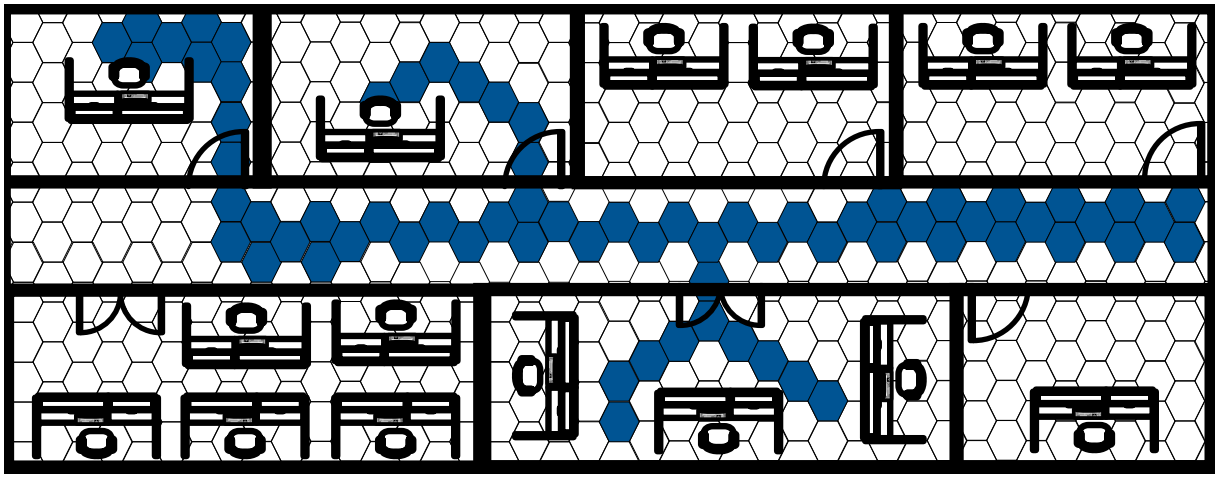

Figure 2.10: Simultaneous localization and mapping.

2.2.3 Simultaneous localization and mapping

The simultaneous localization and mapping (SLAM) extends the localization problem including the estimation of a map. It was developed by the robotics community and the key idea is that a mobile robot can be placed at an unknown location in an unknown environment and incrementally build a consistent map of this environment while simultaneously determining its location within this map [71, 72].

In 2012, Angermann et. al. developed the FootSLAM system resulting from the application of the SLAM problem to the localization of a pedestrian in an indoor environment [26]. The FootSLAM system maps the environment with a regular grid of hexagons and builds a probabilistic map computing the probability that a pedestrian crosses the transition between two adjacent hexagons. The idea beyond this system is that it is probable that a pedestrian walking in an indoor environment passes different times by the same place and thus the estimation can be enhanced considering that the user goes and returns along the same path. Figure 2.10 shows the concept of the FootSLAM where the more likely hexagons are highlighted.

The FootSLAM system computes the odometry of the user using a foot mounted IMU and uses the movement of the user between two epochs to update the particles of a Rao-Blackwellized particle filter. Each particle takes into account a possible path of the user and computes the corresponding hexagonal probabilistic map. At every epoch, the estimated path and probabilistic map of each particle are updated with the measured movement of the user, that is, the probabilities of the transitions between hexagons crossed due to the movement of the user are increased. Thus, whenever the user close the loop and returns to the origin the filter will reward those particles that have gone and returned along

the same path. With this method the drift of the inertial sensors can be eliminated but the filter has the dependence on the closure of the loops. If the walk of the pedestrian does not return to the same place the error in the position estimations will grow as in the typical step and heading systems. The main disadvantage of the system is the computational complexity as every particle must store a probabilistic map of all the environment which can lead to high computational complexity for large environments.

Recently, there appeared works in the literature based on the FootSLAM system, such as the FeetSLAM where the maps of different users are combined [27] or the PocketSLAM where the inertial measurements are obtained from an smartphone placed on the pocket of the user [28].

2.3 Hybrid positioning systems

An hybrid positioning system by definition is a system that combines two or more systems in order to enhance the performance offered by these systems individually. Currently, there are myriads of hybrid positioning systems in the literature that combine the different IPS reviewed so far. Numerous studies have attempted to review the current state of the art of hybrid positioning systems, for example, in 2001, Hightower et. al [73] review the state of the art of positioning systems. Similarly, in 2002, Pahlavan et. al. [74] review the state of the art focusing in systems for indoor environments. More recent revisions are presented in [46, 75] covering hybrid systems of network based technologies. Hybrid methods containing inertial based systems are reviewed in [60]. There are other surveys focused in hybrid methods covering a specific kind of systems like fingerprinting [59, 53], covering a specific technology like UWB [5] or covering a specific device carried by the user like a smartphone [76]. Other examples of surveys published in the last couple of years can be found in [77, 78].

A complete classification of hybrid positioning systems is not feasible due to the large amount of possible combinations of IPS that can form an hybrid system. Therefore, in this section we will review those systems related to the IPS designed in this PhD dissertation. In particular, we will focus on the following three groups:

- **RSS-IMU hybrid systems:** here we include the methods that combine inertial measurements with RSS measurements either by using a propagation model or a fingerprinting approach.
- **Map hybrid systems:** here we embrace the methods that in addition to the RSS and/or IMU measurements also use the map of the building to enhance the

performance of an IPS.

- **Smartphone hybrid systems:** here we include those RSS-IMU and Map hybrid systems that have been specifically designed for smartphones.

2.3.1 RSS-IMU hybrid systems

The availability of wireless networks deployed inside millions of buildings around the world make RSS based positioning systems an attractive option for hybrid systems because there is no need of investing in a wireless infrastructure. Note that, as stated in Section 2.1.1 the RSS can be computed just listening to the network, i. e. without any additional hardware, as far as most of the wireless standards of communication already include the RSS field in the radio packets.

The most common kind of RSS hybrid systems is one that combines it with inertial sensors. The motivation is clear: both systems have complementary errors. The inertial based systems obtain highly accurate positions estimations in the short term while the RSS based systems are less accurate but the estimations of position are time invariant. An example of these kind of hybrid systems is found in [29] where the authors developed a system that combines the position estimation of a WiFi probabilistic fingerprinting with the information of a foot mounted SHS using an EKF for the fusion of the systems. Similarly, in [30, 31] the step information of a hip mounted IMU is combined with the position estimations of a range based RSS system. Jimenez et. al. [32] combine a strapdown foot mounted inertial system with the RSS of RFID tags using an EKF. Table 2.1 summarizes the RSS-IMU hybrid positioning systems showing the main characteristics of the underlying RSS and IMU systems as well as the parameters and results of the experimental evaluation.

2.3.2 Map hybrid systems

The high complexity of the indoor environments with different distributions of walls and furniture that produces NLOS communications between the user and the wireless networks is an inconvenient for IPS because it produces less accurate estimations of the position. However, if the map of the building is a priori known by the user, the high complexity can be an advantage to the IPS as it can constraint the possible positions and improve the accuracy of the estimations. Commonly, the map information is used to enhance the performance of the RSS-IMU hybrid systems. Figure 2.11 shows the estimated trajectory from an inertial system that is affected by drift an how the map information can help us to recover the original path. Typically, the map information is included in the fusion of the

Table 2.1: RSS-IMU hybrid positioning systems

System	Technologies	RSS	IMU		Anchors	Area (m^2)	Error (m)
			Position	Method			
Frank et. al. [29]	WiFi, MEMS	Fingerprinting	Foot	SHS	11	N/A	1.65
Schmid et. al. [30]	WSN, MEMS	Propagation model	Hip	SHS	62	1125	4
Tarrío et. al. [31]	WSN, MEMS	Propagation model	Waist	SHS	9	100	2.3
Jiménez et. al. [32]	RFID, MEMS	Propagation model	Foot	Strapdown	71	2200	1.35

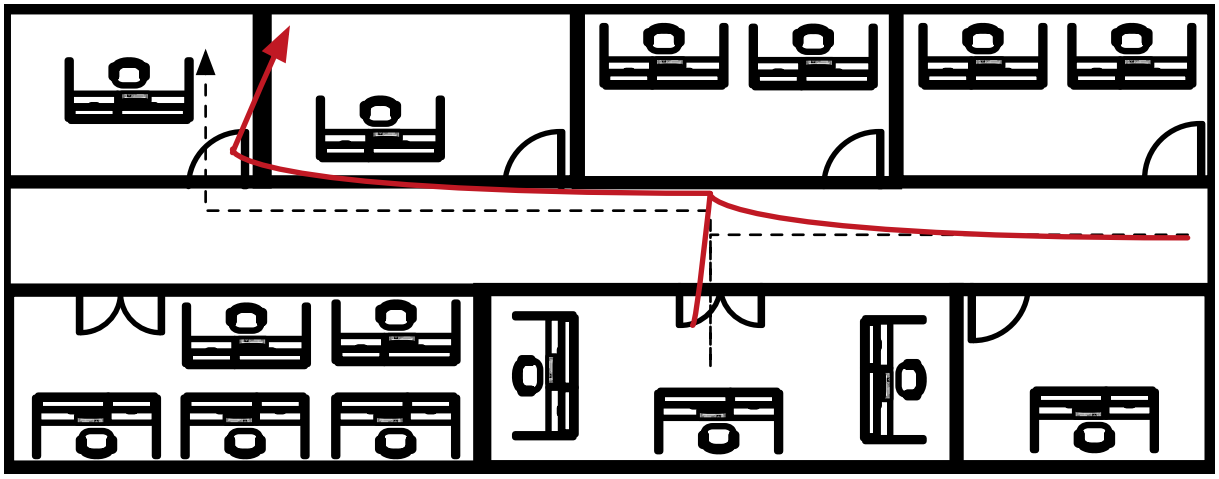

Figure 2.11: Inertial position estimation with drift (red) and corrected path (dashed).

measurements using a particle filter. During the calculation of the weights of each particle, the map constraints are calculated and those particles that have been propagated to impossible locations (as for example crossing a wall) receive a weight of zero preventing the resampling of those particles in the following epoch. For example, in [33] the measurements of a RSS probabilistic fingerprinting method are combined with the measurements of a belt mounted SHS. Then a PF fuses the measurements with the map information. Similarly, in [34] the authors use an equivalent system but the IMU is placed on the foot of the user. There are other examples of hybrid systems with map information as in [35, 36]. Table 2.2 summarizes all of them for the purpose of comparison including the main characteristics of the underlaying systems employed and the experimental evaluation.

2.3.3 Smartphone hybrid systems

The popularization of smartphones among the world converted the smartphone in the perfect device for positioning. Any IPS that can be implemented in a smartphone has the potential to be used by millions of people, granting access to the mass market without the need of investing in devices for positioning. For this reason the research efforts of authors working in the field of pedestrian positioning focused on the smartphone technology during the last years. Furthermore, the different technologies included in the nowadays smartphones allow us to implement hybrid systems using a single device. Note that a smartphone usually includes WiFi, GSM, LTE and Bluetooth radios as well as a 9 DoF IMU among other technologies like GPS.

Examples of IPS based on smartphones can be found in the literature as for example in [37] where the authors present an indoor tracking system for underground public

Table 2.2: Map hybrid positioning systems

System	Technologies	RSS	IMU		Anchors	Area (m^2)	Error	
			Position	Method			Type	Value (m)
Evennou et. al. [33]	WiFi, MEMS	Fingerprinting	Belt	SHS	4	1600	RMSE	1.53
Woodman et. al.[34]	WiFi, MEMS	Fingerprintingl	Foot	SHS	33	8725	90th	0.73
Wang et. al. [35]	WiFi, MEMS	Fingerprinting	N/A	Step	5	1000	RMSE	4.3
Klingbeil et. al. [36]	WSN, MEMS	Proximity	Belt	SHS	9	N/A	RMSE	1.2

transportation based on inertial measurements and information about the route and average time between stops. Other authors estimate the relative position of the smartphone with respect to the user, which is mandatory for the transformation of the inertial measurements from the smartphone coordinate frame to the navigation coordinate frame; in [38], the authors use a least square support vector machine (LS-SVM) for the classification of the smartphone position (hand, pocket, head, etc) and then combine the inertial data with the measurements from a WiFi fingerprinting method using a hidden Markov model (HMM). However, in order to increase the accuracy of the system, the authors typically assume a fixed position of the smartphone; an example can be found in [45] where the authors combine the inertial measurements with RSS and magnetic fingerprinting using an EKF. Other authors employ the SLAM approach in the smartphone combining the inertial measurements with WiFi and magnetic fingerprints [39, 40]. More accurate results can be obtained if the map information is available. In [41] the authors also use a HMM for the fusion of the WiFi and inertial measurements and incorporate the map information. Similarly, [42, 43] combine the WiFi fingerprints with the inertial measurements using a particle filter and in [44] the fusion is done with a Kalman filter. The performance of these systems is summarized in Table 2.3 including the technologies used by the systems, their accuracies and the characteristics of the experimental validation.

Table 2.3: Smartphone positioning systems

System	Technologies				Fusion method	Area (m^2)	Error	
	WiFi	IMU	Magnetic	Map			Type	Value (m)
Pei et. al. [38]	Yes	Yes	No	No	HMM	N/A	RMSE	4.55
Faragher et. al. [39]	Yes	Yes	Yes	Yes	SLAM	450	95th	2.7
Liu et. al. [41]	Yes	Yes	No	Yes	HMM	N/A	RMSE	3.1
Radu et. al. [42]	Yes	Yes	No	Yes	PF	N/A	90th	6
Moder et. al. [43]	Yes	Yes	No	Yes	PF	N/A	90th	2.3
Chen et. al. [44]	Yes	Yes	No	Yes	KF	3800	RMSE	1
Li et. al. [45]	Yes	Yes	Yes	No	EKF	8400	RMSE	2.9

Chapter 3

An overview of Bayesian filtering techniques

During this PhD dissertation we designed three different indoor positioning systems. Common to all of them is the application of the bayesian estimation theory. In particular, the extended Kalman filter is employed, which gives a suboptimal solution to the bayesian filtering problem. In this chapter, we review the bayesian estimation theory and the analytical solutions provided by the Kalman filter and the extended Kalman filter.

The objective in bayesian estimation is to estimate the hidden states $\{\mathbf{x}_0, \mathbf{x}_1, \mathbf{x}_2, \ldots\}$ which are observed from a set of noise measurements $\{\mathbf{z}_1, \mathbf{z}_2, \mathbf{z}_3, \ldots\}$. Particularizing for the indoor positioning problem, the vector to be estimated $\mathbf{x}$ represents the state of the user by means of its position, speed and orientation and $\mathbf{z}$ are the available measurements. The objective of the Bayesian estimation at a given time instant k is to estimate the joint posterior probability density function (PDF) of all the hidden states given all the available measurements, that is,

$$p\left(\mathbf{x}_0, \ldots, \mathbf{x}_k | \mathbf{z}_1, \ldots, \mathbf{z}_k\right). \tag{3.1}$$

If we apply the Bayes rule and reformulate the hidden states as $\mathbf{x}_{0:k} = \mathbf{x}_0, \ldots, \mathbf{x}_k$ and the noisy measurements as $\mathbf{z}_{1:k} = \mathbf{z}_1, \ldots, \mathbf{z}_k$, then we can estimate the joint posterior distribution as [79],

$$p\left(\mathbf{x}_{0:k} | \mathbf{z}_{1:k}\right) = \frac{p\left(\mathbf{z}_{1:k} | \mathbf{x}_{0:k}\right) p\left(\mathbf{x}_{0:k}\right)}{p\left(\mathbf{z}_{1:k}\right)}, \tag{3.2}$$

where $p\left(\mathbf{x}_{0:k}\right)$ is the prior distribution, $p\left(\mathbf{z}_{1:k} | \mathbf{x}_{0:k}\right)$ the likelihood model of the measurements and $p\left(\mathbf{z}_{1:k}\right)$ a normalization constant defined by,

$$p\left(\mathbf{z}_{1:k}\right) = \int p\left(\mathbf{z}_{1:k} | \mathbf{x}_{0:k}\right) p\left(\mathbf{x}_{0:k}\right) d\mathbf{x}_{0:k}. \tag{3.3}$$

Note that following the bayesian approach the posterior distribution must be estimated

every time a new measurement is available. The dimensionality of the posterior distribution increases with the number of measurements. In particular the dimension of the integral in Equation 3.3 grows with time. Therefore, the computation of the integral, and consequently the posterior probability, becomes unaffordable in terms of computational complexity for large sets of measurements. Fortunately, in the indoor positioning problem there are some constraints that can be applied. The position of a pedestrian in two successive time instants cannot be to distant because the velocity of a pedestrian is reduced. Commonly, it is considered that the state of a pedestrian (position, velocity and heading) follows a first order hidden Markov model, where the current state $\mathbf{x}_k$ depends only on the previous state $\mathbf{x}_{k-1}$. Thus, the prior distribution of the states and the likelihood model of the measurements at a given time instant $k = K$ can be now expressed as [79],

$$p\left(\mathbf{x}_{0:K}\right) = p\left(\mathbf{x}_0\right) \prod_{k=1}^{K} p\left(\mathbf{x}_k|\mathbf{x}_{k-1}\right), \tag{3.4}$$

$$p\left(\mathbf{z}_{1:K}|\mathbf{x}_{0:K}\right) = \prod_{k=1}^{K} p\left(\mathbf{z}_k|\mathbf{x}_k\right), \tag{3.5}$$

where the state model $p\left(\mathbf{x}_k|\mathbf{x}_{k-1}\right)$ can be defined as a function of the previous step and the process noise $\mathbf{v}_{k-1}$ [80], that is,

$$\mathbf{x}_k = f_{k-1}\left(\mathbf{x}_{k-1}, \mathbf{v}_{k-1}\right), \tag{3.6}$$

where f_{k-1} is a possibly non linear function. Similarly, the likelihood model of the measurements $p\left(\mathbf{z}_k|\mathbf{x}_k\right)$ can also be expressed as,

$$\mathbf{z}_k = h_k\left(\mathbf{x}_k, \mathbf{w}_k\right), \tag{3.7}$$

where h_k is a possibly nonlinear function of the current state $\mathbf{x}_k$ and the measurement noise $\mathbf{w}_k$.

From the Bayesian perspective, the indoor positioning problem consists on estimating the current state of the pedestrian considering all the available measurements, that is, the PDF $p\left(\mathbf{x}_k|\mathbf{z}_{1:k}\right)$ has to be estimated at each step. In general the Bayesian estimation assumes the knowledge of the prior PDF $p\left(\mathbf{x}_0\right)$ and recursively estimates $p\left(\mathbf{x}_k|\mathbf{z}_{1:k}\right)$ in two stages: *i*) the prediction step and *ii*) the update step.

In the prediction step, the posterior probability is predicted by obtaining the marginal distribution of $\mathbf{x}_k$ given $\mathbf{z}_{1:k}$ from the joint distribution $p\left(\mathbf{x}_k, \mathbf{x}_{k-1}|\mathbf{z}_{1:k-1}\right)$, that is,

$$p\left(\mathbf{x}_k|\mathbf{z}_{1:k-1}\right) = \int p\left(\mathbf{x}_k, \mathbf{x}_{k-1}|\mathbf{z}_{1:k-1}\right) d\mathbf{x}_{k-1}. \tag{3.8}$$

As the state is described as a first order hidden Markov model, the prediction step can be computed based on the state model $p(\mathbf{x}_k|\mathbf{x}_{k-1})$ and the posterior probability computed in the previous state $p(\mathbf{x}_{k-1}|\mathbf{z}_{1:k-1})$ [81], that is,

$$p(\mathbf{x}_k|\mathbf{z}_{1:k-1}) = \int p(\mathbf{x}_k|\mathbf{x}_{k-1})\, p(\mathbf{x}_{k-1}|\mathbf{z}_{1:k-1})\, d\mathbf{x}_{k-1}. \tag{3.9}$$

The update step is applied when the measurement of the time step k is received. Then, the Bayes rule is applied to estimate the posterior PDF, that is,

$$p(\mathbf{x}_k|\mathbf{z}_{1:k}) = \frac{p(\mathbf{z}_k|\mathbf{x}_k)\, p(\mathbf{x}_k|\mathbf{z}_{1:k-1})}{p(\mathbf{z}_k|\mathbf{z}_{1:k-1})}, \tag{3.10}$$

where $p(\mathbf{z}_k|\mathbf{z}_{1:k-1})$ is the normalization constant defined as,

$$p(\mathbf{z}_k|\mathbf{z}_{1:k-1}) = \int p(\mathbf{z}_k|\mathbf{x}_k)\, p(\mathbf{x}_k|\mathbf{z}_{1:k-1})\, d\mathbf{x}_k. \tag{3.11}$$

Assuming the knowledge of the prior PDF $p(\mathbf{x}_0)$ and the state and measurement models, the posterior PDF can be recursively estimated. In general the PDF cannot be analytically solved and numerical methods must be employed. However, under certain assumptions, the PDF can be analytically solved as in the case of the Kalman filter (see Section 3.1) or in the case of the extended Kalman filter (see Section 3.2).

3.1 Kalman filter

The Kalman filter was first presented by Rudolph Emil Kalman in 1960 [82]. The KF provides an analytical solution to the Bayesian estimator becoming the optimum minimum MSE estimator when certain conditions are met [80]. The KF assumes that the posterior PDF is Gaussian at each time step and therefore it can be parametrized by the mean and covariance. If $p(\mathbf{x}_{k-1}|\mathbf{z}_{1:k-1})$ is Gaussian, it can be proved that $p(\mathbf{x}_k|\mathbf{z}_{1:k})$ will be Gaussian if the following assumptions hold [81]:

- The state model is a known linear function.
- The measurement model is a known linear function.
- The process noise is drawn from a known zero mean Gaussian distribution, that is, $\mathbf{v}_k \sim \mathcal{N}(0, \mathbf{Q}_k)$.
- The measurement noise is drawn from a known zero mean Gaussian distribution, that is, $\mathbf{w}_k \sim \mathcal{N}(0, \mathbf{R}_k)$.

- The process noise and the measurement noise are independent.

Therefore, the state and measurement equations can be rewritten as,

$$\mathbf{x}_k = \mathbf{F}_{k-1}\mathbf{x}_{k-1} + \mathbf{v}_{k-1}, \tag{3.12}$$

$$\mathbf{z}_k = \mathbf{H}_k\mathbf{x}_k + \mathbf{w}_k, \tag{3.13}$$

where $\mathbf{F}_{k-1}$ and $\mathbf{H}_k$ are respectively the state matrix and the measurement matrix and can be time variant. In probabilistic terms, the state model and likelihood model of the measurements are Gaussians distributions, that is,

$$p\left(\mathbf{x}_k|\mathbf{x}_{k-1}\right) = \mathcal{N}\left(\mathbf{x}_k; \mathbf{F}_{k-1}\mathbf{x}_{k-1}, \mathbf{Q}_{k-1}\right), \tag{3.14}$$

$$p\left(\mathbf{y}_k|\mathbf{x}_k\right) = \mathcal{N}\left(\mathbf{y}_k; \mathbf{H}_k\mathbf{x}_k, \mathbf{R}_k\right), \tag{3.15}$$

The Kalman filter copies the prediction step and update step structure of the Bayesian estimation. However, in the KF the PDFs are considered Gaussian and therefore they can be parametrized by the mean and covariance. Thus, in the KF, the computation of the PDFs is simplified by just computing the mean and covariance. Particularly, in the prediction step the mean and covariance of the state are predicted from the previous state as follows,

$$\hat{\mathbf{x}}_{k|k-1} = \mathbf{F}_{k-1}\hat{\mathbf{x}}_{k-1|k-1}, \tag{3.16}$$

$$\mathbf{P}_{k|k-1} = \mathbf{F}_{k-1}\mathbf{P}_{k-1|k-1}\mathbf{F}_{k-1}^T + \mathbf{Q}_{k-1}. \tag{3.17}$$

Analyzing again the filter in probabilistic terms, at a given time instant k we assume that the posterior PDF of the previous time instant $k-1$ is available, that is,

$$p\left(\mathbf{x}_{k-1}|\mathbf{z}_{1:k-1}\right) = \mathcal{N}\left(\mathbf{x}_{k-1}; \hat{\mathbf{x}}_{k-1|k-1}, \mathbf{P}_{k-1|k-1}\right). \tag{3.18}$$

Then, the new posterior PDF is predicted using Equations 3.16 and 3.17 as follows:

$$p\left(\mathbf{x}_k|\mathbf{z}_{1:k-1}\right) = \mathcal{N}\left(\mathbf{x}_k; \hat{\mathbf{x}}_{k|k-1}, \mathbf{P}_{k|k-1}\right). \tag{3.19}$$

The derivation of the prediction step of the KF is based on the prediction step of the Bayesian estimation. In order to prove that the solution provided by the KF is equal to the solution of the Bayesian estimation let us introduce Lemma 1 [79].

Lemma 1 *Given two random variables $\boldsymbol{x}$ and $\boldsymbol{y}$ with Gaussian distributions,*

$$p\left(\boldsymbol{x}\right) \sim \mathcal{N}\left(\boldsymbol{a}, \boldsymbol{A}\right),$$

$$p(\boldsymbol{y}|\boldsymbol{x}) \sim \mathcal{N}(\boldsymbol{C}\boldsymbol{x}+\boldsymbol{u}, \boldsymbol{B}),$$

then the joint distribution of $\boldsymbol{x}$ *and* $\boldsymbol{y}$ *and the marginal distribution of* $\boldsymbol{y}$ *are also Gaussian distributions, that is,*

$$p(\boldsymbol{x}, \boldsymbol{y}) \sim \mathcal{N}\left(\begin{bmatrix}\boldsymbol{a}\\ \boldsymbol{C}\boldsymbol{a}+\boldsymbol{u}\end{bmatrix}, \begin{bmatrix}\boldsymbol{A} & \boldsymbol{A}\boldsymbol{C}^T\\ \boldsymbol{C}\boldsymbol{A} & \boldsymbol{C}\boldsymbol{A}\boldsymbol{C}^T+\boldsymbol{B}\end{bmatrix}\right),$$

$$p(\boldsymbol{y}) \sim \mathcal{N}\left(\boldsymbol{C}\boldsymbol{a}+\boldsymbol{u}, \boldsymbol{C}\boldsymbol{A}\boldsymbol{C}^T+\boldsymbol{B}\right).$$

If we apply the Lemma 1 to Equation 3.8 the result is,

$$p(\mathbf{x}_k|\mathbf{z}_{1:k-1}) = \mathcal{N}\left(\mathbf{x}_k; \mathbf{F}_{k-1}\mathbf{x}_{k-1}, \mathbf{F}_{k-1}\mathbf{P}_{k-1|k-1}\mathbf{F}_{k-1}^T + \mathbf{Q}_{k-1}\right). \tag{3.20}$$

Note that the results obtained by Equation 3.20 are equal to the results in Equation 3.19.

Similarly, the update step modifies the predictions using the available measurements at time k and the so called Kalman gain $\mathbf{K}_k$, that is,

$$\hat{\mathbf{x}}_{k|k} = \hat{\mathbf{x}}_{k|k-1} + \mathbf{K}_k\left(\mathbf{z}_k - \mathbf{H}_k\hat{\mathbf{x}}_{k|k-1}\right), \tag{3.21}$$

$$\mathbf{P}_{k|k} = \left(\mathbf{I} - \mathbf{K}_k\mathbf{H}_k\right)\mathbf{P}_{k|k-1}, \tag{3.22}$$

where $\mathbf{I}$ is the identity matrix. The Kalman gain is derived in order to minimize the MSE of the state estimation [83], that is,

$$\mathbf{K}_k = \mathbf{P}_{k|k-1}\mathbf{H}_k^T\left(\mathbf{R}_k + \mathbf{H}_k\mathbf{P}_{k|k-1}\mathbf{H}_k^T\right)^{-1}. \tag{3.23}$$

Repeating the analysis in probabilistic terms, we update the posterior PDF of the state as,

$$p(\mathbf{x}_k|\mathbf{z}_{1:k}) = \mathcal{N}\left(\mathbf{x}_k; \hat{\mathbf{x}}_{k|k}, \mathbf{P}_{k|k}\right). \tag{3.24}$$

In order to prove that the closed solution of the KF update step is equal to the Bayesian solution let us introduce Lemma 2 [79].

Lemma 2 *Given two random variables* $\boldsymbol{x}$ *and* $\boldsymbol{y}$ *with the following joint probability distribution,*

$$p(\boldsymbol{x}, \boldsymbol{y}) \sim \mathcal{N}\left(\begin{bmatrix}\boldsymbol{a}\\ \boldsymbol{b}\end{bmatrix}, \begin{bmatrix}\boldsymbol{A} & \boldsymbol{C}^T\\ \boldsymbol{C} & \boldsymbol{B}\end{bmatrix}\right),$$

then the marginal and conditional distributions of $\boldsymbol{x}$ *and* $\boldsymbol{y}$ *are given as,*

$$p(\boldsymbol{x}) \sim \mathcal{N}(\boldsymbol{a}, \boldsymbol{A}),$$

$$p(\boldsymbol{y}) \sim \mathcal{N}(\boldsymbol{b}, \boldsymbol{B}),$$
$$p(\boldsymbol{x}|\boldsymbol{y}) \sim \mathcal{N}\left(\boldsymbol{a} + \boldsymbol{C}\boldsymbol{B}^{-1}(\boldsymbol{y} - \boldsymbol{b}), \boldsymbol{A} - \boldsymbol{C}\boldsymbol{B}^{-1}\boldsymbol{C}^{T}\right).$$
$$p(\boldsymbol{y}|\boldsymbol{x}) \sim \mathcal{N}\left(\boldsymbol{b} + \boldsymbol{C}^{T}\boldsymbol{A}^{-1}(\boldsymbol{x} - \boldsymbol{a}), \boldsymbol{B} - \boldsymbol{C}^{T}\boldsymbol{A}^{-1}\boldsymbol{C}\right).$$

The update step of the Bayesian estimation computes the posterior PDF $p(\mathbf{x}_k|\mathbf{z}_{1:k})$. Let us first compute the joint distribution of $\mathbf{x}_k$ and $\mathbf{z}_k$ given the set of past measurements, that is, $p(\mathbf{x}_k, \mathbf{z}_k|\mathbf{z}_{1:k-1})$. From Lemma 1 the joint probability distribution is given as,

$$p(\mathbf{x}_k, \mathbf{z}_k|\mathbf{z}_{1:k-1}) = \mathcal{N}\left(\begin{bmatrix}\hat{\mathbf{x}}_{k|k-1} \\ \mathbf{H}_k\hat{\mathbf{x}}_{k|k-1}\end{bmatrix}, \begin{bmatrix}\mathbf{P}_{k|k-1} & \mathbf{P}_{k|k-1}\mathbf{H}_k^T \\ \mathbf{H}_k\mathbf{P}_{k|k-1} & \mathbf{H}_k\mathbf{P}_{k|k-1}\mathbf{H}_k^T + \mathbf{R}\end{bmatrix}\right), \tag{3.25}$$

Then, we apply the Lemma 2 to the joint probability distribution $p(\mathbf{x}_k, \mathbf{z}_k|\mathbf{z}_{1:k-1})$ in order to obtain the conditional distribution $p(\mathbf{x}_k|\mathbf{z}_k, \mathbf{z}_{1:k-1}) = p(\mathbf{x}_k|\mathbf{z}_{1:k})$, that is,

$$p(\mathbf{x}_k|\mathbf{z}_{1:k}) = \mathcal{N}\left(\hat{\mathbf{x}}_{k|k}, \mathbf{P}_{k|k}\right), \tag{3.26}$$

where $\hat{\mathbf{x}}_{k|k}$ and $\mathbf{P}_{k|k}$ are,

$$\hat{\mathbf{x}}_{k|k-1} = \hat{\mathbf{x}}_{k|k-1} + \mathbf{P}_{k|k-1}\mathbf{H}_k^T(\mathbf{H}_k\mathbf{P}_{k|k-1}\mathbf{H}_k^T + \mathbf{R})^{-1}(\mathbf{z}_k - \mathbf{H}_k\hat{\mathbf{x}}_{k|k-1}), \tag{3.27}$$

$$\mathbf{P}_{k|k} = \mathbf{P}_{k|k-1} - \mathbf{P}_{k|k-1}\mathbf{H}_k^T(\mathbf{H}_k\mathbf{P}_{k|k-1}\mathbf{H}_k^T + \mathbf{R})^{-1}\mathbf{H}_k\mathbf{P}_{k|k-1}, \tag{3.28}$$

which is exactly the same solution provided by the Kalman filter. An interesting characteristic of the KF is that even when the Gaussian assumption is not hold, the Kalman filter is the optimal linear MMSE estimator [84]. This fact explains why the Kalman filter has been used widely in the literature as it provides accurate estimations with relatively low computational complexity.

3.2 Extended Kalman filter

The assumptions of the optimality of the Kalman filter are in general highly restrictive. Although the Gaussian distributions are commonly found in the nature, the relationships between two physical magnitudes are commonly non linear. For example, in our work the position of a pedestrian observed from range measurements will be described by a non linear measurement model (see Section 2.1.1). The Extended Kalman filter is designed as a suboptimal solution for these cases where the non linear functions are linearized about the mean using a first order Taylor series approximation [79]. In the EKF we assume that the process and measurement noises are additive. Then, we describe the state and measurement models as,

$$\mathbf{x}_k = f_{k-1}(\mathbf{x}_{k-1}) + \mathbf{v}_{k-1}, \tag{3.29}$$

$$\mathbf{z}_k = h_k\left(\mathbf{x}_k\right) + \mathbf{w}_k. \tag{3.30}$$

Afterwards, the equations are linearized about the estimate in the previous time step [80] , that is,

$$f_{k-1}\left(\mathbf{x}_k\right) \approx f_{k-1}\left(\hat{\mathbf{x}}_{k-1|k-1}\right) + \hat{\mathbf{F}}_{k-1}\left(\mathbf{x}_{k-1} - \hat{\mathbf{x}}_{k-1|k-1}\right), \tag{3.31}$$

where $\hat{\mathbf{F}}_{k-1}$ is now the Jacobian matrix, that is,

$$\hat{\mathbf{F}}_{k-1} = \left.\frac{\partial f_{k-1}\left(\mathbf{x}_{k-1}\right)}{\partial \mathbf{x}_{k-1}}\right|_{\mathbf{x}_{k-1}=\hat{\mathbf{x}}_{k-1|k-1}}. \tag{3.32}$$

Similarly, the measurement model is approximated as,

$$h_k\left(\mathbf{x}_k\right) \approx h_k\left(\hat{\mathbf{x}}_{k|k-1}\right) + \hat{\mathbf{H}}_k\left(\mathbf{x}_k - \hat{\mathbf{x}}_{k|k-1}\right), \tag{3.33}$$

where $\hat{\mathbf{H}}_k$ is also the Jacobian matrix, that is,

$$\hat{\mathbf{H}}_k = \left.\frac{\partial h_k\left(\mathbf{x}_k\right)}{\partial \mathbf{x}_k}\right|_{\mathbf{x}_k=\hat{\mathbf{x}}_{k|k-1}}. \tag{3.34}$$

The estimation process of the EKF is similar to the KF. In particular, the non linear functions are used to predict the state and measurements and the Jacobian matrices are employed for the prediction of the covariances and the computation of the Kalman gain. The EKF steps are as follows,

$$\hat{\mathbf{x}}_{k|k-1} = f_{k-1}\left(\hat{\mathbf{x}}_{k-1|k-1}\right), \tag{3.35}$$

$$\mathbf{P}_{k|k-1} = \hat{\mathbf{F}}_{k-1}\mathbf{P}_{k-1|k-1}\hat{\mathbf{F}}_{k-1}^T + \mathbf{Q}_{k-1}, \tag{3.36}$$

$$\mathbf{K}_k = \mathbf{P}_{k|k-1}\hat{\mathbf{H}}_k^T\left(\mathbf{R}_k + \hat{\mathbf{H}}_k\mathbf{P}_{k|k-1}\hat{\mathbf{H}}_k^T\right)^{-1}, \tag{3.37}$$

$$\hat{\mathbf{x}}_{k|k} = \hat{\mathbf{x}}_{k|k-1} + \mathbf{K}_k\left(\mathbf{z}_k - h_k\left(\hat{\mathbf{x}}_{k|k-1}\right)\right), \tag{3.38}$$

$$\mathbf{P}_{k|k} = \left(\mathbf{I} - \mathbf{K}_k\hat{\mathbf{H}}_k\right)\mathbf{P}_{k|k-1}. \tag{3.39}$$

Note that the EKF employs non linear functions and therefore the random variables employed will no longer be normal after the non linear transformations. The EKF has no optimal properties and its accuracy depends on the accuracy of the linearization performed [80]. Nevertheless, the EKF achieves accurate results for certain applications like in the indoor positioning problems described in this PhD dissertation.

Chapter 4

Inertial-aided Indoor Tracking System for Wireless Sensor Networks

In this chapter, we begin the study of indoor positioning systems based on wireless sensor networks. The expansion of the internet of things in the last years has popularized the deployment of WSNs to control and interact with the environment, i.e. in alignment with the ideas of smart cities and smart buildings. Therefore IPS designers can take advantage of this deployment to build IPS on top of the networks without increasing the cost of the positioning system. Following the idea of reducing the cost of the system, in this chapter we present an indoor tracking system based on the RSS because these techniques do not require additional hardware to be implemented. Furthermore, the RSS can be read without being part of the network, that is, just listening to the network packets. The main problem when dealing with applications using pure RSS based localization methods is that, we experience an accuracy limitation. The reason is that the RSS observations are error-prone mainly due to the well known wireless channel variability. This fact impinges directly on the performance of most of the RSS based localization methods proposed in the literature as stated in Section 2.1.1. Similarly, the inertial based sensors provide accurate solutions for the short term but the error grows with time due to the inertial drift. In this chapter, we combine both strategies in an hybrid architecture to exploit the benefits of both systems and increase the performance of the resulting IPS.

4.1 Introduction

This chapter describes a RSS-IMU hybrid system, similar to the ones reviewed in Section 2.3.1, that combines RSS measurements form a WSN with inertial measurements from a belt mounted IMU. In general, the literature of RSS-IMU hybrid systems is focused on the

improvement of the measurements used by the fusion filter. Most works try to enhance the accuracy of the RSS-based position estimations or the accuracy of the speed and heading estimations from the inertial measurements. However, far too little attention has been paid to the configuration of the fusion filters in order to effectively combine the inertial and RSS measurements. In this chapter we address this problem and we design two different methods for the automatic configuration of the extended Kalman filter.

First of all we analyse the statistical characteristics of the RSS based position measurements. Following this analysis, two automatic methods for the tuning of the measurement noise covariance matrix of the EKF are designed: *i*) the Power Threshold Covariance Matrix Tuning (PT-CMT) method; and *ii*) the Distance Statistics Covariance Matrix Tuning (DS-CMT) method. These methods allow the EKF to benefit from the goodness of the inertial sensors in the short term and, assisted by the RSS measurements, extend their accuracy also in the long term. Finally, both methods have been tested experimentally. To the best of the author's knowledge, there are no other works considering the covariance matrix tuning of the EKF in the context of indoor hybrid positioning solutions for WSNs based on inertial and RSS measurements.

The main contributions of this chapter follow:

- The analysis of the RSS measurements statistics and its impact in the accuracy of the RSS based position estimations.
- The design of the PT-CMT method for the automatic configuration of the EKF.
- The design of the DS-CMT method for the automatic configuration of the EKF.
- The experimental validation of the proposed methods.

This chapter is organized as follows: Section 4.2 introduces the system architecture. Sections 4.3 and 4.4 detail the proposed system whereas Section 4.5 presents the experimental validation. Finally, the conclusions are presented in Section 4.6.

4.2 System Architecture

Let us consider a wireless sensor network deployed in an arbitrary indoor area. There are N anchor nodes in the network with known positions,

$$\mathbf{s}_i = \begin{bmatrix} x & y \end{bmatrix}^T, \tag{4.1}$$

where x, y are the respective Cartesian coordinates and $i = 1, 2, ...N$ is the index. Lets also consider a pedestrian that carries an additional node with unknown position,

$$\mathbf{m}_k = \begin{bmatrix} x_k & y_k \end{bmatrix}^T, \tag{4.2}$$

where k stands for the time index with corresponding sampling period T. The node carried by the pedestrian, the mobile node, listens to the network packets in order to get the RSS values of each radio link between $\mathbf{s}_i$ and $\mathbf{m}_k$. The mobile node includes a 3-axis accelerometer, a 3-axis magnetometer and a 3-axis gyroscope. These sensors are sampled several times at every time instant k obtaining the vectors of measurements from the accelerometer $\mathbf{a}_{x,k}$, $\mathbf{a}_{y,k}$, $\mathbf{a}_{z,k}$, magnetometer $\mathbf{b}_{x,k}$, $\mathbf{b}_{y,k}$, $\mathbf{b}_{z,k}$ and gyroscope $\mathbf{c}_{x,k}$, $\mathbf{c}_{y,k}$, $\mathbf{c}_{z,k}$. The subscripts x, y, z denote the respective sensor measurement axis.

Additionally, let us consider the following state space representation of the mobile node. First, the state variables are,

$$\mathbf{x}_k = \begin{bmatrix} x_k & y_k & v_k & \theta_k \end{bmatrix}^T, \tag{4.3}$$

where x_k, y_k represent the position of the mobile node at the k-th time instant in Cartesian coordinates, v_k is its speed and θ_k its heading. Taking into account that the pedestrian motion fits well to a constant velocity model, we work with the following state space model,

$$\mathbf{x}_k = f_{k-1}\left(\mathbf{x}_{k-1}\right) + \mathbf{v}_{k-1}, \tag{4.4}$$

where $\mathbf{v}_{k-1}$ is a zero mean Gaussian noise with covariance matrix $\mathbf{Q}$ and $f_{k-1}\left(\mathbf{x}_{k-1}\right)$ is the state model function that describes the constant velocity model with the velocity represented in polar coordinates. Namely,

$$f_{k-1}\left(\mathbf{x}_{k-1}\right) = \begin{bmatrix} 1 & 0 & T\cos\theta_{k-1} & 0 \\ 0 & 1 & T\sin\theta_{k-1} & 0 \\ 0 & 0 & 1 & 0 \\ 0 & 0 & 0 & 1 \end{bmatrix} \mathbf{x}_{k-1}. \tag{4.5}$$

This chapter presents a pedestrian tracking system based on an EKF, which combines RSS and inertial measurements using the architecture depicted in Figure 4.1. The system architecture is divided into three blocks,

- The pre-processing block that transforms the available set of RSS and inertial measurements into measurements of the state variables.
- The covariance matrix tuning block that tunes the measurement noise covariance matrix of the EKF based on the analysis of the RSS based distance estimation statistics.

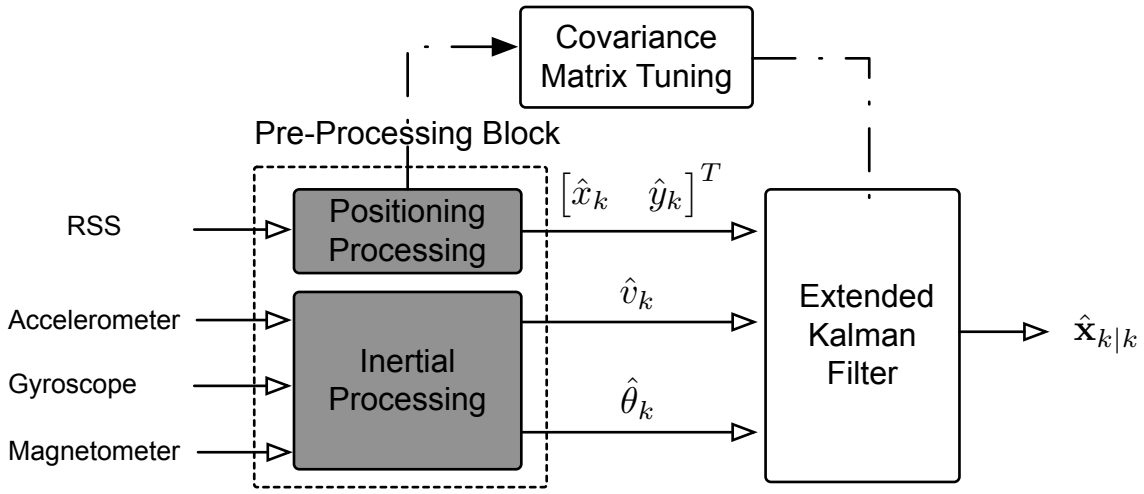

Figure 4.1: Navigation system architecture.

- The EKF block that reduces the positioning error thanks to the kinematic model and the information given by the previous blocks.

The pre-processing block is divided into two sub-blocks: *i*) the positioning processing sub-block, which transforms the RSS measurements into measurements of the mobile node position $\begin{bmatrix}\hat{x}_k & \hat{y}_k\end{bmatrix}$ and *ii*) the inertial processing sub-block, which estimates the speed and heading of the mobile node $\hat{v}_k$, $\hat{\theta}_k$ from the inertial measurements.

The EKF block uses the measurements of the state variables, the statistical information about the model and the previous state estimation $\hat{\mathbf{x}}_{k-1|k-1}$ to compute a refined estimation of the state vector $\hat{\mathbf{x}}_{k|k}$. This refined estimation achieves high accuracy thanks to the two novel measurement noise covariance matrix tuning methods introduced in Section 4.4.1.

In what follows, we first describe how the set of RSS values and the inertial measurements are pre-processed and, afterwards, we discuss our particular configuration of the EKF to take into account the statistics of the measurements.

4.3 Pre-Processing Block

This section describes: i) the propagation model (log-distance path loss model) used to obtain distance measurements from RSS readings; ii) how the distance measurements are then converted to a position estimation by means of the weighted least squares (WLS) algorithm; and iii) the methods employed to extract heading and speed information from the IMU readings. All the techniques and models described in this section have been chosen according to complexity, versatility and acceptation criteria, that is, we selected

computationally low complex (to be implemented in a WSN node) and widely used solutions in the literature.

4.3.1 Positioning Processing Sub-Block

The positioning processing sub-block obtains a position estimation from the received RSS values. In this chapter we employ the least squares (LS) approach, which obtains the position of the mobile node as the position that minimizes the squared error of the measured distances [84]. Notwithstanding, the ideas developed here can be easily extrapolated to other RSS based location methods [46].

Using the LS method, the first step is to estimate the distance between the mobile node and the anchor nodes. As stated in Section 2.1.1 this is typically done using the log-distance path loss model, that is,

$$RSS_{\mathbf{s}_i \to \mathbf{m}_k, k} = P_{1m} - 10\alpha \log_{10} d_{\mathbf{s}_i \to \mathbf{m}_k} - \gamma, \tag{4.6}$$

where $d_{\mathbf{s}_i \to \mathbf{m}_k}$ is the distance to the i-th node, P_{1m} is the received power at 1 meter from the transmitter, α is the path loss exponent and $\gamma \sim \mathcal{N}\left(0, \sigma_\gamma^2\right)$ is a zero mean Gaussian noise that models the shadowing effects. Note that the parameters of the model, i.e. P_{1m} and α, have to be experimentally obtained for each scenario, which requires a small measurement campaign to adjust the model to the scenario.

The maximum likelihood estimator of the distance between an anchor node and the mobile node is [9]:

$$\hat{d}_{\mathbf{s}_i \to \mathbf{m}_k} = 10^{\frac{RSS_{\mathbf{s}_i \to \mathbf{m}_k, k} - P_{1m}}{10\alpha}}, \tag{4.7}$$

where $\hat{d}_{\mathbf{s}_i \to \mathbf{m}_k}$ is the estimated distance to the i-th node. Note that the distance estimation does not follow a Gaussian distribution due to the exponential relationship between the distance and the RSS value. In fact, the distance estimation follows a log-normal distribution [9], that is

$$\ln \hat{d}_{\mathbf{s}_i \to \mathbf{m}_k} \sim \mathcal{N}\left(\ln d_{\mathbf{s}_i \to \mathbf{m}_k}, \sigma_d^2\right), \tag{4.8}$$

where $\sigma_d = (\sigma_\gamma \ln 10) / (10\alpha)$ is the standard deviation. Moreover, the mean and variance of the distance estimation are,

$$\mathrm{E}\left[\hat{d}_{\mathbf{s}_i \to \mathbf{m}_k}\right] = d_{\mathbf{s}_i \to \mathbf{m}_k} e^{\sigma_d^2/2}, \tag{4.9}$$

$$\mathrm{Var}\left[\hat{d}_{\mathbf{s}_i \to \mathbf{m}_k}\right] = d_{\mathbf{s}_i \to \mathbf{m}_k}^2 e^{\sigma_d^2}\left(e^{\sigma_d^2} - 1\right), \tag{4.10}$$

Therefore the estimator is biased with a bias directly proportional to the distance value. Note also that the variance exhibits a quadratic growth with the distance value.

Such statistical characteristic of $\hat{d}_{\mathbf{s}_i \to \mathbf{m}_k}$ makes the estimation of small distances more reliable than the estimation of large ones, which should also be considered in the design of localization algorithms.

The LS approach estimates the mobile node position in order to minimize the overall squared error of the distances estimated. Note that for a given realization of the LS approach, the distances estimated from different nodes have different accuracies. In order to take this into account, we use the well-known weighted LS (WLS) alternative [85, 86]. It computes the current position of the mobile node as the solution of the following minimization problem,

$$\min_{\hat{\mathbf{m}}_k} J = \sum_{i \in \mathcal{R}} \omega_i \left(\hat{d}_{\mathbf{s}_i \to \mathbf{m}_k} - \|\mathbf{s}_i - \hat{\mathbf{m}}_k\| \right)^2, \tag{4.11}$$

where $\mathcal{R}$ is the set of RSS values available at the k-th time instant and $\omega_i = 1/\text{Var}\left[\hat{d}_{\mathbf{s}_i \to \mathbf{m}_k}\right]$ are the weights [86]. The problem in (4.11) can be solved in an iterative way following the gradient descent approach [85], that is,

$$\hat{\mathbf{m}}_{k,(l)} = \hat{\mathbf{m}}_{k,(l-1)} + \delta_{(l)} \sum_{i \in \mathcal{R}} \omega_i (\hat{d}_i - \|\hat{\mathbf{s}}_i - \hat{\mathbf{m}}_{k,(l-1)}\|) \tilde{\mathbf{q}}_{i,(l-1)}, \tag{4.12}$$

where l is the iteration index, $0 < \delta_{(l)} \ll 1$ is the step size, and $\tilde{\mathbf{q}}_{i,(l-1)}$ is a unitary vector,

$$\tilde{\mathbf{q}}_{i,(l-1)} = \frac{\left(\hat{\mathbf{s}}_i - \hat{\mathbf{m}}_{k,(l-1)}\right)}{\|\hat{\mathbf{s}}_i - \hat{\mathbf{m}}_{k,(l-1)}\|}. \tag{4.13}$$

4.3.2 Inertial Processing Sub-Block

The inertial processing sub-block transforms the inertial observations into estimations of the speed and heading of the mobile node. In this work, we place the IMU in the middle of the back at the waist level (see Figure 4.2) for the user comfortability and versatility (it is much easier to fix a small device on a belt than on a shoe). However this placement has two main disadvantages: *i*) the ZUPT strategy cannot be used for correcting the inertial drift [25]; and *ii*) the sensor axes have to be perfectly aligned with the system axes in order to avoid misalignment errors. Note that we do not consider perfect alignment, hence our system copes with small alignment errors (due to the user manual adjustment) instead. Nevertheless, these disadvantages are circumvented thanks to the use of the designed measurement noise covariance matrix tuning methods (see Section 4.4), which allow us to achieve accuracies similar to the ones obtained with the foot mounted hybrid systems.

Let us first focus on the speed computation block, where $\hat{v}_k$ is estimated as the product of the number of steps per second times the length of each step, since we assume a constant

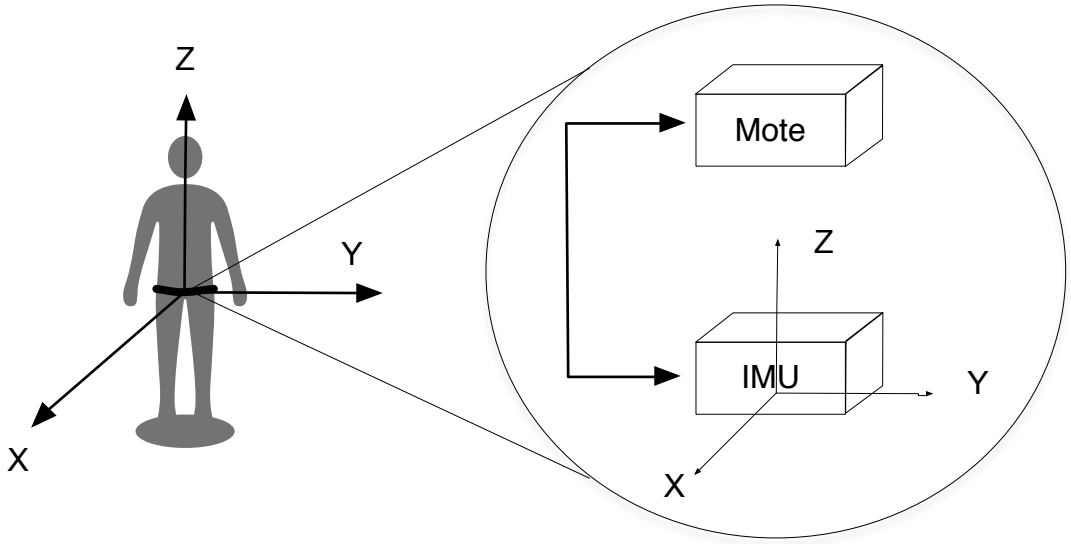

Figure 4.2: System axes.

step length per user l_{step}. In order to compute the number of steps per second, we work with the modulus of the acceleration as far as it is not affected by the particular alignment of the sensor. The corresponding discrete signal is first filtered (see Figure 4.3) using a low pass linear phase finite impulse response (FIR) filter (order 20 and 1.5 Hz cut-off frequency) in order to mitigate the higher frequency accelerations due for example to sensor vibrations and that are not of interest [87]. Finally the number of local maximums (M_{max}) that are above a predefined threshold is computed and we obtain $\hat{v}_k$ as,

$$\hat{v}_k = \frac{M_{max}}{T} l_{step}. \tag{4.14}$$

Second, the heading or speed direction of the mobile node is computed using a combination of magnetometer and gyroscope measurements. The magnetometer gives vector information of the main magnetic field, which is usually the earth magnetic field. Therefore, it is possible to obtain the angle between the magnetic field and the mobile node [88]. Hence, using the initial angle measurement as a reference, the heading of the sensor at each moment is obtained as,

$$\hat{\theta}_{mag,k} = \tan^{-1} \frac{\bar{\mathbf{b}}_{y,k}}{\bar{\mathbf{b}}_{x,k}} - \hat{\theta}_{mag,0}, \tag{4.15}$$

where $\hat{\theta}_{mag,k}$ is the heading estimation from the magnetometer at time-instant k and $\bar{\mathbf{b}}_{x,k}$, $\bar{\mathbf{b}}_{y,k}$ are the mean of the magnetic field readings at the k-th period in the x and y axis, respectively. Note that the magnetometer provides long term stability but suffers from local alterations in the magnetic field produced, for example, by home appliances, which

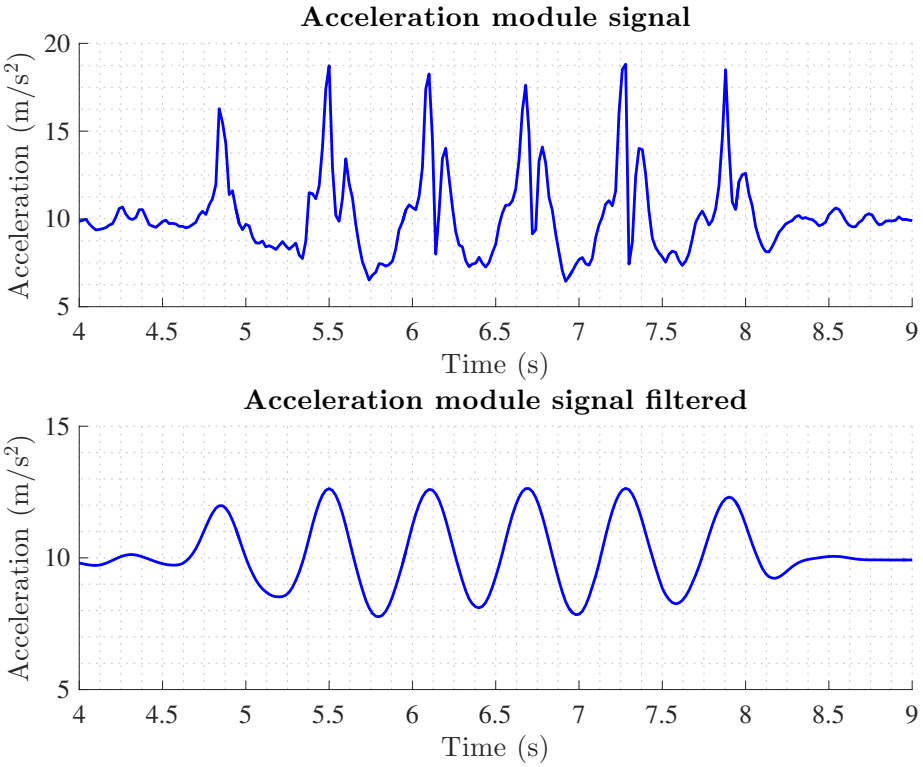

Figure 4.3: Module of the acceleration signal: original and filtered.

introduce errors in the measurements. Alternatively, the change of heading of the mobile node during an specific interval can be obtained by means of integrating the gyroscope signal, since it provides information about the angular speed. In this case, external sources of interference are not considered but the drift of the sensors plays an important role. As shown in [89], the combination of both measurements provides a relatively accurate estimate of the heading and mitigates the particular drawbacks associated to each type of sensors. Mathematically, the combination is expressed as,

$$\hat{\theta}_k = (1 - W)\left(\hat{\theta}_{k-1} + \Omega_k T\right) + W\hat{\theta}_{mag,k}, \tag{4.16}$$

where $\hat{\theta}_k$ is the heading estimation at time instant k, W the weighting factor and$\Omega_{\ k}$ the integration of the measurements of the yaw axis of the gyroscope signal at the k-th period [36].

In what follows, we describe how the EKF is configured to take advantage of the statistical information of the RSS measurements in order to benefit from the goodness of the inertial measurements also in the long term. Obviously, more sophisticated positioning and inertial pre-processing blocks will lead to better system performance, but important is that the ideas developed next can be easily extrapolated to possible modifications in the pre-processing blocks.

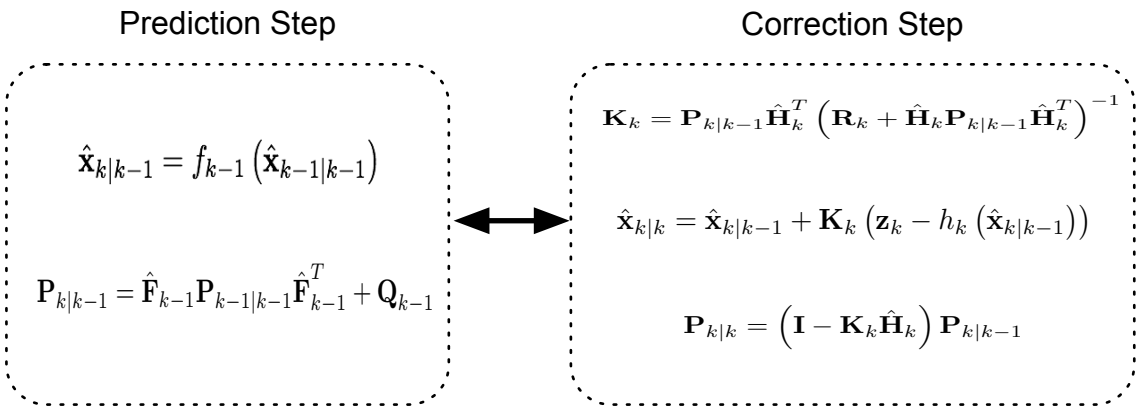

Figure 4.4: Equations of the extended Kalman Filter.

4.4 Novel Distance Statistics Based Adaptive Extended Kalman Filter

In this section, two novel configuration methods of the EKF are presented. These new methods are based on the statistical characteristics of the distance estimations, which are used for computing the position measurements. In this way the EKF takes into account the different degrees of reliability in the positioning data and the overall accuracy of the system is increased as a result.

Figure 4.4 summarizes the equations of the EKF presented in Section 3.2. The kinematic model employed is the constant velocity model defined in Equation 4.5 and the Jacobian matrix of the model function is given as,

$$\hat{\mathbf{F}}_{k-1} = \begin{bmatrix} 1 & 0 & T\cos(\theta^k) & -T\sin(\theta^k)v^k \\ 0 & 1 & T\sin(\theta^k) & T\cos(\theta^k)v^k \\ 0 & 0 & 1 & 0 \\ 0 & 0 & 0 & 1 \end{bmatrix}. \tag{4.17}$$

The performance of the filter depends on the existing measurement noise as expected. However, an accurate adjustment of the measurement noise covariance matrix $\mathbf{R}$ is not straightforward and in practice most works adopt an ad-hoc solution [29, 90, 30]. This ad-hoc adjustment is not efficient due to the variations of the statistics of the distance measurements (see Section 4.3.1). In Section 4.4.1 we propose two different methods to tune the measurement noise covariance matrix based on those statistics.

4.4.1 Covariance Matrix Tuning

This section presents two automatic methods that exploit the different degrees of reliability in the measurements to adjust the corresponding covariance matrix. They are based on the statistical characteristics of the distance estimations in indoor environments and allow us to design a system with simple inertial algorithms with similar performance than other more complex strategies (e.g. foot mounted hybrid systems).

The proposed methods are: *i*) the power threshold covariance matrix tuning method (PT-CMT); and *ii*) the distance statistics covariance matrix tuning method (DS-CMT). On the one hand, the PT-CMT method is a simple solution that considers two degrees of reliability in the measurements. It is designed for indoor areas with many small rooms (e.g. houses or offices). On the other hand, the DS-CMT takes into account the whole range of reliabilities. This method is specially designed for indoor open areas (e.g. large halls, museums, university classrooms).

Before introducing the methods, let us define the measurement noise covariance matrix as,

$$\mathbf{R} = \begin{bmatrix} \mathbf{C} & \mathbf{0} \\ \mathbf{0} & \begin{bmatrix} \sigma_V^2 & 0 \\ 0 & \sigma_\theta^2 \end{bmatrix} \end{bmatrix}, \tag{4.18}$$

where $\mathbf{C}$ is the noise covariance matrix of the position measurements, σ_V^2 is the variance of the speed measurements and σ_θ^2 is the variance of the heading measurements. Both σ_V^2 and σ_θ^2 are considered time invariant in our work whereas the distance statistics modify $\mathbf{C}$. Note that we are modifying the parameters of the matrix $\mathbf{R}$ based on the RSS statistics, therefore we will not modify the variance of the measurements obtained from the inertial sensors.

Figure 4.5 shows the bias and the variance of the distance estimation as a function of the distance itself according to (4.9)-(4.10). Note the exponential growth of the variance and also the linear increase in the bias. Consequently, the closer the mobile node is to an anchor node, the higher the reliability of the estimated distance.

Power Threshold Covariance Matrix Tuning (PT-CMT)

The PT-CMT method considers two types of position measurements: *i*) highly reliable measurements when the node is close to an anchor node; and *ii*) low reliable measurements in the other cases. This distinction is made in terms of power by comparing the received power to a given threshold P_{th}. When the highest RSS (the position computation involves several RSS values from different anchor nodes) or P_{max} is higher than P_{th}, then the

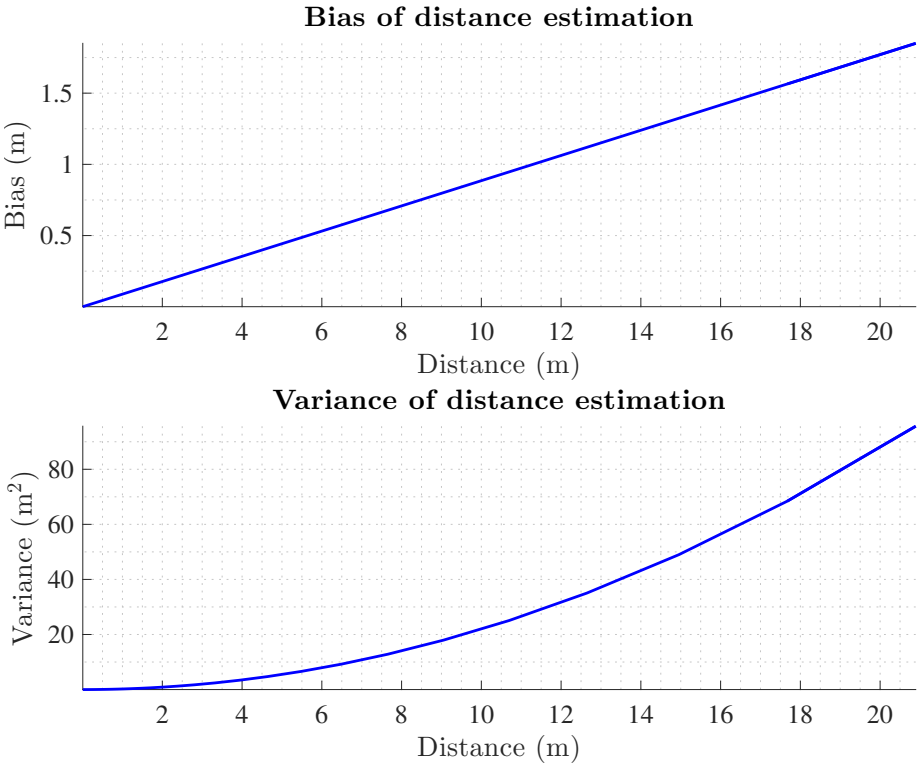

Figure 4.5: Bias and Variance of the distance estimation.

position estimation of the mobile node is directly the location of the anchor node with the highest RSS. Note that in that case there is no need to estimate the position using the WLS approach. Note also that in order to minimize the errors in the distinction of the measurements reliability, an adequate value of P_{th} is necessary. In particular we consider that the node is close to an anchor node whenever the distance between them is lower than 1 meter. Therefore, following the log-distance path loss model the power threshold is selected to be greater than the value of the received power at 1 meter to the transmitter P_{1m}. Finally, the tuning of the covariance matrix is defined as:

$$\mathbf{C} = \begin{cases} \epsilon\mathbf{I} & if \quad P_{max} \geq P_{th} \\ \sigma_p^2\mathbf{I} & if \quad P_{max} < P_{th} \end{cases}, \tag{4.19}$$

where $\epsilon \ll 1$ and σ_p^2 is a standard value of the variance defined by the user.

The PT-CMT method is designed to be applied in indoor areas with small rooms and narrow corridors, as for example in houses or offices. In these scenarios an adequate placement of the anchor nodes will produce highly reliable measurements frequently. For example, consider a node placed below the frame of a door or in a corridor.

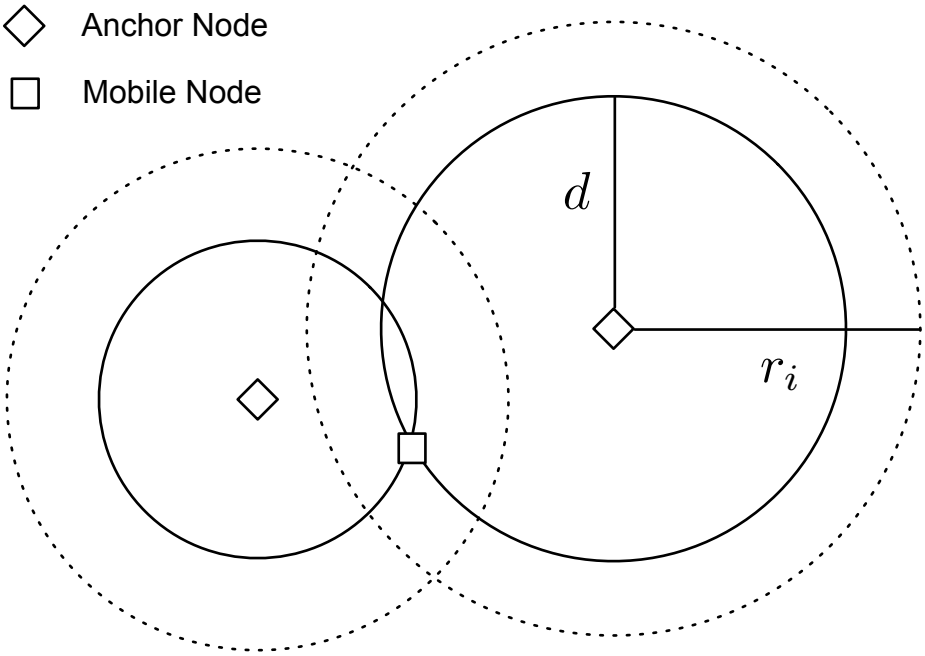

Figure 4.6: Basics of the DS-CMT method.

Distance Statistics Covariance Matrix Tuning (DS-CMT)

In open indoor areas such as large halls or museums the previous hypothesis is no longer valid, that is, the trajectory of the mobile node is not necessarily close to any anchor node at any point. Therefore, the PT-CMT method is not adequate. In the DS-CMT method each position has a different degree of reliability that depends on the individual distances to the anchor nodes. In the following, we describe how the degree of reliability is computed and how the covariance matrix of the EKF is adjusted afterwards.

First of all, the probability density function of the distance estimation from the anchor's position $\mathbf{s}_i$ to the mobile node position $\mathbf{m}_k$ is defined as [91],

$$f(\chi) = \begin{cases} \frac{1}{\sqrt{2\pi}\sigma_{d\chi}} \exp \frac{\left(\ln \chi - \ln d_{\mathbf{s}_i \to \mathbf{m}_k}\right)^2}{-2\sigma_d^2} & if\ \chi > 0 \\ 0 & if \chi \leq 0 \end{cases}. \tag{4.20}$$

From the PDF of the distance estimation it is possible to define a confidence region (see Figure 4.6) where the mobile node will be with a given probability p defined by the user. This confidence region is a circle centered on the anchor's node location and with radius r_i fulfilling $p\left(d_{\mathbf{s}_i \to \mathbf{m}_k} \leq r_i\right) = p$. Notwithstanding, the mean and variance of the

distance are unknown and therefore we use the estimated values, that is,

$$\int_{0^+}^{r_i} \frac{1}{\sqrt{2\pi}\hat{\sigma}_d \chi} \exp \frac{\left(\ln \chi - \ln \hat{d}_{\mathbf{s}_i \to \mathbf{m}_k}\right)^2}{-2\hat{\sigma}_d^2} \mathrm{d}\chi \approx p, \tag{4.21}$$

where $\hat{\sigma}_d = (\hat{\sigma}_\gamma \ln 10) / (10\hat{\alpha})$ and $\hat{\sigma}_\gamma$, $\hat{\alpha}$ are parameters of the log-distance path loss model obtained in the system calibration.

The reliability of the position estimations depends on the area resultant of the intersection of all the confidence region of the anchor nodes. The computation of this area is not straightforward therefore in this work we will approximate this area by the confidence region of the closest anchor node. Note that the mobile node is simultaneously inside all the confidence regions with high probability (p=0.95 in our case) and the smaller region corresponds with the closest anchor node. Note also that the approximated area will always be greater than the real one so our approximation can be considered as an upper bound of the real area.

Finally the measurement noise covariance matrix of the EKF is adjusted using the radius of the smaller confidence region $r_{i_{min}}$, that is,

$$\mathbf{C} = r_{i_{min}}^2 \mathbf{I}. \tag{4.22}$$

Next section evaluates the performance enhancements achieved thanks to the proposed DSB-EKF.

4.5 Experimental Validation

In the experimental validation, we test the performance of the system using the Iris motes [92] from Crossbow, equipped with the ATmega 1281 microcontroller [93] and the rf230 radio chip [94]. The IMU used is the 9DOF Sensor Stick from Sparkfun, which includes a 3 axis accelerometer (ADXL345 [95]), a 3 axis magnetometer (HMC5883L [96]) and a 3 axis gyroscope (ITG-3200 [97]).

The anchor nodes are configured to broadcast a packet every second with an output power of 0 dBm. The mobile node (a node connected to the IMU stick) is attached to the person with the help of a belt. The accelerometer is sampled at 50 Hz and the magnetometer and gyroscope at 15 Hz. Finally, there is one more mote connected to a computer that acts as a gateway. This mote receives a message from the mobile node every second and stores the data in the computer. The position estimation is computed by the EKF every second.

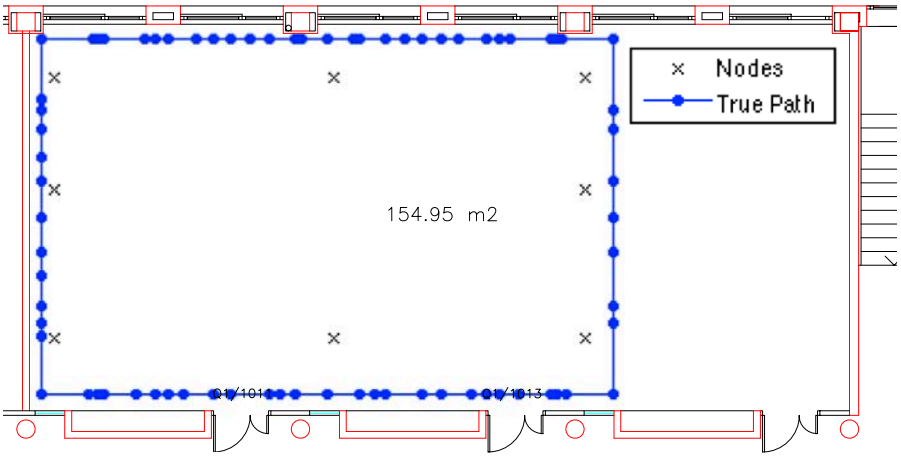

Figure 4.7: Scenario 1 (size 8.6 m x 18 m).

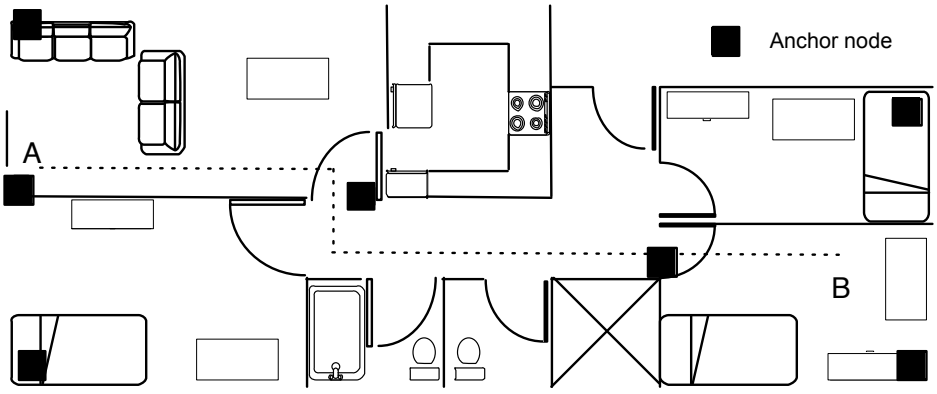

Figure 4.8: Scenario 2 (size 5.6 m x 13.6 m).

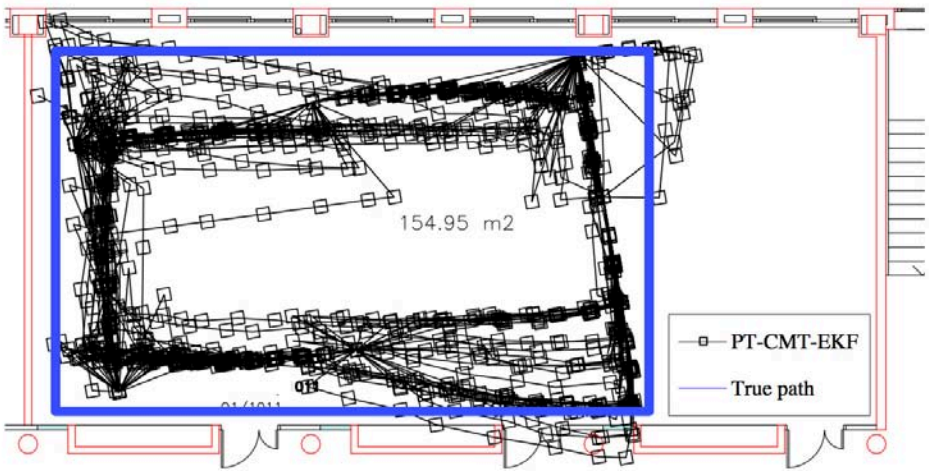

Figure 4.9: PT-CMT in Scenario 1 (size 8.6 m x 18 m).

In order to evaluate the performance of the proposed technique, the system is tested in two different scenarios. The Scenario 1 is a big classroom of 154.95 m^2 that is representative of a large indoor area and it is covered with 8 anchor motes as shown in Figure 4.7, there is one node every 19.3 m^2. The true path is a square trajectory of 46.4 m length.

Scenario 2 is a house with an area of 76.16 m (5.6 m x 13.6 m) covered with 8 motes (See Figure 4.8), that is, one node for every 9.52 m^2. Therefore, this scenario is representative of an indoor area with small rooms and corridors. The defined path starts at point A, goes to point B and returns to point A as depicted in Figure 4.8. There are stops programmed at points A and B of 15 seconds duration.

Common to both scenarios is the duration of the test, which is fixed to 20 minutes. Note that this duration is enough to evaluate the long term stability of the algorithms presented as far as, typically, inertial based positioning methods deviate in seconds or a few minutes in the best cases. The tests are repeated ten times and averaged afterwards. The power threshold of the PT-CMT strategy is set to -61 dBm for Scenario 1 and to -63 dBm for Scenario 2.

During the experimental validation we compare the results of an EKF configured with the PT-CMT method, an EKF configured with the DS-CMT method and a reference case with an EKF manually configured, that is, different values are tested and the ones that minimize the positioning error are selected. In the following, these systems are referred to as PT-CMT-EKF, DS-CMT-EKF and Basic-EKF.

Let us first focus on Scenario 1. Figures 4.9 and 4.10 include an example of the estimated paths of the PT-CMT-EKF and DS-CMT-EKF systems. The reader can appreciate the higher accuracy of the DS-CMT-EKF system compared to the PT-CMT-EKF. In the

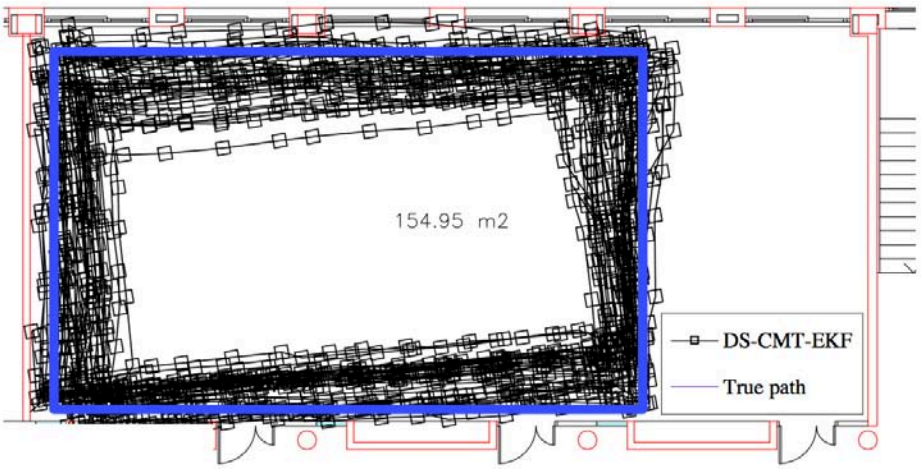

Figure 4.10: DS-CMT in Scenario 1 (size 8.6 m x 18 m).

different tests carried out the root mean squared error (RMSE) achieved is 1 m for the DS-CMT-EKF and 1.3 m for the PT-CMT-EKF, which represents an improvement of 23%. This improvement is due to the characteristics of the Scenario 1, i.e. an open area where the mobile node does not pass near the anchor nodes and therefore the PT-CMT-EKF is not the best option. Furthermore, both methods outperform the accuracy of the Basic-EKF as shown in Table 4.1. Specifically, the improvement in accuracy is 9% and 30% for the PT-CMT-EKF and DS-CMT-EKF, respectively.

Table 4.1: Results of the experimental validation in terms of RMSE

	Basic-EKF	PT-CMT-EKF	DS-CMT-EKF
Scenario 1	1.43	1.3	1
Scenario 2	1.05	0.64	0.87

Note that in general the RMSE does not fully represent the real performance of a system. Instead, the cumulative distribution function (CDF) of the positioning errors provides more information. The CDF has been calculated for both methods and plotted in Figure 4.11. We appreciate that the error is below 2.62 m in 90% of the occasions for the Basic-EKF. This error is 2.29 m for the PT-CMT-EKF and it is significantly reduced to 1.77 m in the case of the DS-CMT-EKF. The improvement of both methods over the Basic-EKF in terms of CDF is 12.6% and 32.5% for the PT-CMT-EKF and DS-CMT-EKF, respectively.

Considering now the Scenario 2, an example of the estimated paths for both methods is shown in Figure 4.12 and Figure 4.13. In this case the performance of the algorithms

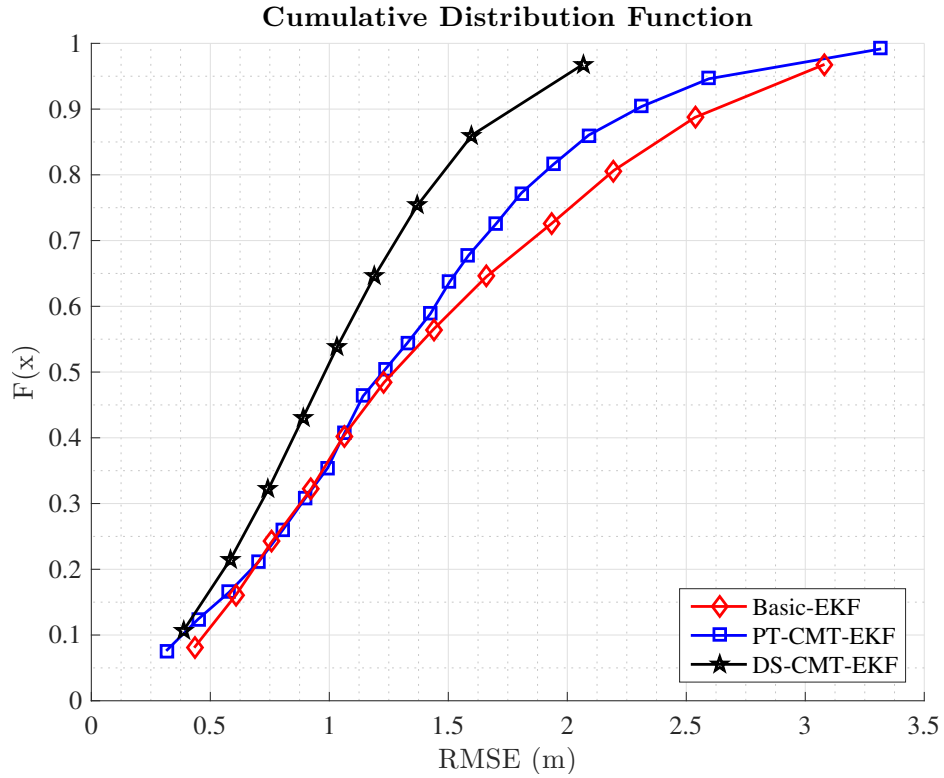

Figure 4.11: Cumulative Distributed Function of the error in the Scenario 1.

follows a different pattern and it is the PT-CMT-EKF who presents better results. The tests carried out show a RMSE of 0.87 m for the DS-CMT-EKF and 0.64 m for the PT-CMT-EKF, which represents an improvement of 26%. Again, both methods outperform the accuracy obtained by the Basic-EKF (see Table 4.1). In particular, the improvement is 39% for the PT-CMT-EKF and and 17% DS-CMT-EKF. Moreover, Figure 4.14 shows the CDF for Scenario 2. If we analyse again the error in the 90% of the cases, we observe that it is situated at 1.79 m for the Basic-EKF. This error is below 1.5 m for the DS-CMT-EKF and 1.32 m for the PT-CMT-EKF. The resultant improvement in accuracy, in terms of CDF, over the Basic-EKF is 26% for the PT-CMT-EKF and 16% for the DS-CMT-EKF Note that in this case, the trajectory of the mobile node is often very close to the anchor nodes and this explains the superior performance of the PT-CMT-EKF.

Finally, we evaluate the different methods as a function of the number of anchor nodes, which strongly influences the performance of the techniques. Table 4.2 summarizes the 90th percentile of the CDF for two different number of anchor nodes $N = 8$ and $N = 6$. As it is expected the accuracy of the system is degraded when less anchor nodes are available. Particularly remarkable is the behavior of the DS-CMT-EKF, whose performance is slightly degraded with the number of nodes. Contrarily, the PT-CMT-EKF is clearly degraded because close anchor nodes are not present along the trajectory.

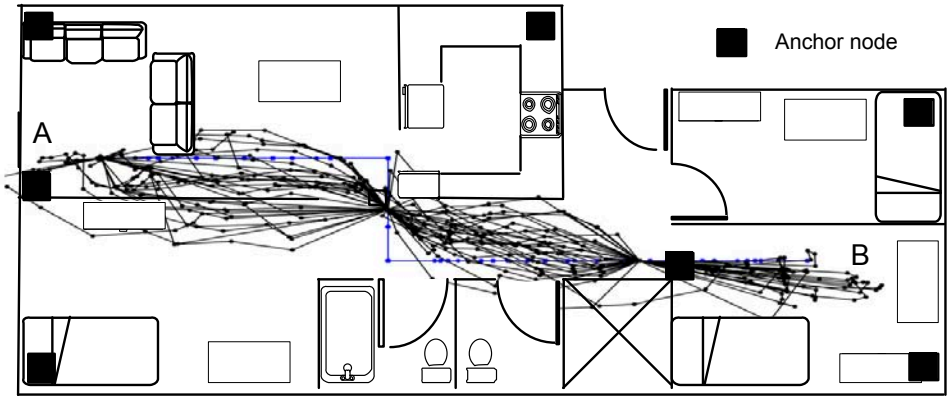

Figure 4.12: PT-CMT in Scenario 2 (size 5.6 m x 13.6 m).

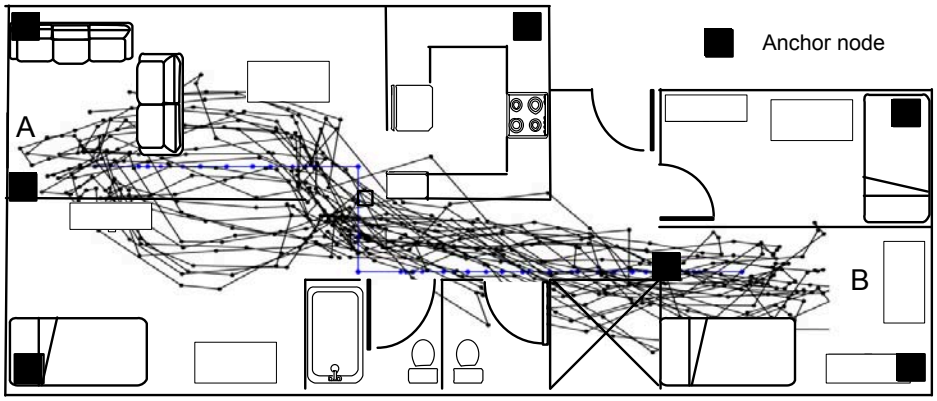

Figure 4.13: DS-CMT in Scenario 2 (size 5.6 m x 13.6 m).

Table 4.2: Results of the experimental validation in terms of 90th percentile

	Basic-EKF		PT-CMT-EKF		DS-CMT-EKF	
	8 nodes	6 nodes	8 nodes	6 nodes	8 nodes	6 nodes
Scenario 1	2.62	2.93	2.29	2.68	1.77	1.93
Scenario 2	1.79	2.17	1.32	1.69	1.5	1.66

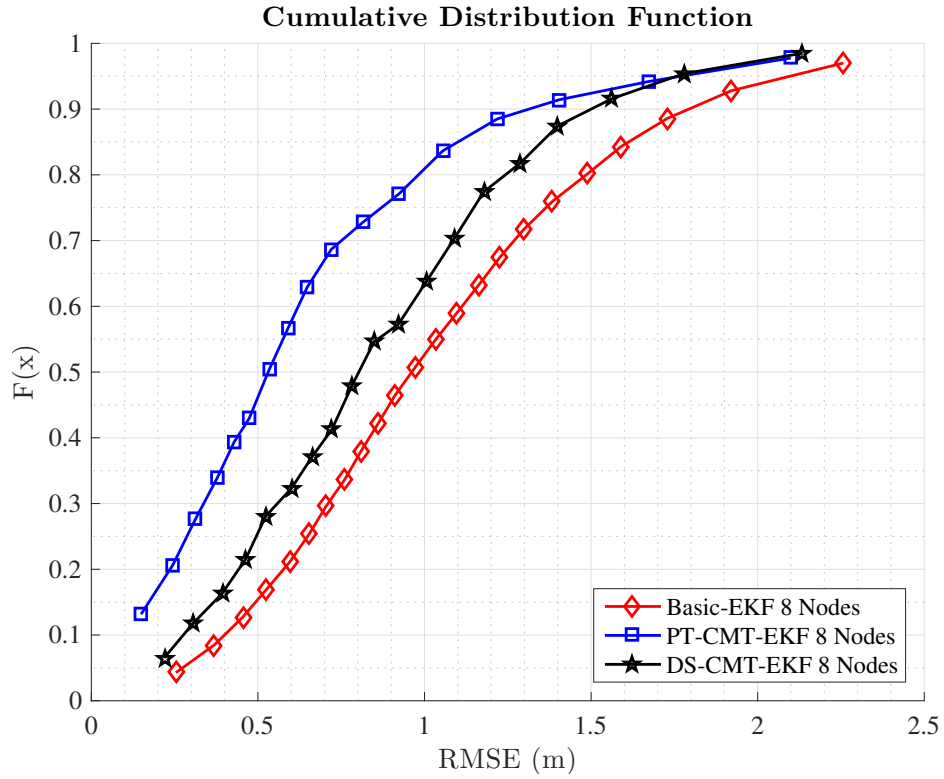

Figure 4.14: Cumulative Distributed Function of the error in the Scenario 2.

Notice that our solutions extend in both scenarios the short-term accuracy of the inertial sensors over time as desired. Note also that the presented covariance matrix tuning methods do not avoid the drift of the inertial sensors but they are able to bound this drift by tuning the measurement noise covariance matrix of the EKF taking into account the statistics of the distance readings. That is because the proposed methods are able to convey the low MSE of the good position measurements to the output of the EKF. Furthermore, the presented methods achieve similar accuracies to other hybrid systems using more complex inertial algorithms like the ZUPT strategy for the foot mounted inertial algorithms [32, 29, 60]. In particular, our proposed systems achieve accuracies around the meter (i.e. the same as foot mounted hybrid systems) and this accuracy is maintained over a long period of time, that is, the accuracy remains around 1 meter during a 20 minutes test.

4.6 Conclusions

In this chapter we presented an enhanced inertial-aided indoor tracking system for WSNs based on the extended Kalman filter. Our system combines distance measurements extracted from the RSS of a set of anchor nodes together with inertial measurements obtained

from an on-board IMU. It is well-known that dead reckoning solutions provide good accuracies in the short term but not in the long term. On the contrary, RSS based position estimations are not so accurate but stable in time. In this chapter, we statistically analysed the RSS based position measurements and designed two covariance matrix tuning methods that automatically adjust some of the filter parameters, in particular the coefficients of the measurement noise covariance matrix. The PT-CMT method suits indoor scenarios with many small rooms and the DS-CMT method is better for indoor open areas. In summary, we showed that it is possible to design simple EKF based solutions that efficiently combine observations with different degrees of reliability.

The system has been experimentally validated in two different representative indoor scenarios with different densities of nodes and the proposed enhancements in the EKF reduce the positioning RMSE with respect to a regular EKF up to 39% in the scenarios tested. As a result, the proposed system is kept simple in terms of computational complexity, the accuracy is around the meter in terms of RMSE and also kept in the long term as it is shown in Section 4.5 during a 20 minutes test. Therefore, our contribution suits applications that require the tracking of objects or people inside buildings.

Chapter 5

Indoor Pedestrian Tracking by On-body Multiple Receivers

In this chapter, we continue the study of indoor positioning systems based on wireless sensor networks extending the problem to the multiple receiver case. The multiple receiver scheme is exploited to improve the accuracy of the designed IPS and to estimate the speed and heading of the user without the use of inertial sensors. The motivation is the reduction of the computational complexity of the system. The WSNs devices are designed for low complex systems with low measurement rates in order to enlarge the duration of the batteries. The use of inertial sensors in WSNs increase the complexity as they must be sampled several times every second to be able to recognize the movement of the user. Moreover, the computation of the relative orientation generally implies the use of additional Kalman filter variations, typically the EKF or the UKF, as stated in Section 2.2.2. Furthermore, the placement of the receivers around the body of the user allows us to exploit the attenuation of the human body, which will be different for each receiver, in order to infer the relative orientation between the user and the anchor node. The result is a pure RSS based localization system that can respond to changes in the orientation of the user without the need of using inertial sensors, with the correspondent saving in terms of computational cost.

5.1 Introduction

This chapter describes the design of an indoor positioning system, based on the RSS measurements received from a WSN, employing multiple receivers deployed in the body of the user. The multiple receiver architecture is not common in the literature of IPS. In fact, most authors prefer to employ hybrid architectures involving RSS and inertial

measurements (see Section 2.3) because it can benefit from the time invariant RSS based position estimations and the speed and heading estimations based on the inertial measurements. However, in this chapter we show that the speed and heading of the user can also be estimated employing a multiple receiver architecture. To do so, we employ machine learning techniques to find patterns in the data and estimate the distance and relative angle between the user and each anchor node. Then, we combine the measurements to find the estimations of position, speed and heading and finally, we use an EKF for the fusion of the position and velocity measurements. Furthermore, the system has been experimentally validated. To the best of the author's knowledge, there are no other works considering the multiple receiver architecture for pure RSS based systems based on WSNs.

The main contributions of this chapter follow:

- Design of a multiple receiver architecture for IPS.
- Design of algorithms based on a machine learning pipeline that estimate the speed and heading of the user.
- The experimental validation of the system that proves the generalization of the ML algorithms, that is, the algorithms are trained in one scenario and tested in other scenarios.

The rest of the chapter is organized as follows: Section 5.2 introduces the system architecture. Section 5.3 introduces the ML techniques employed in this work whereas Section 5.4 details the methods used in the estimation of distances and angles. Section 5.5 explains the algorithms used to estimate the position and heading of the user and Section 5.6 details the EKF. Section 5.7 presents the experimental validation and finally, the conclusions are presented in Section 5.8.

5.2 System Architecture

As in Chapter 4 let us consider an arbitrary indoor area with N anchor nodes with known positions,

$$\mathbf{s}_i = \begin{bmatrix} x & y \end{bmatrix}^T, \tag{5.1}$$

where x, y are the respective Cartesian coordinates and $i = 1, 2, ..., N$ is the index. Now, instead of one receiver we consider L receiver nodes placed on the body of the user defining a set,

$$\mathcal{R} = \{\mathrm{Rx}_1, \mathrm{Rx}_2, ..., \mathrm{Rx}_L\}. \tag{5.2}$$

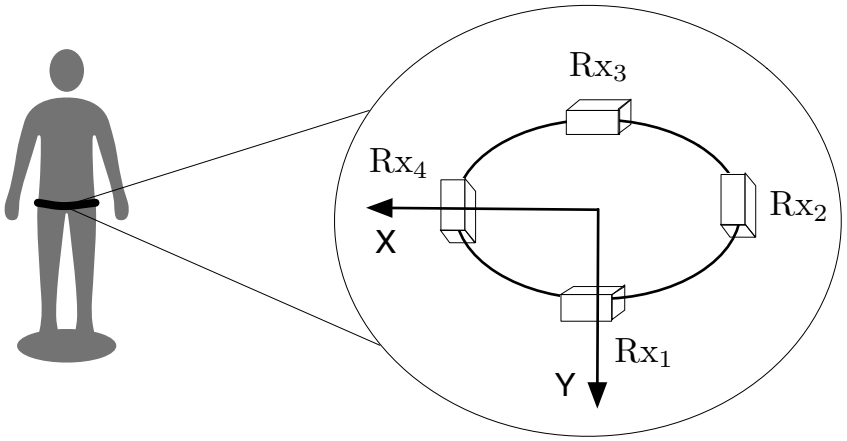

Figure 5.1: Distribution of the receivers on the user's body.

The relative position of every node in $\mathcal{R}$ is known in the body reference system (see Figure 5.1). However, due to the user's mobility, the absolute position is unknown. Since the aim of this work is the tracking of the user, we consider the position of the receivers to be the position of the user itself, that is,

$$\mathbf{m}_k = \begin{bmatrix} x_k & y_k \end{bmatrix}^T, \tag{5.3}$$

where k stands for the time index with corresponding sampling period T. The receivers periodically listen to the network packets and compute the RSS from all the anchors nodes inside their communications range. Specifically, in this work we have employed four receiver nodes ($L = 4$) placed on a belt with ninety degrees of separation as depicted in Figure 5.1.

This chapter presents and indoor positioning system based on RSS measurements, machine learning algorithms and an EKF. The architecture of the system (see Figure 5.2) is divided into three blocks:

- The RSS processing block that processes the RSS measurements using ML techniques to obtain estimations of the user's speed and the distance and angle between the user and the anchor nodes.

- The measurement block where we obtain the position and heading of the mobile node using the distances and angles estimated in the first block.

- The filtering block that estimates the user's position using an EKF that takes into account a constant velocity model.

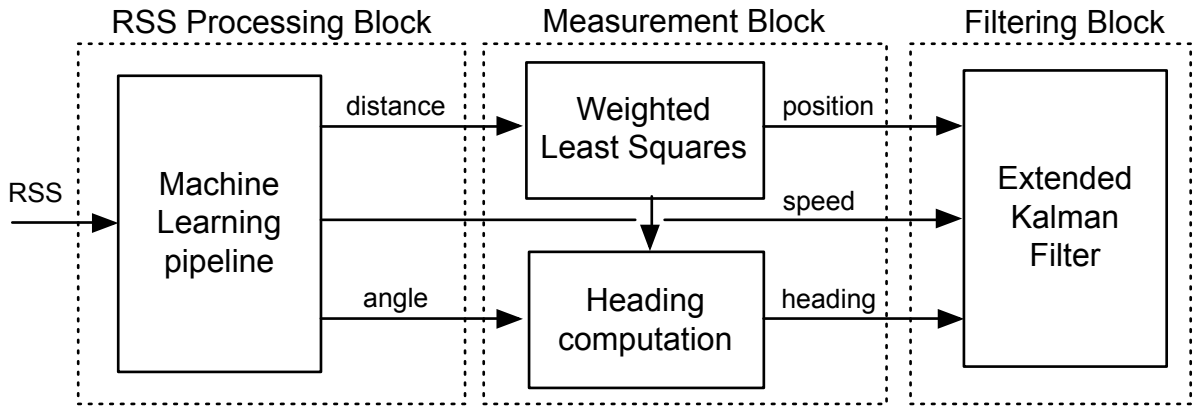

Figure 5.2: System Architecture.

Next section introduces the ML techniques used in this work whereas Sections 5.4 to 5.6 detail each of the described system blocks.

5.3 Background in Machine Learning

This section provides a brief introduction to the ML techniques used in this work. ML techniques are algorithms developed for searching patterns in data and predict new outcomes. Typically, the algorithms apply an adaptive model $f(\cdot)$ to the input data $\boldsymbol{\xi}$ (i.e. the features in the ML terminology) in order to find the output variable of interest η.

In order to find the parameters of the model, a database of m different pairs $\boldsymbol{\xi}, \eta$ (supervised learning) is necessary. We divide the database into three groups: i) the training set which includes m^t samples (around 60 % of the available data); ii) the cross validation set which includes m^{cv} samples (about 20 % and different from the data included in the training set); and iii) the test set which includes the remaining data in the database.

ML techniques can be classified into two different groups. If the output η is one of a finite discrete number of categories we are dealing with a classification problem. Otherwise, it is a regression problem. In this work we have employed a classification technique (neural network) and a regression technique (linear regression).

5.3.1 Linear Regression

In linear regression, the goal is to estimate the regression function $\eta = f(\boldsymbol{\xi})$. Since a linear relationship between η and $\boldsymbol{\xi}$ is assumed in linear regression, we can write [98, Sec. 3.2]

$$\eta = f(\boldsymbol{\xi}) = \beta_0 + \sum_{i=1}^{A} \beta_i \xi_i, \tag{5.4}$$

where A is the number of features, β_i the parameters and β_0 is a bias parameter that adjusts the model to any fixed offset in the data. It is helpful to define an additional dummy feature $\xi_0 = 1$ so that,

$$\eta = f(\boldsymbol{\xi}) = \boldsymbol{\beta}^T \boldsymbol{\xi}, \tag{5.5}$$

where $\boldsymbol{\beta} = \left[\beta_0, \ldots, \beta_A\right]^T$ and $\boldsymbol{\xi} = \left[1, \xi_1, \ldots, \xi_A\right]^T$. Note that $f(\boldsymbol{\xi})$ is linear on the parameters β_i but we are not restricted to linear models with respect to $\boldsymbol{\xi}$. In other words, artificially created inputs such as transformations of the inputs (e.g. logarithm, square-root, etc.), polynomial expansions (e.g. $\xi_1 \cdot \xi_2, \xi_1^2$, etc.) and others may be added. These extra features introduce non linear models as regards $\boldsymbol{\xi}$.

Once the model is defined, it is necessary to find out the values of β_i that best fit our training set. The goal is to learn from the training set which are the parameters that best fit the data to the model and, accordingly, we define a cost function that measures how good our knowledge is. Commonly this cost function is the residual sum of squares, that is

$$J(\boldsymbol{\beta}) = \sum_{i=1}^{m^t} \left(\eta_i - f(\boldsymbol{\xi}_i)\right)^2, \tag{5.6}$$

and hence in linear regression we find the values of $\boldsymbol{\beta}$ as

$$\boldsymbol{\beta}^* = \underset{\boldsymbol{\beta}}{\operatorname{argmin}}\ J(\boldsymbol{\beta}). \tag{5.7}$$

Finally, it is common in linear regression to use regularisation in order to mitigate the over-fitting problem [98, Sec. 3.4.1]. This problem appears when the training set is small compared to the complexity of the model, roughly speaking, when the degrees of freedom in our model suffice or nearly suffice to fit all the data in the training set. Note that in such cases, outliers in the training set become representative when they shall not. Our common regularisation method, i.e. L2-regularisation consists simply in shrinking the size of the elements inside $\boldsymbol{\beta}$ and thus avoiding the best possible fit (which may be over-fitted). Mathematically, $J(\boldsymbol{\beta})$ is modified as

$$J^r(\boldsymbol{\beta}) = \sum_{i=1}^{m^t} \left(\eta_i - f(\boldsymbol{\xi}_i)\right)^2 + \lambda \sum_{i=1}^{A} \beta_i^2, \tag{5.8}$$

where $\lambda > 0$ is the regularisation parameter. We use the cross-validation set to check the goodness of the proposed model (measured with $J(\boldsymbol{\beta})$) and select the value of λ. The test set is used to check the performance of the algorithm (for the best value of λ chosen).

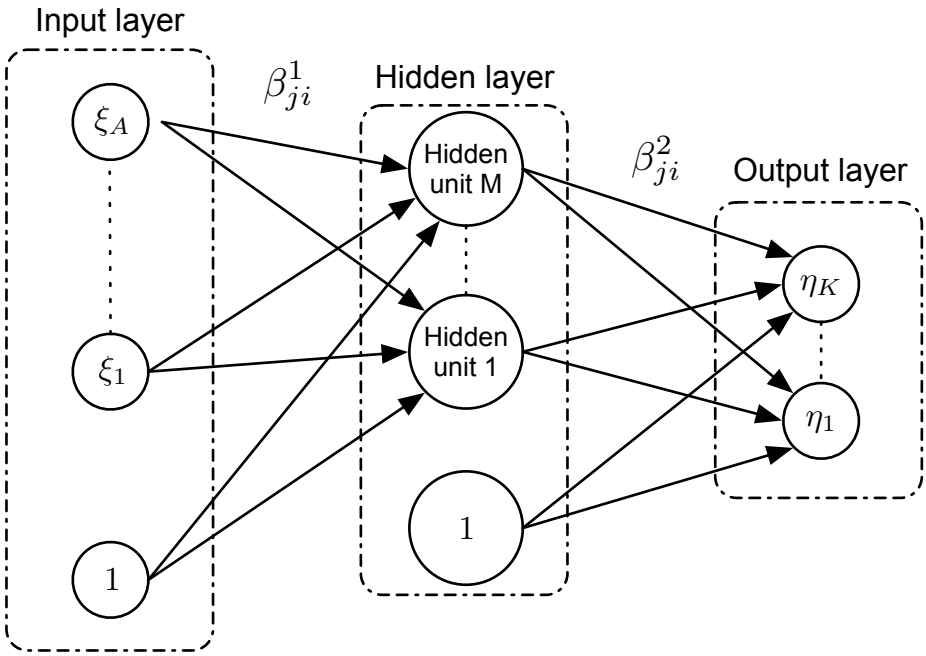

Figure 5.3: Neural network architecture.

5.3.2 Feedforward Neural Network

A feedforward neural network is a supervised method used for classification. Generally, a neural network comprises an input layer, an output layer and an arbitrary number of hidden layers. In this section and for the sake of simplicity, we will consider a three layer NN with a single hidden layer as depicted in Figure 5.3.

Let us first consider the general binary case so that $\eta_i = 0$ if $\boldsymbol{\xi}_i$ belongs to class $\mathcal{C}_0$ and $\eta_i = 1$ if $\boldsymbol{\xi}_i$ belongs to class $\mathcal{C}_1$.

In the neural network method, we assume the following probabilities of the classes given the input data [99, Sec. 5.2],

$$p(\mathcal{C}_0|\boldsymbol{\xi}) = f(\boldsymbol{\xi}) \quad \text{and} \quad p(\mathcal{C}_1|\boldsymbol{\xi}) = 1 - p(\mathcal{C}_0|\boldsymbol{\xi}), \tag{5.9}$$

where the adaptive model $f(\boldsymbol{\xi})$ is defined as,

$$f(\boldsymbol{\xi}) = \mathcal{G}\left(\sum_{j=1}^{M} \beta^2_{1j} \mathcal{G}\left(\sum_{i=1}^{A} \beta^1_{ji}\xi_i + \beta^1_{j0}\right) + \beta^2_{10}\right), \tag{5.10}$$

where A is the number of input units, M the number of hidden units, the superscript l indicates the corresponding parameters from layer l to layer $l+1$ and $\mathcal{G}(g)$ is the activation function. In this work we employ the sigmoid function $\mathcal{G}(g) = (1 + e^{-g})^{-1}$. This S-shaped

function ranges between 0 when $g \to -\infty$ and 1 when $g \to \infty$. In order to obtain the parameters that best fit the training set, we minimize the following cost function,

$$J(\mathcal{B}) = -\frac{1}{m^t} \sum_{i=1}^{m^t} \eta_i \ln\left(f(\boldsymbol{\xi}_i)\right) + (1-\eta_i) \ln\left(1 - f(\boldsymbol{\xi}_i)\right), \tag{5.11}$$

where $\mathcal{B}$ denotes the set of all β parameters. As in linear regression, a slightly modified cost function allows us to mitigate the undesired effects produced by outliers, that is,

$$\begin{aligned} J^r(\mathcal{B}) = & -\tfrac{1}{m^t} \textstyle\sum_{i=1}^{m^t} \eta_i \ln\left(f(\boldsymbol{\xi_i})\right) + (1-\eta_i) \ln\left(1 - f(\boldsymbol{\xi_i})\right) \\ & + \tfrac{\lambda}{2m^t} \textstyle\sum_{l=1}^{S-1} \sum_{i=1}^{s_l} \sum_{j=1}^{s_{l+1}} \left(\beta_{ji}^l\right)^2, \end{aligned} \tag{5.12}$$

where S is the number of layers of the neural network and s_l the number of units in the l-th layer. The learning process is also similar. We first set $\lambda = 0$ and use error backpropagation [99, Sec. 5.3] and gradient descent based methods to learn the values of $\mathcal{B}$ that best classify the data in the training set. Afterwards we use the cross-validation set to find a good value of λ and finally, the test set is used to measure the algorithm performance.

In the case of interest, we shall distinguish among $K > 2$ classes and so we have used the one-versus-all strategy [100] where the output layer of the NN has K different units. The k-th classifier estimates the probability that the current input features belong to class $\mathcal{C}_k$. Once all K probabilities are computed, the class with the highest value is chosen.

5.4 RSS Processing Block

This section details the ML algorithms employed to obtain estimations of distance and angle between the user and the anchor nodes. In order to improve the accuracy of the different estimations (distance and angle) we classify the data into groups using a ML pipeline. The block diagram of the pipeline is depicted in Figure 5.4. First, we use a neural network to predict whether the user is walking or standing. Then, we predict whether the corresponding anchor node is far ($d > 7\,\mathrm{m}$) or near ($d < 7\,\mathrm{m}$). This criterion has been selected based on the analysis of the data collected in a calibration campaign. Finally, we estimate the distance and angle between the user and the anchor node. The advantage of using the proposed ML pipeline is that the samples are classified into groups with similar statistical patterns, thus increasing the overall system accuracy. In other words, distance and angle estimations use two different sets of model parameters, respectively: one set for $d > 7\,\mathrm{m}$ and another set for $d < 7\,\mathrm{m}$.

In the following, we detail the ML methods used for the estimation of the distance and

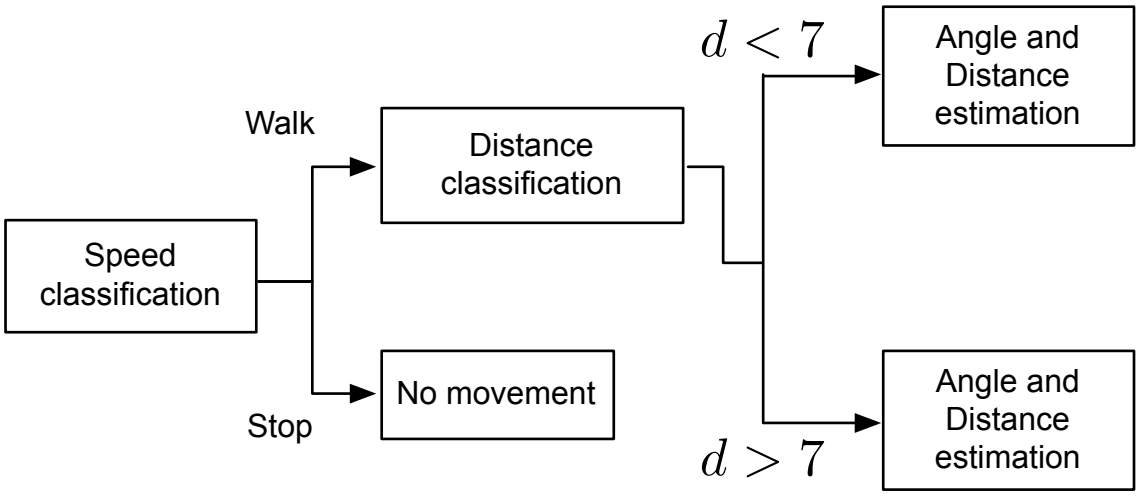

Figure 5.4: Machine Learning pipeline.

angle. All of them share the same input features $\boldsymbol{\xi}$, that is,

$$\left[\overline{RSS}_{\mathbf{s}_i \to \mathrm{Rx}_1} \quad \overline{RSS}_{\mathbf{s}_i \to \mathrm{Rx}_2} \quad \overline{RSS}_{\mathbf{s}_i \to \mathrm{Rx}_3} \quad \overline{RSS}_{\mathbf{s}_i \to \mathrm{Rx}_4} \quad \sigma^2_{\mathrm{Rx}_1} \quad \sigma^2_{\mathrm{Rx}_2} \quad \sigma^2_{\mathrm{Rx}_3} \quad \sigma^2_{\mathrm{Rx}_4}\right]^T, \quad (5.13)$$

where $\overline{RSS}_{\mathbf{s}_i \to \mathrm{Rx}_i}$ and $\sigma^2_{\mathrm{Rx}_i}$ are respectively the mean and variance of the RSS measurements received during the last position update period. In order to obtain an accurate estimation of the variance a large number of samples are necessary. This implies a large number of transmissions and therefore, the lifetime of the battery powered WSN is seriously reduced. In this work we compute the variance with only a few samples as our goal is to obtain a coarse estimation of the variance and assist the ML algorithms in the data classification process. Note that, as shown in Section 5.7, this coarse estimation suffices to obtain an accurate position estimation.

The training of ML methods can be computationally expensive, particularly in the case of NN with high number of layers and units. Notwithstanding, it can be done off-line before the installation of the positioning system. Once the parameters of the model are selected the estimation can be done with simple algebra equations with low computational complexity. Furthermore, in order to prove the generalization of the ML algorithms employed here, we have trained the parameters of the models in one scenario and applied the same parameters to all the tested scenarios.

5.4.1 Speed Classification

The first step in the ML pipeline is the speed classification. The samples of the database are divided into two groups depending on the movement of the user: *i*) standing and *ii*) walking. This division is motivated by the different statistical pattern of the RSS samples

of the two groups. In fact, the movement of the user impinges directly on the variance of the RSS measurements. Particularly, the variance of the measurements increases when the user is walking because the movement of the user as well as the oscillations of the receiver nodes (with respect to the user's body if they are not strongly fixed) favour fast fading effects and thus an increase in the variance.

The speed classification is performed using a feedforward neural network (see Section 5.3.2) with 3 layers: *i*) an input layer with 8 units (see Equation 5.13); *ii*) a single hidden layer with 10 units; and *iii*) an output layer with a single unit. In this work we use L2-regularisation with $\lambda = 1$ to avoid over-fitting (see Equation 5.12).

The output of the NN is a binary variable that tells us if the user is walking or standing. This can also be interpreted as a discrete speed estimation with two possible velocities, zero and a constant velocity value that can be specific for each user (1 m/s in our case). Note that whenever the user is standing there is no need to update the estimated trajectory. Therefore, the system stops until new measurements are available. The accuracy of the speed classification method in our test set is approximately 93%.

5.4.2 Distance Classification

Typically, the estimation of distances from RSS measurements has been done according to a path loss model. As stated in Section 5.4, in this work we use ML techniques to compute distance estimations from RSS measurements. ML techniques are more flexible as they are not restricted to the configuration of the specific parameters of a model. However, the overall performance of the ML techniques can be improved using information from a path loss model. Particularly, we use the dual slope model which considers that the slope of the RSS decay with distance will change after a critical distance. We emulate this model with ML techniques by adding a new step in the ML pipeline: distance classification. This step classifies the data into two different sets: *i*) near anchor RSS measurements ($d < 7\,\mathrm{m}$); and *ii*) far anchor RSS measurements ($d > 7\,\mathrm{m}$). The distance threshold is selected based on the data extracted on a experimental validation campaign. By applying different algorithms to each of the cases, we have confirmed in our experiments that not only distance estimations improve but also heading estimations. The reason is that the partial blockage of the line of sight by the user's body is reduced with distance [101].

The distance classification is done with a feedforward neural network that uses L2-regularisation ($\lambda = 1$) and 3 layers: *i*) an input layer with 8 units (see Equation 5.13); *ii*) a single hidden layer with 10 units; and *iii*) an output layer with a single unit.

The accuracy of the NN employed in the distance classification method is approximately

88% in our test set.

5.4.3 Distance Estimation

Contrary to other typical indoor positioning systems in the literature, in this work we estimate the distance from the RSS measurements using a ML algorithm instead of using the typical log-distance path loss model [8]. The reason is that this model is developed for the single receiver case and does not take into account the scenario proposed in this work where the user carries multiple receivers on the body. Note that it is not straightforward to adapt the log-distance path loss model to the multiple receiver case as each receiver will need a specific function for modelling the attenuation depending on its position on the user's body.

During the estimation process, we first classify the data samples by the speed of the user (walk or stop) and by the distance to the anchor node ($d < 7\,\text{m}$ or $d > 7\,\text{m}$). Then, we use a linear regression method (see Section 5.3.1) to obtain the distance estimation. The cost function used to obtain the parameters $\boldsymbol{\beta}$ can be found in (5.8) and the regularisation parameter is set to $\lambda = 1$.

The mean squared error (MSE) of the distance estimations evaluated in the test set is 0.7 for the case $d < 7\,\text{m}$ and 4 otherwise. Note that the maximum distance in the test set is approximately 17 m.

5.4.4 Angle Estimation

Let us define the angle between the user and the anchor node ϕ as the angle between two vectors: *i*) the direction vector of the user $\vec{u} = \begin{bmatrix} u_x & u_y \end{bmatrix}$ and *ii*) the vector formed by the user's and anchor's position $\vec{ms} = \begin{bmatrix} ms_x & ms_y \end{bmatrix}$. Figure 5.5 shows the definition of the vectors and angles employed in this section.

In order to find the angle ϕ we exploit the effect of the body attenuation on the wireless signals. As the receiver nodes are distributed around the body, each one of them will be affected differently and therefore it will suffer from a different attenuation. Indeed, our experiments show that this pattern is stronger when the user is close to the anchor node and vanishes with distance. This fact allows us to estimate the angle ϕ from the RSS of the set of receiver nodes $\mathcal{R}$. Again, the estimation of the angle is done using a NN and two different models are trained, one for short distances ($d < 7\,\text{m}$) and another one for large distances ($d > 7\,\text{m}$). Although the estimation of angle is a regression problem, as the angle is a continuous variable, we estimate here the angle as a classification problem by

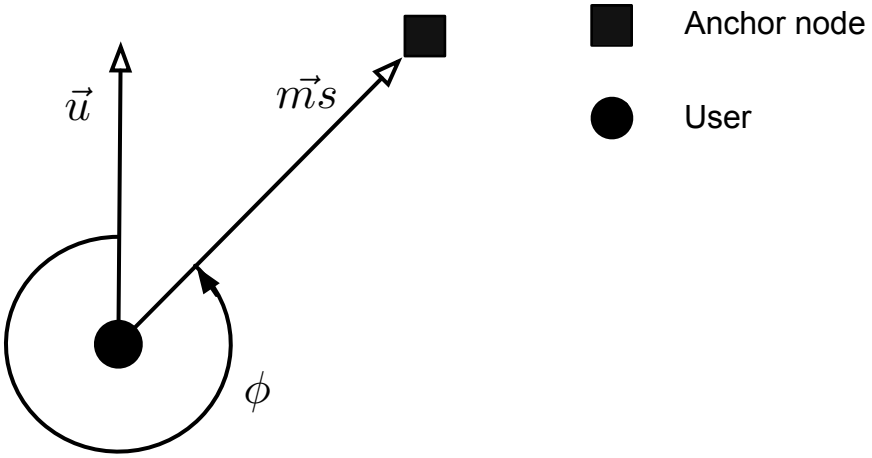

Figure 5.5: Angle between an anchor node and the user.

dividing all the possible angles into four categories with mean angles 0º, 90º, 180º and 270º. Note that due to the characteristics of indoor scenarios, it is reasonable to assume that the user will usually walk following straight trajectories with turns of 90 degrees and therefore this classification suffices to enhance the position estimation of the user as shown in Section 5.7.

In this case, the feedforward neural network employed is a three layer network with 8 units in the input layer, 30 units in the hidden layer and $K = 4$ units in the output layer. The regularisation parameter is set to 1. The accuracy obtained using the test set is approximately 75% for the close anchor node case and 62% for the far anchor node case.

5.5 Measurements Block

In this section the algorithms used to convert the estimations of distance and angle into estimations of position and heading are described.

5.5.1 Position Computation

The position of the mobile node is computed using a weighted least squares algorithm as in Chapter 4. The WLS combines all the distance estimations available in a positioning update period in order to minimize the overall squared error of the distance measurements. In other words, the position of the mobile node is computed as the solution to the following

minimization problem,

$$\min_{\hat{\mathbf{m}}_k} J = \sum_{i \in \mathcal{D}} \omega_i \left(\hat{d}_i - \|\mathbf{s}_i - \hat{\mathbf{m}}_k\| \right)^2, \tag{5.14}$$

where $\mathcal{D}$ is the set of distance measurements obtained in Section 5.4.3 [86] and ω_i are the weights of the algorithm. Note that we have different distance estimations due to the classification procedure of the ML pipeline. Therefore, the accuracy of the distance estimations is different depending on the classification and hence, it is meaningful to assign different weights to estimations with different accuracies [102]. We fix the different weights to be the inverse of the MSE obtained in Section 5.4.3. The problem in (5.14) can be solved in an iterative way following a gradient descent approach [85],

$$\hat{\mathbf{m}}_{k,(l)} = \hat{\mathbf{m}}_{k,(l-1)} + \delta_{(l)} \sum_{i \in \mathcal{D}} \omega_i (\hat{d}_i - \|\hat{\mathbf{s}}_i - \hat{\mathbf{m}}_{k,(l-1)}\|) \tilde{q}_{i,(l-1)}, \tag{5.15}$$

where l is the iteration index, $0 < \delta_{(l)} \ll 1$ is the step size, and $\tilde{q}_{i,(l-1)}$ is a unitary vector,

$$\tilde{q}_{i,(l-1)} = \frac{\left(\hat{\mathbf{s}}_i - \hat{\mathbf{m}}_{k,(l-1)}\right)}{\|\hat{\mathbf{s}}_i - \hat{\mathbf{m}}_{k,(l-1)}\|}. \tag{5.16}$$

5.5.2 Heading Computation

This section computes the heading of the user from the angle estimations in Section 5.4.4 and the position estimation in Section 5.5.1. The heading of the user θ is defined as the angle between the y axis of the cartesian coordinate system and the vector $\vec{u}$. Figure 5.6 shows the angles employed in the calculation of the heading of the user.

In order to obtain the heading we first compute the angle between the y axis and the vector $\vec{ms} = \begin{bmatrix} ms_x & ms_y \end{bmatrix}^T$, that is,

$$\psi_i = \begin{cases} \nu_i \ if \ ms_x \leq 0 \\ 2\pi - \nu_i \ if \ ms_x > 0 \end{cases}, \tag{5.17}$$

where the subscript i denotes the i-th anchor node and ν_i is defined as

$$\nu_i = \arccos \frac{\vec{y} \cdot \vec{ms}}{\|\vec{y}\| \|\vec{ms}\|}, \tag{5.18}$$

being $\vec{y} = \begin{bmatrix} 0 & 1 \end{bmatrix}^T$. Then, we obtain the heading of the user as

$$\hat{\theta}_i = \psi_i - \phi_i. \tag{5.19}$$

Note that the position of the user is unknown, therefore we will use the estimated position $\hat{\mathbf{m}}_k$ instead. Note also that we obtain a different heading estimation for each one of the anchor nodes. Therefore, we compute the average of the estimations in order to obtain the definitive heading estimation $\hat{\theta}_k$.

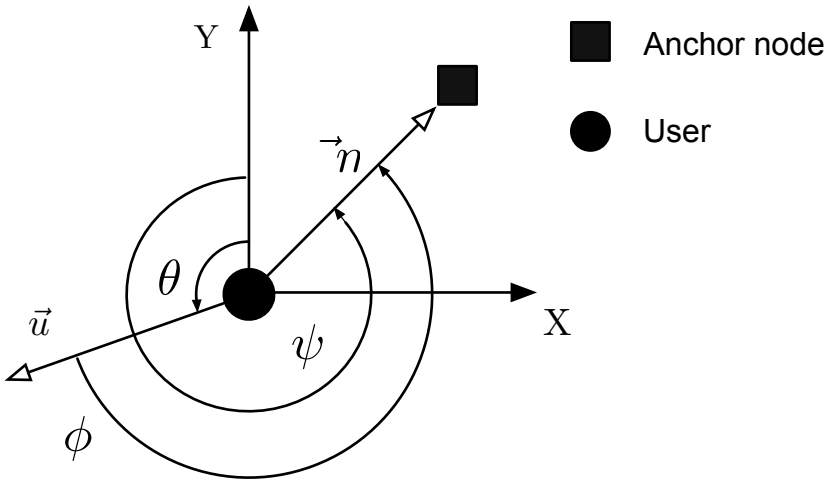

Figure 5.6: Heading of the user.

5.6 Filtering Block

The last step in our system architecture is the Filtering Block. This step combines the estimations of the previous blocks (that is, position, speed and heading) into a single filter that outputs an enhanced estimation of the position of the user. In this chapter, we also employed the EKF as in Chapter 4.

Let us model again the state of a person in a two dimensional space by means of its position and speed,

$$\mathbf{x}_k = \begin{bmatrix} x_k & y_k & v_k & \theta_k \end{bmatrix}^T, \tag{5.20}$$

where x_k, y_k represent the position in Cartesian coordinates, v_k is the speed and θ_k the heading. The movement of the person is defined as a discrete-time dynamic system,

$$\mathbf{x}_k = f_{k-1}\left(\mathbf{x}_{k-1}\right) + \mathbf{v}_{k-1}, \tag{5.21}$$

where $f_{k-1}\left(\mathbf{x}_{k-1}\right)$ is the state model function and $\mathbf{v}_{k-1}$ is a zero mean Gaussian noise with covariance matrix $\mathbf{Q}$. The state model employed is the same as in Chapter 4, which is a modification of the constant velocity model that takes into account that the velocity is represented in polar coordinates, that is,

$$f_{k-1}\left(\mathbf{x}_{k-1}\right) = \begin{bmatrix} 1 & 0 & T\cos\theta_{k-1} & 0 \\ 0 & 1 & T\sin\theta_{k-1} & 0 \\ 0 & 0 & 1 & 0 \\ 0 & 0 & 0 & 1 \end{bmatrix} \mathbf{x}_{k-1}, \tag{5.22}$$

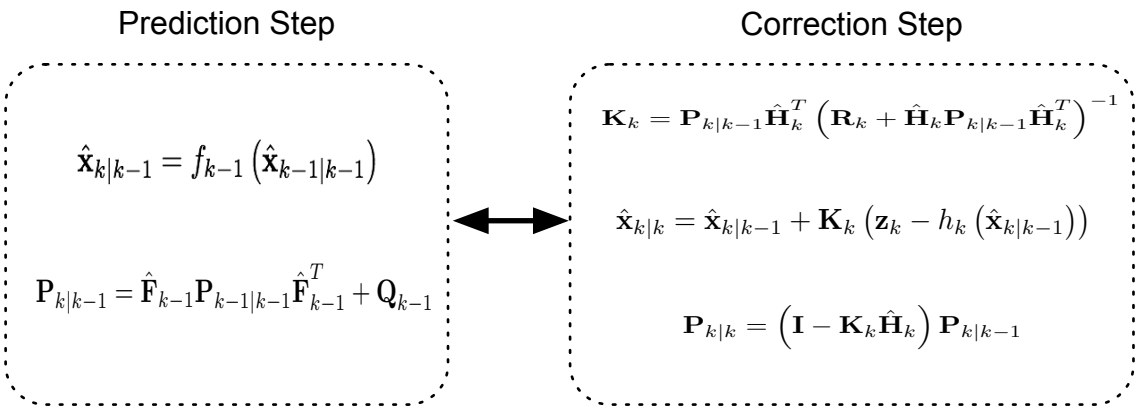

Figure 5.7: Equations of the Extended Kalman Filter.

where T is the time period between measurements and the Jacobian matrix of the model function is given as,

$$\hat{\mathbf{F}}_{k-1} = \begin{bmatrix} 1 & 0 & T\cos(\theta^k) & -T\sin(\theta^k)v^k \\ 0 & 1 & T\sin(\theta^k) & T\cos(\theta^k)v^k \\ 0 & 0 & 1 & 0 \\ 0 & 0 & 0 & 1 \end{bmatrix}. \tag{5.23}$$

The equations of the EKF used for the estimation of the user's position are depicted in Figure 5.7. The filter combines the position and heading measurements taking into account the kinematic model of the user's movement. In particular, covariance matrices $\mathbf{Q}$ and $\mathbf{R}$ (of the state vector and noise, respectively) are the parameters to adjust. In this work we assume that the state variables and measurement variables are independent and therefore we configure their covariance matrices as diagonal matrices. The values of the variances are manually configured based on our experimental results. The specific values used are

$$\mathbf{Q} = diag(\begin{bmatrix} 5 & 5 & 0.5 & 0.5 \end{bmatrix}), \tag{5.24}$$

$$\mathbf{R} = diag(\begin{bmatrix} 1 & 1 & 0.1 & 0.5 \end{bmatrix}). \tag{5.25}$$

Note that we could have used here a similar configuration method as the ones described in Chapter 4. However, the employment of such techniques will difficult the validation of the designed systems as it will be difficult to know if the improvements of the system are due to the proposed multiple receiver architecture or due to the configuration methods. Furthermore, the methods employed in Chapter 4 are designed for a single receiver architecture and its adaptation to the multiple receiver architecture is not straightforward. For these reasons, we decided here to manually configure the EKF and we leave the adaptation of the configuration methods to the multiple receiver architecture as a future

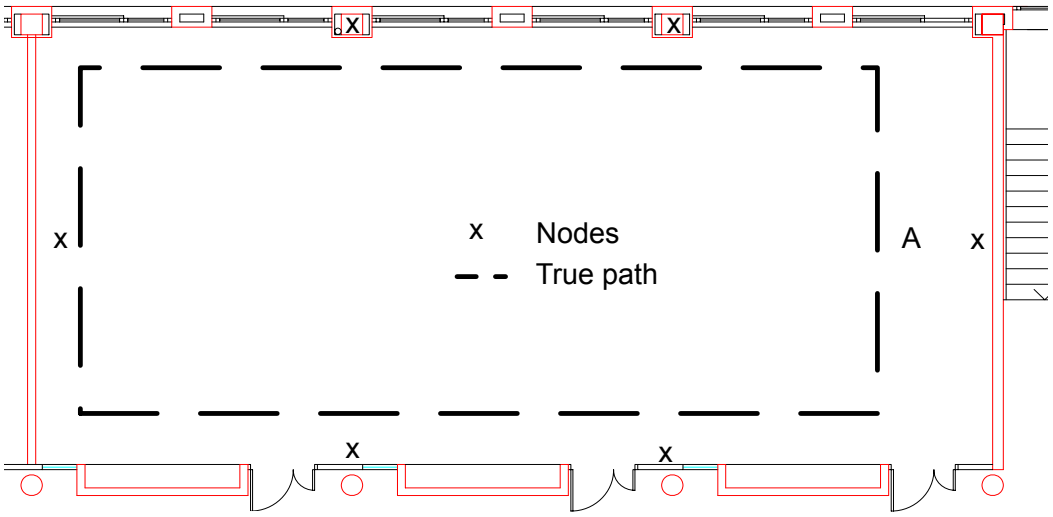

Figure 5.8: Scenario 1-A.

line of work (see Section 7.2). The following section validates the performance of the designed pedestrian tracking system in a real environment.

5.7 Experimental Validation

In the experimental validation, we test the performance of the system using the Z1 motes from Zolertia [103], equipped with the MSP430 microcontroller [104] and the CC2420 radio chip [105].

The anchor nodes are configured to broadcast a packet every 250 ms. The on-body receivers send a packet every second with the mean and variance of the RSS received since the previous transmission. This packet is received by an extra mote acting as a gateway. It sends the data to the computer, where it is finally stored.

In order to evaluate the performance of the proposed technique, we have tested the system in three different scenarios. The first scenario is a big classroom of 154.8 m^2 (8.6 m x 18 m). We have distributed 6 anchor nodes, that is, a node every 25.8 m^2. In this scenario we have tested two different trajectories. On the one hand, Trajectory 1 is a rectangular path with a length of 44 m (see Figure 5.8). On the other hand, Trajectory 2 has an 8-shape and a length of 74.4 m (see Figure 5.9). Note that we include a stop in the path, in both trajectories, in order to test the response of the system to an abrupt change of the user's speed (the place of the stop is marked with the letter A in the figures). In the following, these trajectories are referred to as Scenario 1-A and Scenario 1-B.

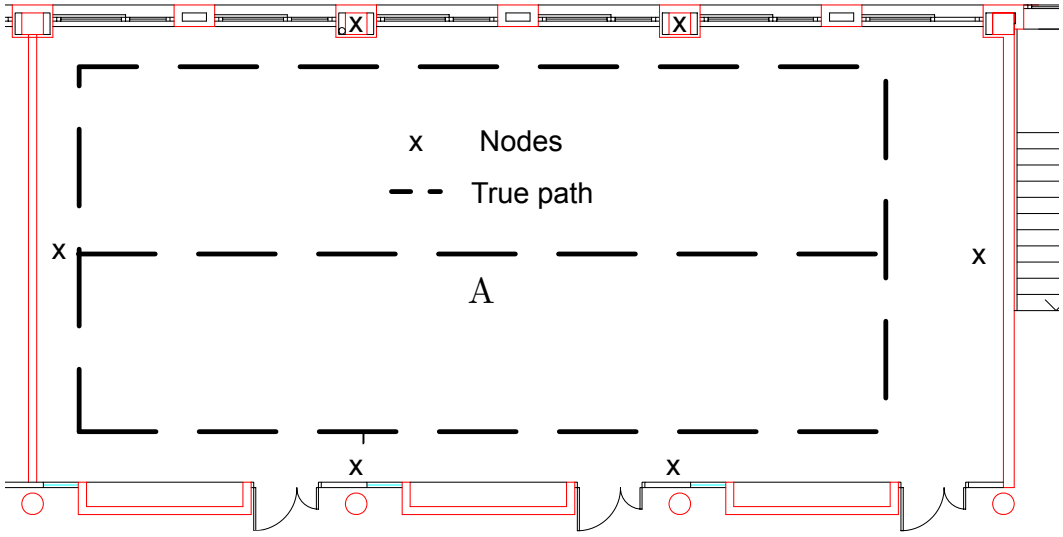

Figure 5.9: Scenario 1-B.

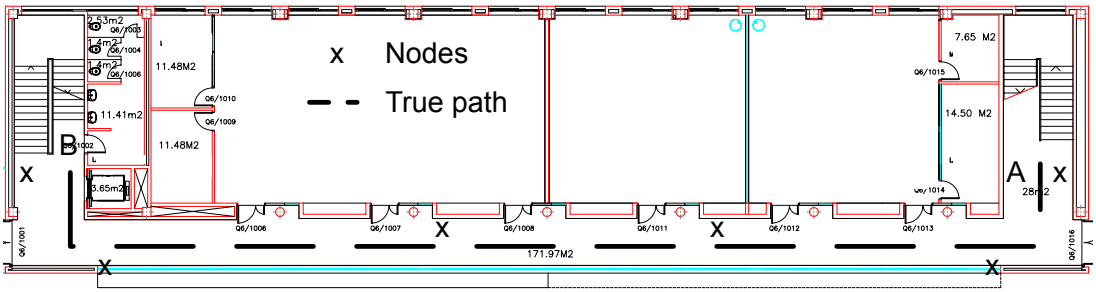

Figure 5.10: Scenario 2.

The second scenario is a long corridor inside a large building. It has an area of 533.12 m^2 (11.2 × 47.6 meters) and it is also covered with 6 motes (a node every 88.8 m^2). The scenario is shown in Figure 5.10. The path starts at point A and goes to B before going back to A. During the path the user stops every time it reaches the points A or B.

The third scenario is a house. It has an area of approximately 100 m^2 and it is also covered with 6 motes (a node every 16.6 m^2). The mobile node goes back and forth between points A and B following the depicted trajectory (Figure 5.11). At both points A and B, the user stops for a while.

Common to the three scenarios are the user's speed and the duration of the stops. The user walks at pedestrian speed (around 1 m/s) and the duration of the stops is randomly selected by the user, typically with a duration between 10 and 30 seconds.

In order to show the behavior of the designed system during the experimental validation we compare four different methods:

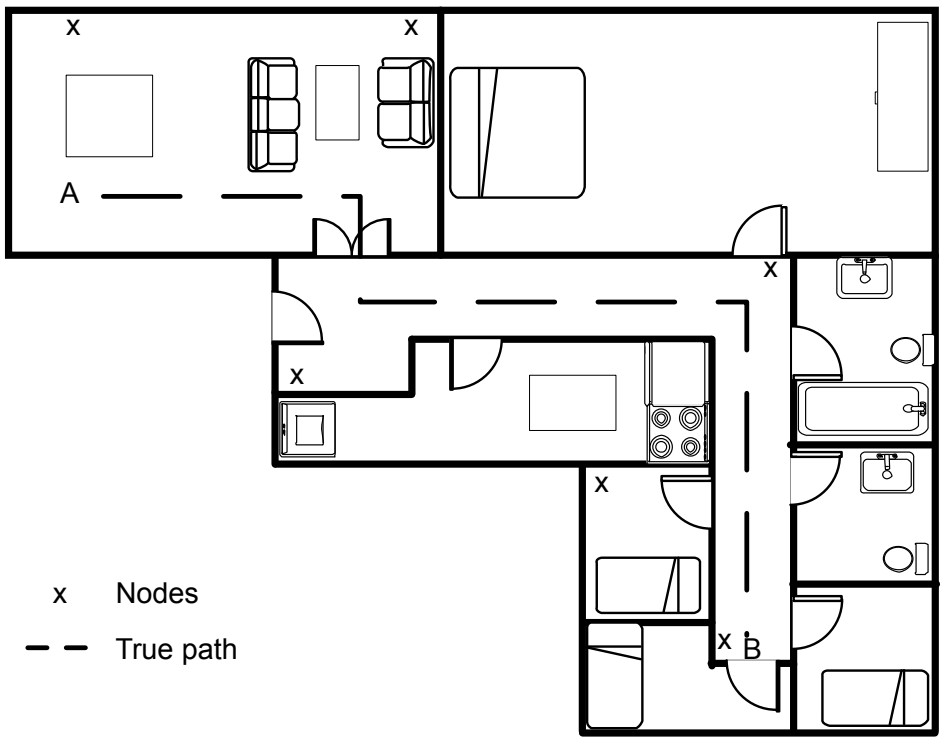

Figure 5.11: Scenario 3.

- **WLS-ML:** a WLS based on the distance obtained using linear regression (see Section 5.4.3).
- **EKF-ML-I:** an EKF based on the position estimations of the previous WLS and the binary speed estimation (see Section 5.4.1).
- **EKF-ML-II:** the designed system, an EKF with position, speed and heading estimations obtained using a NN (see Section 5.4.4 and 5.5.2).
- **LS-1RX:** a baseline method with a LS based on the RSS of only one receiver.

Note that the different ML algorithms are trained with data from Scenario 1-B and applied to all the scenarios. The aim is to evaluate how dependent on the particular scenario our method is. For this reason we have selected three different scenarios with very different densities of anchor nodes (from one node every 16.6 m^2 to one node every 88.8 m^2) and different structures (a classroom, a long corridor and a flat).

For the purpose of evaluating the positioning accuracy of the designed systems, each trajectory has been repeated several times and the results shown in this section are the average of all the experimental tests performed.

Table 5.1: Results of the experimental validation in terms of RMSE

	LS-1RX	WLS-ML	EKF-ML-I	EKF-ML-II
Scenario 1-A	3.66	1.4	1.37	1.14
Scenario 1-B	2.29	1.23	0.95	0.82
Scenario 2	8.15	1.83	1.70	1.57
Scenario 3	5.14	1.60	1.20	1.13

Table 5.1 shows the results obtained during the experimental validation in terms of the RMSE. Results show the outstanding improvement in the positioning accuracy of the multiple receivers case (WLS-ML) in comparison with the single receiver case (LS-1RX). Furthermore, the combination of position and speed measurements by means of an EKF (EKF-ML-I) results in improvements between 4% and 24% regarding positioning accuracy. Finally, if we also include the heading measurements to the EKF (EKF-ML-II) the positioning accuracy is improved between 18% and 32%.

Let us now compare the performance of the methods in terms of the CDF. In order to compare the positioning systems using the CDF we will consider the value of the RMSE when the CDF equals 0.9. This means that the error committed by the algorithm is below this threshold value in 90% of the cases. Table 5.2 summarizes 90% percentile of the validated systems and scenarios. Note the overall high accuracy achieved in the different scenarios. The errors committed are below 2.08 m for scenarios 1-A, 1-B and 3 (areas of approximately 100 m^2) and 3.04 m for Scenario 2 (area of 533.12 m^2).

Table 5.2: Results of the experimental validations in terms of 90% percentile

	LS-1RX	WLS-ML	EKF-ML-I	EKF-ML-II
Scenario 1-A	4.96	2.50	2.15	2.08
Scenario 1-B	4.66	2.15	1.87	1.48
Scenario 2	13.18	3.24	3.16	3.04
Scenario 3	7.30	2.26	1.70	1.53

The experimental validation shows that the positioning accuracy of the proposed system with multiple receivers on the body clearly outperforms the accuracy of a single receiver system. In addition, the system is able to compute the heading of the user from the RSS measurements, and thanks to the EKF the system accuracy experiments

an average increase of 25% in the scenarios tested. Furthermore, the system has been validated in different types of scenarios using the same model parameters, which proves the generalization of the estimations performed using the proposed ML techniques.

Finally, note that the designed system achieves positioning accuracies similar to other systems in the literature based on inertial sensors [29, 32, 60, 106] and that the main drawbacks of these techniques, generally related to the drift of the inertial sensors in the long term, are circumvented thanks to the multiple receiver architecture.

5.8 Conclusions

In this chapter we developed a pedestrian tracking system for indoor scenarios. It is designed to work only with the RSS measurements of a set of anchor nodes from a WSN. The main novelty in our method is the placement of multiple receivers on the user's body. In this way, distance estimations are improved as expected but, more important, the angle between the user and the anchor nodes can now be estimated. The angle estimation is possible due to the attenuation effect of the human body in the wireless signals. Moreover, the estimations are performed with low computational complexity thanks to the application of two ML techniques: *i*) linear regression; and *ii*) neural networks. Afterwards, distance and angle estimations are processed in order to obtain preliminary estimations of the position and heading of the user, which are finally refined with an EKF using a constant velocity kinematic model.

Contrarily to most of the pedestrian tracking systems in the literature, the designed system avoids the use of inertial sensors and, accordingly, does not suffer from temporal drifts and hence its positioning accuracy is time invariant. The system has been experimentally validated in different scenarios including a flat, a university classroom and a long corridor achieving in all cases a positioning accuracy around 1 meter.

Chapter 6

Pedestrian Tracking System for Smartphones and Smartwatches

The popularization of smartphones and smartwatches is an interesting opportunity for reducing the infrastructure cost of the positioning systems and at the same time facilitates the adaptation of IPS to mass market applications. Nowadays, smartphones include inertial sensors that can be used in pedestrian dead reckoning algorithms for the estimation of the user's position. Both smartphones and smartwatches include WiFi capabilities allowing the computation of the received signal strength. Therefore, it is possible to design RSS-IMU hybrid systems for current commercial smartphones. In this chapter we extend the multiple receiver scheme to the smartphone and smartwatch case. That is, we combine the estimation of the speed and heading of the user obtained form the inertial sensors embedded in the smartphone with the RSS measurements of both, the smartphone and the smartwatch. The result is an IPS that can be installed in commercial smartphones and smartwatches and so it can be employed for mass market applications.

6.1 Introduction

This chapter describes the design of an indoor positioning system for smartphones and smartwatches that combines the RSS measurements of a multiple receiver architecture with inertial measurements. The system is designed with the aim of being applied in mass market applications so it has to take into account that it will be installed in buildings where the configuration of the WiFI network is fixed. To do so, we analyze the implications of using a WiFi network designed for communication purposes in an indoor positioning system when the designer cannot control the network configuration. The main disadvantages are detailed and in consequence, a new method for the combination of RSS measurements

is designed. Then, we design a hybrid positioning system by combining the RSS based position estimations with a pocket navigation system based on the measurements of a low cost IMU embedded in a smartphone placed in the pocket of the user. Finally, the proposed system is experimentally tested employing commercial smartphones.

The main contributions of this chapter follow:

- The design of an indoor positioning system based on inertial measurements and the combination of RSS measurements from different sources (a smartphone and a smartwatch) using a GMM algorithm that improves the accuracy of the distance estimations.
- The identification and evaluation of the network deployment and network management issues produced by the lack of control over the WiFi network that negatively affect the performance of positioning systems.
- The experimental validation of the designed positioning system in a real scenario of $6000\,\mathrm{m}^2$ without any control over the network and using commercial smartphones.

The rest of this chapter is organized as follows: Section 6.2 introduces the architecture of the system. Section 6.3 details the algorithms employed to obtain the speed and the heading of the user from the inertial measurements. In Section 6.4, we describe the method used for computing the position estimation from the RSS measurements. The combination of inertial and RSS measurements is explained in Section 6.5, and Section 6.6 presents the experimental validation. Finally, the conclusions of the work are presented in Section 6.7.

6.2 System Architecture

Let us consider an arbitrary indoor area with a WiFi network formed by N anchor nodes with known positions,

$$\mathbf{s}_i = \begin{bmatrix} x & y \end{bmatrix}^T, \tag{6.1}$$

where x, y are the respective Cartesian coordinates and $i = 1, ..., N$ is the index. Lets also consider a pedestrian user freely moving around the area with unknown position defined by:

$$\mathbf{m}_k = \begin{bmatrix} x_k & y_k \end{bmatrix}^T, \tag{6.2}$$

where k stands for the k-th time instant. The user carries a smartphone in the pocket that includes a 3-axis accelerometer and a 3-axis gyroscope. These sensors are sampled several times at every time instant k obtaining the vectors of measurements from the

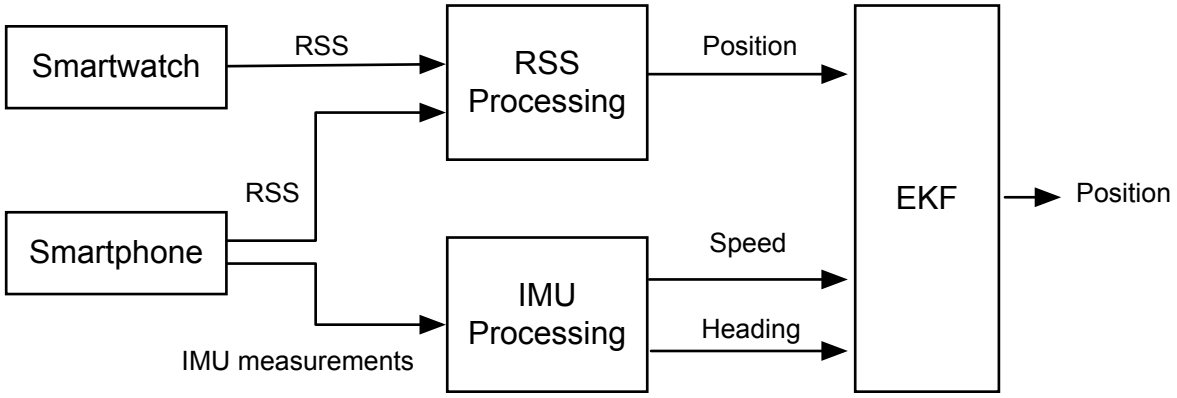

Figure 6.1: System architecture.

accelerometer $\mathbf{a}_{x,k}$, $\mathbf{a}_{y,k}$, $\mathbf{a}_{z,k}$ and gyroscope $\mathbf{c}_{x,k}$, $\mathbf{c}_{y,k}$, $\mathbf{c}_{z,k}$. The subscripts x, y, z denote the respective sensor measurement axis. The smartphone periodically scans the WiFi channels every second and provides a set of measurements of the RSS from the anchor nodes, that is,

$$\mathcal{R}_p = \{\mathrm{Rx}_1, \mathrm{Rx}_2, ..., \mathrm{Rx}_N\}. \tag{6.3}$$

We also consider that the user wears a smartwatch, which scans the WiFi channels every second and provides a set of RSS measurements, that is,

$$\mathcal{R}_w = \{\mathrm{Rx}_1, \mathrm{Rx}_2, ..., \mathrm{Rx}_N\}. \tag{6.4}$$

In this chapter, we combine all of the measurements provided by the smartphone and the smartwatch to compute an enhanced estimation of the user's position. The architecture of the system (see Figure 6.1) is divided into three blocks: *i*) the IMU processing block; *ii*) the RSS processing block; and *iii*) the filtering block. In the first block, we obtain the speed and heading of the user using the IMU readings of the smartphone. In the second block, the RSS measurements received by the smartphone and the smartwatch are combined and processed to obtain estimations of the user's position. Finally, in the third block, the estimations obtained in the first two blocks are combined using an EKF that takes into account a constant velocity model as in Chapter 4 and Chapter 5.

6.3 IMU Processing Block

The IMU processing block estimates the user's speed and heading from the measurements of the inertial sensors embedded in the smartphone. This is done in two steps as indicated

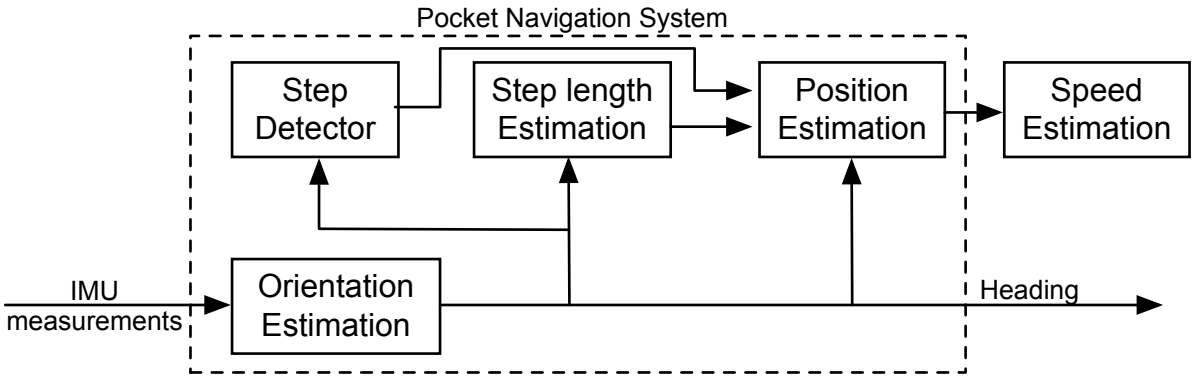

Figure 6.2: IMU processing block.

in Figure 6.2. In the first step, the pocket navigation system uses the inertial measurements to estimate the user's position and orientation defined by the Euler angles, i.e., roll, pitch and yaw, also known as heading. In the second step, the position estimate is used to derive the speed of the user. The two parts of the inertial measurements' processing are presented in the next sections.

Note that the pocket navigation system is based on the inertial measurements of a low cost IMU embedded in a commercial smartphone running an Android OS. The smartphone is configured to provide measurements at a rate of 100 Hz. Unfortunately, the rate obtained is not exactly 100 Hz, and it will vary depending on the amount of processes running at the same time on the smartphone. This behavior impinges directly on the performance of the PDR algorithms because the design measurement rate does not always match the operational measurement rate. Moreover, they have to cope with the typical large bias of the low cost IMU embedded in commercial smartphones.

6.3.1 Pocket Navigation System

This section describes the pocket navigation system employed here, which is presented in detail in [23] and the references therein. This system estimates the user's position using inertial measurements collected with a smartphone placed in the user's pocket.

The position is estimated through the step and heading approach. This recursive method estimates the position as follows:

$$x_k = x_{k-1} + l_{step_k} \times \cos(\theta_k), \tag{6.5}$$

$$y_k = y_{k-1} + l_{step_k} \times \sin(\theta_k), \tag{6.6}$$

where (x_k, y_k) is the x-y position of the user at time k, (x_{k-1}, y_{k-1}) is the x-y position of the user at the previous time $k-1$, l_{step_k} is the step length at time k and θ_k is the heading estimate at time k.

The block diagram of the pocket navigation system is presented in the dashed box in Figure 6.2. The first subsystem is the orientation estimator. It uses turn rate and acceleration measurements to estimate the Euler angles, i.e., roll, pitch and heading, of the user's thigh.

The orientation estimation subsystem implements an unscented Kalman filter whose states are the Euler angles and the biases of the gyroscopes. The prediction stage of the filter integrates the turn rate measurements to obtain the Euler angles, whereas the biases are estimated with an auto-regressive model. The update stage of the filter corrects the orientation using the acceleration measurements. Further details can be found in [107].

The pitch and the heading of the orientation estimation block are used in the next stages of the pocket navigation system. On the one hand, the heading is used for the position estimation as indicated by Equations 6.5 and 6.6. On the other hand, the pitch is used to detect step occurrences and estimate the step lengths, a method that was first proposed in [108]. For completeness, a brief overview is provided below.

The left diagram of Figure 6.3 presents the maximum and the minimum elongation of the thigh during the walk. These are indicated by ρ_{max} and ρ_{min}, respectively. Let us consider that the smartphone is on the thigh of the leg in red depicted in Figure 6.3. The maximum elongation corresponds to one step of the leg with the IMU, in this case, the leg with the smartphone. Thus, by detecting the maximums of the thigh pitch, step occurrences can be reliably detected [23]. Figure 6.3 also shows the evolution of the thigh pitch during eight steps.

Once a step is detected, its length needs to be estimated. The step length is estimated through the amplitude of the thigh pitch ($\Delta\rho$). The latter is defined as the difference between the maximum and minimum elongation of the thigh with the smartphone; see Figure 6.3:

$$\Delta\rho = \rho_{max} - \rho_{min}, \tag{6.7}$$

The authors in [108] show that the relationship between the step length (l_{step}) and the amplitude of the thigh pitch ($\Delta\rho$) can be represented by a first order model:

$$l_{step} = a \times \Delta\rho + b, \tag{6.8}$$

where a and b are the parameters of the model that can be universal or can be estimated for each user.

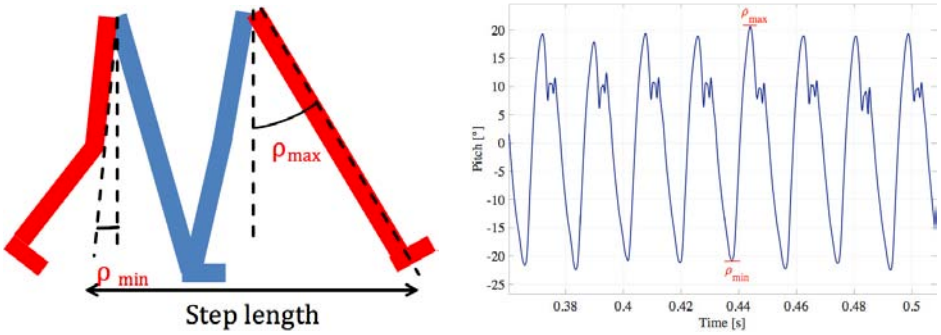

Figure 6.3: (**Left**) Maximum and minimum elongation of the red leg while walking; (**right**) Thigh pitch while walking. Each step can be detected by detecting each maximum of the pitch angle estimation (blue curve).

By successively detecting maximums and minimums of the thigh pitch, not only steps can detected but also the step length can be estimated. This in combination with the heading estimated in the attitude estimation block, allows for a tracking of the user's position.

6.3.2 Speed Estimation

The EKF of Figure 6.1 requires an estimation of the user's speed. The latter is obtained by deriving the position estimate of the pocket navigation system in Figure 6.2.

This is done as follows:

$$v_k = \frac{\mathbf{p}_k - \mathbf{p}_{k-1}}{\Delta k}, \tag{6.9}$$

where v_k is the velocity at time k, $\mathbf{p}_k$ and $\mathbf{p}_{k-1}$ are the position estimates at times k and $k-1$, respectively, andΔ k is the time increment between the position samples $\mathbf{p}_k$ and $\mathbf{p}_{k-1}$. The time increment, Δk, is calculated using the sampling time of each position estimate produced by the pocket navigation system. Then, we convert the speed to polar coordinates because the EKF uses a constant velocity model expressed in polar coordinates.

6.4 RSS Processing Block

This section details the algorithms employed to obtain position estimations from the RSS measurements. As stated in Section 2.1.1 the position estimation is divided into two steps. First, the RSS is computed from an existing wireless network and transformed to distance estimations following a path loss model. Afterwards, the distance estimations are combined through a multilateration method to obtain the position estimation. The

network selection is crucial for the design of an indoor positioning system. Among all possible network technologies that provide RSS measurements (WiFi, LTE, UWB, WSN, Bluetooth, etc.), we choose the WiFi technology because it has an outstanding advantage among all of the others: WiFi networks are currently deployed around the world in millions of buildings. Moreover, almost all the nowadays commercial smartphones include a WiFi transceiver. Therefore, our system can be used in mass market applications without investing in the network infrastructure. Unfortunately, WiFi networks are typically designed for communications and not for positioning applications. This fact generates some issues that must be amended in order to minimize the error of the positioning system. These issues can be divided into two groups: *i*) network deployment issues; and *ii*) network management issues.

6.4.1 Network Deployment Issues

The design of the network deployment for communication purposes tries to maximize the coverage area of the network with the minimum possible number of nodes. There are some constraints that can be applied to the minimization as for example to assure a minimum QoS for the network in all the area. These constraints can increase the number of anchor nodes, but generally, network designers are reluctant to increase the number of nodes as this increases the cost of the network infrastructure. This main design objective is contrary to the interest of positioning systems. The main issues follow:

- **Reception from at least three anchor nodes:** it is necessary to receive from at least three anchor nodes in order to obtain a 2D position estimation. Due to the low density of anchor nodes, there will be areas where the user will not receive from three of them. Note that this issue is magnified when the user only receives measurements from one anchor node.

- **Distance to anchors:** the mean distance between any anchor node and the mobile user is inversely proportional to the number of nodes. In combination with larger estimation errors at longer distances (see Section 4.3.1), the mean distance will affect the accuracy of the position estimations.

- **Collinearity of anchor nodes:** collinear anchors produce higher position estimation errors. The deployment of the nodes in a communication network does not take into account the collinearity of the nodes. Disregarding this issue will impinge on the performance of the positioning system.

6.4.2 Network Management Issues

The management of a communication network can respond to many different objectives, so it is difficult to analyze them in general. Notwithstanding, there are several configuration issues that can affect the performance of a positioning system:

- **Transmitted power:** beyond the obvious relationship between distance and RSS, which is directly related to the transmitted power, the transmitted power also affects the coverage area of the anchor nodes, which can lead to the issues commented in the network deployment section (reception from at least three anchor nodes and distance to anchors).
- **WiFi channel:** without controlling the network, the user is unaware of the transmission channel of the anchor nodes. Therefore, it has to scan all of the frequency channels in order to obtain the RSS, which increases the measurement time and reduces the number of measurements. Note that a reduction in the number of measurements means a reduction in the number of different anchor nodes received simultaneously.
- **Beacon period of anchor nodes:** anchor nodes periodically send beacon signals, which are used to estimate the RSS. The periodicity of these signals affects directly the performance of the positioning system, as it determines the number of RSS estimations available for the user.
- **Synchronization between anchor nodes:** the synchronization between the anchor nodes is critical if we want to obtain at least three simultaneous RSS readings in order to compute a 2D position estimation.

The above issues can appear alone or in groups in an indoor positioning system. These issues are not commonly treated in the literature, as total control of the network is typically assumed. They are amended in the network configuration and design phase. However, without controlling the WiFi network, new ways of designing indoor positioning systems have to be considered. In this chapter, we consider the introduction of a secondary receiver that ameliorates these issues. Focusing on mass market applications, we consider a smartwatch as the second receiver. These devices are nowadays increasing in popularity among consumers, and it is expected that they will be widely used in the near future.

The benefits of using a smartwatch as a secondary receiver in our system are mainly two: *i*) an improvement in the accuracy of the distance estimations; and *ii*) an increase in the number of measurements. On the one hand, the improvement in the accuracy of the

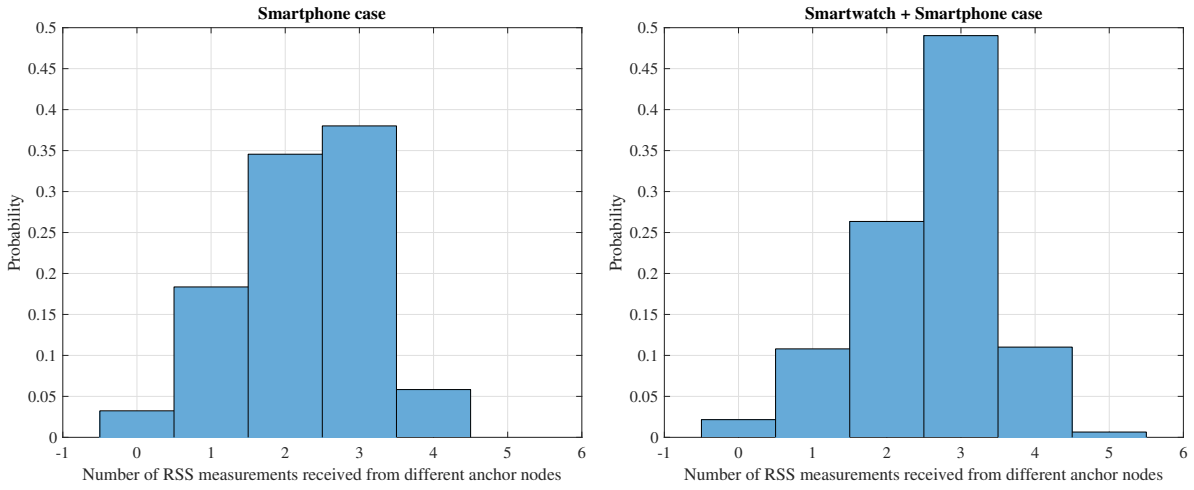

(a) (b)

Figure 6.4: Normalized histograms of the number of RSS measurements received from different anchor nodes at each time instant: (**a**) case of only using the smartphone for the measurements (**b**) case of using the smartphone and the smartwatch.

distance estimations is achieved thanks to the combination of the RSS measurements from multiple devices. By combining the RSS of two sources, the variability of the measurements is reduced. Note that we can consider noise in both measurements to be statistically independent. Therefore, the accuracy of the distance estimation is increased. On the other hand, the increase in the number of measurements is produced by the fact that we have two devices independently scanning the WiFi channels, and therefore, the odds of receiving more measurements are increased.

Figure 6.4 shows the normalized histogram of the number of RSS measurements from different anchor nodes received by the system at each time instant. In Case A, only the smartphone is used to obtain the measurements, and in Case B, the smartphone and smartwatch measurements are used. An increase of the number of times that the system has received from three or more different anchor nodes can be observed, which results in an increase in the accuracy of the position estimation, as is shown in Section 6.6. Particularly, in Case A, the number of times that the system has received from more than three anchor nodes represents 44% of times, whereas in Case B, this number rises up to 61%.

6.4.3 Distance Estimation

As stated in Section 2.1.1, the estimation of distance from the RSS uses the log-distance path loss model [8], that is,

$$P = P_{1m} - 10\alpha \log_{10} d - \gamma, \tag{6.10}$$

where P is the received power, P_{1m} is the received power at one meter from the transmitter, α is the path loss exponent, d is the distance and $\gamma \sim \mathcal{N}\left(0, \sigma_\gamma^2\right)$ models the shadowing effects. Considering this model, the RSS follows a Gaussian distribution:

$$P \sim \mathcal{N}\left(P_{1m} - 10\alpha \log_{10} d, \sigma_\gamma^2\right). \tag{6.11}$$

However, this model was developed for the single receiver case and does not take into account the scenario proposed in this work where the user carries two different receivers. In Chapter 5 we addressed the estimation of distance based on multiple receivers using a ML pipeline to classify the data and a linear regression method to estimate the distance. The ML approach used in Chapter 5 allowed us to estimate not only the distance but also the speed and heading of the user based on the RSS of multiple receivers. In this chapter, we only seek to estimate the distance from the RSS measurements because the speed and heading of the user are estimated from the inertial measurements as stated in Section 6.3.1. We propose to estimate the PDF of the distance based on the RSS measurements using Gaussian mixture models (GMM). Note that if we attempt to jointly estimate the PDF of the distance to the anchor, the speed and the heading of the user based on the RSS we will have to deal with a higher dimension distribution. Thus increasing the overall complexity of the problem.

The idea behind the mixture models is to obtain a new distribution from a linear combination of known distributions, Gaussian in the case of GMM. By using a sufficient number of Gaussians and by adjusting their means and covariances, as well as the coefficients in the linear combination, almost any continuous density can be approximated to arbitrary accuracy [99]. We consider a superposition of K Gaussian distributions of the form,

$$p(X) = \sum_{k=1}^{K} \pi_k \mathcal{N}(X; \mu_k, \Sigma_k), \tag{6.12}$$

where π_k are the so-called mixing coefficients and μ_k and$\Sigma_{\ k}$ are, respectively, the mean and covariance of the Gaussian densities used (also known as components of the mixture). We can also express the PDF as a marginal density [99], that is,

$$p(X) = \sum_{k=1}^{K} p(k)\, p(X|k), \tag{6.13}$$

where we can view $p(k) = \pi_k$ as the prior probability of choosing the k-th component and $p(X|k) = \mathcal{N}(X|\mu_k, \Sigma_k)$ as the probability of X conditioned on k. Following this interpretation, we can also compute the posterior probability $p(k|X)$, that is,

$$p(k|X) = \frac{\pi_k \mathcal{N}(X; \mu_k, \Sigma_k)}{\sum_{j=1}^{K} \pi_j \mathcal{N}(X; \mu_j, \Sigma_j)}, \tag{6.14}$$

which are also called responsibilities because it can be viewed as the responsibility of the k-th component of the mixture to explain the observation X.

In order to use the GMM in the distance estimation, we need to compute the parameters of the model, i.e., π_k, μ_k and$\Sigma_{\ k}$, from a set of observations obtained in a calibration phase. Lets us denote $\mathbf{X}$ as the set of N observations obtained from the calibration phase, that is a set of N vectors $\left[\mathcal{R}_p,\ \mathcal{R}_w,\ d\right]$, where $\mathcal{R}_p$ are the RSS received by the smartphone, $\mathcal{R}_w$ the RSS received by the smartwatch and d the real distance from the user to the anchor node. Assuming that the data points are drawn independently from the distribution, the log-likelihood function is given by,

$$\ln p\left(\mathbf{X};\pi_k,\mu_k,\Sigma_k\right)=\sum_{n=1}^{N}\ln\left(\sum_{k=1}^{K}\pi_k\mathcal{N}\left(X_n;\mu_k,\Sigma_k\right)\right). \tag{6.15}$$

We compute the parameters of the model as the values that maximize the log-likelihood function. The maximization of the log-likelihood function of a GMM is a complex problem and does not have a closed solution. Traditionally, the maximization problem is solved using the expectation maximization (EM) algorithm [109]. The EM algorithm is an iterative method that maximizes the log-likelihood function in each iteration following a two step procedure [99]: *i*) the expectation step (E-step); and *ii*) the maximization step (M-step). In the E-step, we compute the so-called responsibilities $p\left(k|X_n\right)$ from the current estimation of the parameters, that is,

$$p\left(k|X_n\right)=\frac{\pi_k\mathcal{N}\left(X_n;\mu_k,\Sigma_k\right)}{\sum_{j=1}^{K}\pi_j\mathcal{N}\left(X_n;\mu_j,\Sigma_j\right)}, \tag{6.16}$$

while in the M-step, we re-estimate the parameters using the computed responsibilities, that is,

$$\mu_k^{new}=\frac{1}{N_k}\sum_{n=1}^{N}p\left(k|X_n\right)x_n, \tag{6.17}$$

$$\sigma_k^{new}=\frac{1}{N_k}\sum_{n=1}^{N}p\left(k|X_n\right)\left(X_n-\mu_k^{new}\right)\left(X_n-\mu_k^{new}\right)^T, \tag{6.18}$$

$$\pi_k^{new}=\frac{N_k}{N}, \tag{6.19}$$

where:

$$N_k=\sum_{n=1}^{N}p\left(k|X_n\right). \tag{6.20}$$

These two steps are iteratively repeated until the increment of the log-likelihood function in the current iteration is below a convergence threshold.

As previously stated in this chapter, we do not have any control of the wireless network. This will produce a lack of synchronization between the RSS measurements of the receivers, and therefore, we have to consider different situations:

- **Case A:** in this case, we obtain a measurement of the RSS from a specific anchor node in both receivers at a quasi-simultaneous time. Then, we can compute the estimated distance using the RSS obtained by both devices. Therefore, we define a vector of observation $X = \left[RSS_p,\ RSS_w,\ d\right]$.

- **Case B:** in this case, we receive RSS measurements only from the smartphone. Then, we define the observation vector as $X = \left[RSS_p,\ d\right]$.

- **Case C:** this is similar to Case B, but we receive RSS measurements from the smartwatch instead of the smartphone; the observation vector is $X = \left[RSS_w,\ d\right]$.

We use a different GMM for each one of the three cases, that is we estimate the parameters π_k, μ_k and$\Sigma_{\ k}$ for the log likelihood function of each one of the cases. The difference between the models is the vector of observations X. Once we have estimated the parameters of the models using the data obtained in the calibration phase and the EM algorithm, we estimate the distance solving the following maximization problem:

$$\hat{d} = \max_{\hat{d}} \ln p\left(\mathbf{X}; \pi_k, \mu_k, \Sigma_k\right), \tag{6.21}$$

where the maximization of the log-likelihood function is done with respect to the distance because it is the only unknown variable in the vector of observation X; the RSS_p and RSS_w variables are known as they are the RSS measurements received from the smartphone and the smartwatch.

6.4.4 Position Computation

The estimation of position based on RSS measurements is usually done using a multilateration method as stated in Section 2.1.1. In this chapter as in previous Chapters 4 and 5, we use a weighted least squares algorithm. For the sake of readability we repeat here the steps of the WLS. The WLS estimates the position of the user as the solution to the following minimization problem [85],

$$\min_{\hat{\mathbf{m}}_k} J = \sum_{i \in \mathcal{D}} \omega_i \left(\hat{d}_i - \|\mathbf{s}_i - \hat{\mathbf{m}}_k\|\right)^2, \tag{6.22}$$

where $\mathcal{D}$ is the set of distance measurements available at time instant k and $\omega_i = \frac{1}{(\hat{d}_i)^2}$ are the weights of the algorithm [86]. Note that due to the logarithmic relationship between the RSS and the distance, the accuracy of the estimations depends on the distance to be estimated itself [9], and hence, it is meaningful to assign different weights to estimations with different accuracies [102]. The problem in Equation 6.22 can be solved in an iterative way following a gradient descent approach, that is,

$$\hat{\mathbf{m}}_{k,(l)} = \hat{\mathbf{m}}_{k,(l-1)} + \delta_{(l)} \sum_{i \in \mathcal{R}} \omega_i (\hat{d}_i - \|\hat{\mathbf{s}}_i - \hat{\mathbf{m}}_{k,(l-1)}\|) \tilde{\mathbf{q}}_{i,(l-1)}, \tag{6.23}$$

where l is the iteration index, $0 < \delta_{(l)} \ll 1$ is the step size, and $\tilde{\mathbf{q}}_{i,(l-1)}$ is a unitary vector,

$$\tilde{\mathbf{q}}_{i,(l-1)} = \frac{\left(\hat{\mathbf{s}}_i - \hat{\mathbf{m}}_{k,(l-1)}\right)}{\|\hat{\mathbf{s}}_i - \hat{\mathbf{m}}_{k,(l-1)}\|}. \tag{6.24}$$

6.5 Filtering Block

The third block of the system architecture is the filtering block. Here, we combine the estimations of the position, speed and heading of the user into a single filter that outputs an enhanced estimation of the user's position. Again the filter employed for the fusion of the measurements is the EKF as in previous chapters.

Let us model again the state of a person in a two dimensional space by means of its position and velocity,

$$\mathbf{x}_k = \begin{bmatrix} x_k & y_k & v_k & \theta_k \end{bmatrix}^T, \tag{6.25}$$

where x_k, y_k represent the position in Cartesian coordinates, v_k is the speed and θ_k the heading of the user. The movement of the person is defined as a discrete time dynamic system,

$$\mathbf{x}_k = f_{k-1}(\mathbf{x}_{k-1}) + \mathbf{v}_{k-1}, \tag{6.26}$$

where $f_{k-1}(\mathbf{x}_{k-1})$ is the state model function and $\mathbf{v}_{k-1}$ is a zero mean Gaussian noise with covariance matrix $\mathbf{Q}$. The state model is a modification of the constant velocity model that takes into account that the velocity is represented in polar coordinates, that is,

$$f_{k-1}(\mathbf{x}_{k-1}) = \begin{bmatrix} 1 & 0 & T\cos\theta_{k-1} & 0 \\ 0 & 1 & T\sin\theta_{k-1} & 0 \\ 0 & 0 & 1 & 0 \\ 0 & 0 & 0 & 1 \end{bmatrix} \mathbf{x}_{k-1}, \tag{6.27}$$

where T is the time period between measurements. The equations of the EKF used for the estimation of the user's position are depicted in Figure 6.5. In particular, the Jacobian

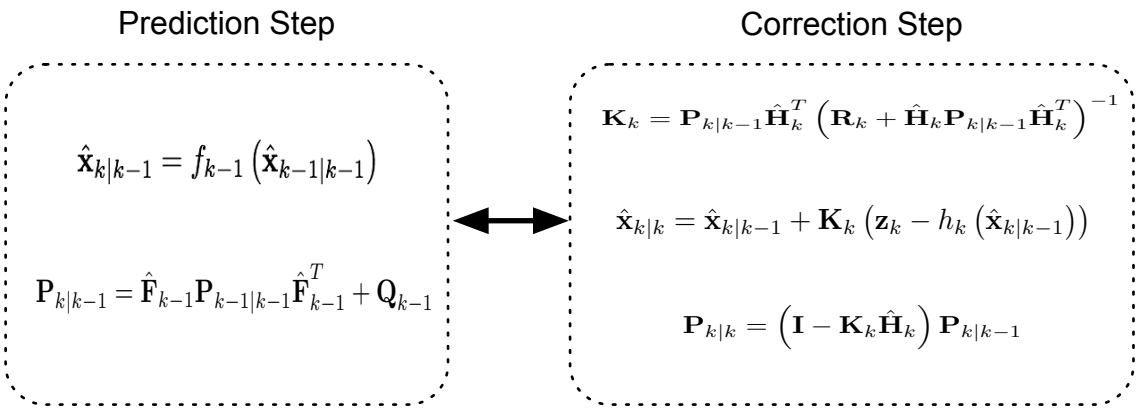

Figure 6.5: Equations of the Extended Kalman Filter.

matrix of the model function employed is,

$$\hat{\mathbf{F}}_{k-1} = \begin{bmatrix} 1 & 0 & T\cos(\theta^k) & -T\sin(\theta^k)v^k \\ 0 & 1 & T\sin(\theta^k) & T\cos(\theta^k)v^k \\ 0 & 0 & 1 & 0 \\ 0 & 0 & 0 & 1 \end{bmatrix}. \tag{6.28}$$

As stated in previous chapters, the EKF exploits the statistics of the measurements in order to produce an enhanced estimation of the state vector. These statistics are considered to be known by the designer and are introduced to the filter through the configuration of the covariance matrices $\mathbf{Q}$ and $\mathbf{R}$. In this chapter, we assume that the state variables and measurement variables are independent, and therefore, we configure their covariance matrices as diagonal matrices. The values of the variances are manually configured based on our experimental results. The specific values used are:

$$\mathbf{Q} = diag\left(\begin{bmatrix} 0.5 & 0.5 & 3 & 3 \end{bmatrix}\right), \tag{6.29}$$

$$\mathbf{R} = diag\left(\begin{bmatrix} 75 & 75 & 0.5 & 0.05 \end{bmatrix}\right), \tag{6.30}$$

Note that as in Chapter 5 we prefer here to manually configure the EKF instead of employing a method similar to the ones designed in Chapter 4. The reasons are the same than in Chapter 5. We do not want to mask the origin of the improvements obtained by the designed system with the improvements of the configuration methods of the EKF. Furthermore, we also employ here a multiple receiver architecture and as previously stated, the adaptation of the configuration methods to the multiple receiver architecture is left as a future line of work (see Section 7.2). The following section validates the performance of the designed pedestrian tracking system in a real environment.

Figure 6.6: Path 1 and odometry obtained with the pocket navigation system.

6.6 Experimental Validation

In this section, we test the performance of the indoor positioning system designed. To evaluate the performance, we have used a Motorola Moto G2 LTE smartphone and a Nexus 5 smartphone, which will take the roll of the smartwatch once attached to the wrist of the user. Both smartphones include a 6-DoF IMU with an accelerometer and a gyroscope. The sensors are sampled with a frequency of 100 Hz with our own designed Android application that also scans the WiFi channels to obtain the RSS measurements. As stated in Section 6.3, the obtained frequency is not always 100 Hz, and our system has to adapt to small changes in the measurement rate. The system updates the estimation of the user's position every second using the inertial and RSS measurements received since the last estimation update.

The scenario of validation is the first floor of the Engineering School at *Universitat Autònoma de Barcelona* (see Figure 6.6). The scenario is an area of approximately 6000 m^2 covered with 14 WiFi access points (marked with grey squares in Figure 6.6) that will act as the anchor nodes of the system, that is an anchor node every 428.5 m^2. Note that, there is no control about the configuration nor the placement of the anchor nodes as far as we are using the available WiFi network at the building. Note also that the distribution of the anchor nodes is not uniform around the area, and there are zones far from any of the anchor nodes, zones with high density of anchor nodes and zones with collinear anchors nodes. This is the reason for choosing this scenario; the selected scenario presents all of the typical issues of a communication network described in Section 6.4.

Figure 6.7: Path 2 and odometry obtained with the pocket navigation system.

In order to evaluate the indoor positioning system, we have considered three different paths. Figure 6.6 depicts the trajectory of Path 1 with a length of 620 m. The second path, i.e., Path 2, is shown in Figure 6.7, and it has a length of 420 m. Finally, Path 3 is shown in Figure 6.8, and it has a length of 338 m.

During the experimental validation, we compare five different methods: *i*) a step length and heading estimation algorithm based on the inertial measurements from the smartphone; *ii*) a WLS approach based on the distance estimations obtained from the RSS measurements of the smartphone; *iii*) an EKF that combines the estimations of the previous WLS (based only on the smartphone) with the inertial measurements; *iv*) a WLS based on the distance estimation obtained from the combination of the RSS measurements of the smartphone and the smartwatch; and *v*) an EKF that combines the inertial measurements with the WLS based on the smart combination of the smartphone and smartwatch. In the following, these methods are referred to as IMU, WLS-phone, EKF-phone, WLS-smart and EKF-smart, respectively.

In order to evaluate the performance of the different methods, we compute the real path of the user using a series of landmarks deployed around the building. We ask the user of the system to press a button every time that he/she goes near a landmark. Then, the times are stored, and the real path is calculated by assuming a constant speed of the user between two landmarks. With the appropriate number of landmarks, the resultant error of the obtained real path can be considered negligible.

Table 6.1 shows the results obtained during the experimental validation in terms of the RMSE. We have selected the paths in order to be representative of a real scenario. For this reason, we have selected two paths where the IMU has a considerable drift (Path 1

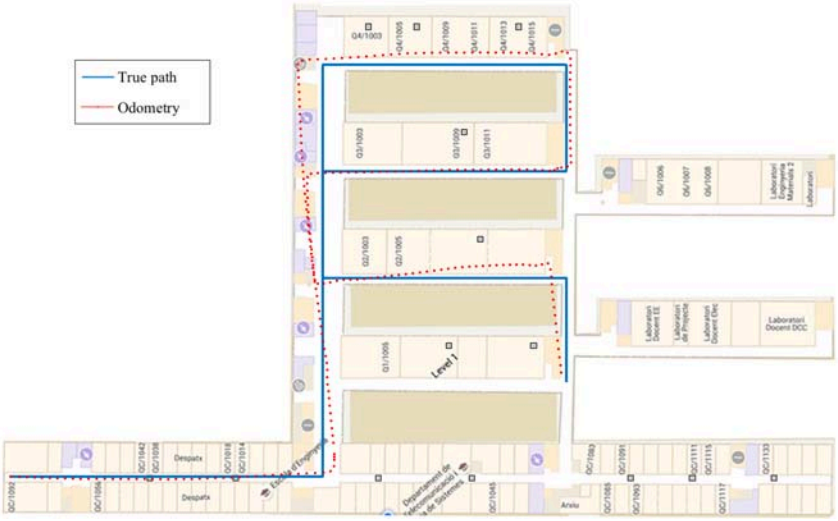

Figure 6.8: Path 3 and odometry obtained with the pocket navigation system.

and Path 2) and one path where the drift of the IMU is small (Path 3). The odometry of the selected paths is shown in Figures 6.6 to 6.8. Results show the improvement in the positioning accuracy due to the use of a second mobile receiver. In particular, the improvement of the WLS-smart over the WLS-phone is around 30% in the case of Path 1, 23% in Path 2 and 37.5% in Path 3. For the EKF-smart system, the improvement over the EKF-phone is around 35% in the case of Path 1, 19% in the case of Path 2 and 22% in Path 3. If we consider the improvement of the EKF-smart system compared with the IMU system, we obtain an improvement of 56% for Path 1, 35% for Path 2 and 12.5% for Path 3.

Table 6.1: Results of the experimental validation in terms of RMSE. t

	Smartphone			**Smartphone & Smartwatch**	
	IMU	**WLS-Phone**	**EKF-Phone**	**WLS-Smart**	**EKF-Smart**
Path 1	5.4	5.6	3.7	3.9	2.4
Path 2	5.2	5.3	4.2	4.1	3.4
Path 3	1.6	4	1.8	2.5	1.4

The comparison between the WLS-smart method and the WLS-phone method gives us an idea about the improvement produced by the use of a second receiver in the system. The increment in the accuracy of the estimation is produced by two main factors. First, the combination of the RSS from the smartphone and the smartwatch results in an increment in the accuracy of the distance estimation. Second, the use of two receivers increases the

number of measurements available. Specifically, the increase in the number of measurements is 35% in Path 1, 25% in Path 2 and 28% in Path 3. These results confirm that the use of a second receiver ameliorates the problems of RSS based methods implemented with third party WiFi networks stated in Section 6.4. Similarly, the comparison between the IMU method and the smart-EKF shows the benefits of combining inertial measurements with RSS measurements because the PDR system employed obtains high accurate position estimations in the short term, but deviates with time. Contrarily, the accuracy of the RSS position estimations is lower, but time invariant.

A special case of interest appears in Path 3 when we compare the accuracy of the EKF-phone method with the IMU method. In this case, the combination of inertial and RSS measurements from the smartphone has worse performance than the use of only the IMU measurements. This effect is produced by the general configuration of the parameters of the EKF (see Section 6.5) as the configuration is fixed for all of the cases the EKF cannot adapt to the increase in the accuracy of the IMU measurements, increasing the importance of the IMU measurements in the output of the EKF. Instead, the IMU measurements are fused exactly in the same way, so the output does not improve the accuracy of the single IMU system in this case. Note that this effect is not present in the EKF-smart system because the combination of RSS measurements from the two sources increases the accuracy of the position measurements (see WLS-smart), and in this case, the difference between the accuracy of the IMU and RSS measurements is similar for the three paths; therefore, the actual filter configuration is robust to the different scenarios and the EKF-smart system always outperforms the accuracy of the other systems.

Table 6.2: Results of the experimental validation in terms of the 90 percentile.

	Smartphone			**Smartphone & Smartwatch**	
	IMU	**WLS-Phone**	**EKF-Phone**	**WLS-Smart**	**EKF-Smart**
Path 1	12.8	11	7.8	8.5	4.4
Path 2	7.9	10	7.3	8	6.3
Path 3	3	5.6	3.1	5	2.9

Again as in previous chapters, we include also the analysis of the behavior of the designed systems in terms of the cumulative distribution function. In order to compare the positioning systems employed in this work, we will consider the value of the RMSE when the CDF equals 0.9. This means that the error committed by the algorithm is below this threshold value in 90% of the cases. Table 6.2 summarizes the 90 percentiles of the validated systems. The complete CDFs are shown in Figure 6.9 for the case of Path 1,

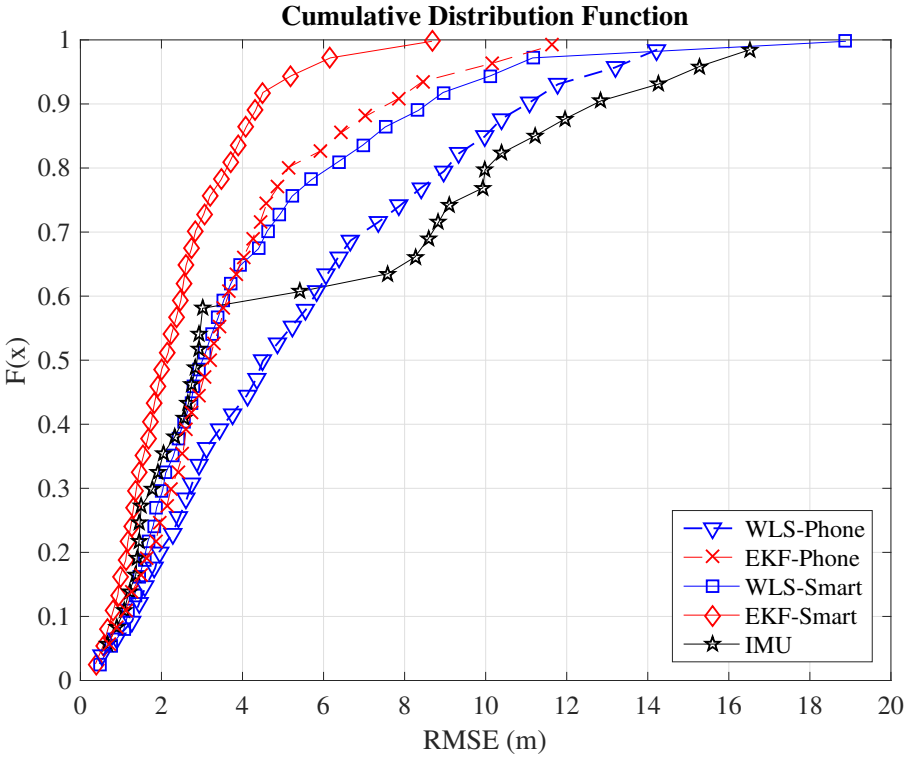

Figure 6.9: CDF of the positioning estimation error in Path 1.

Figure 6.10 for the case of Path 2 and Figure 6.11 for Path 3. From the figures, we can observe how the EKF-smart outperforms all of the other systems. It can also be observed how the error committed by our system is almost always below 2.9 m, 4.4 m and 6.3 m, which can be considered high accuracies taking into account the area of the scenario, which is 6000 m^2. If we compare the accuracy of our system with other indoor positioning systems based on smartphones, we can see that our system outperforms similar systems based on hybrid measurements [38, 41, 45] and obtains accuracies similar to the ones obtained by hybrid systems that include additional map information for the sensor fusion [42, 43, 44].

The experimental validation shows the benefits of introducing a smartwatch in an indoor positioning system based on a smartphone. The positioning accuracy obtained from the RSS measurements of the WiFi network is increased, and therefore, the overall solution including also the inertial measurements shows better performance. In fact, in the scenarios tested, the increment in accuracy from the initial PDR algorithm to the EKF-smart methods goes from 12.5% up to 56%. Furthermore, the system has been designed for being used in conjunction with a third party WiFi network, and the experimental validation has proven the adaptability of our system and its ability to obtain accurate position estimations.

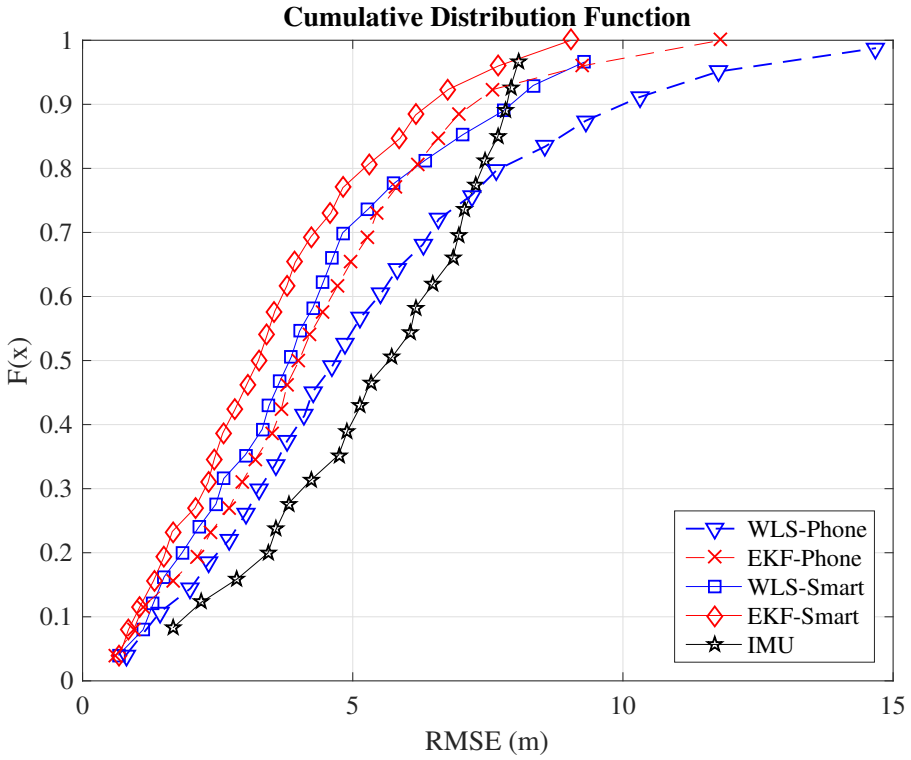

Figure 6.10: CDF of the positioning estimation error in Path 2.

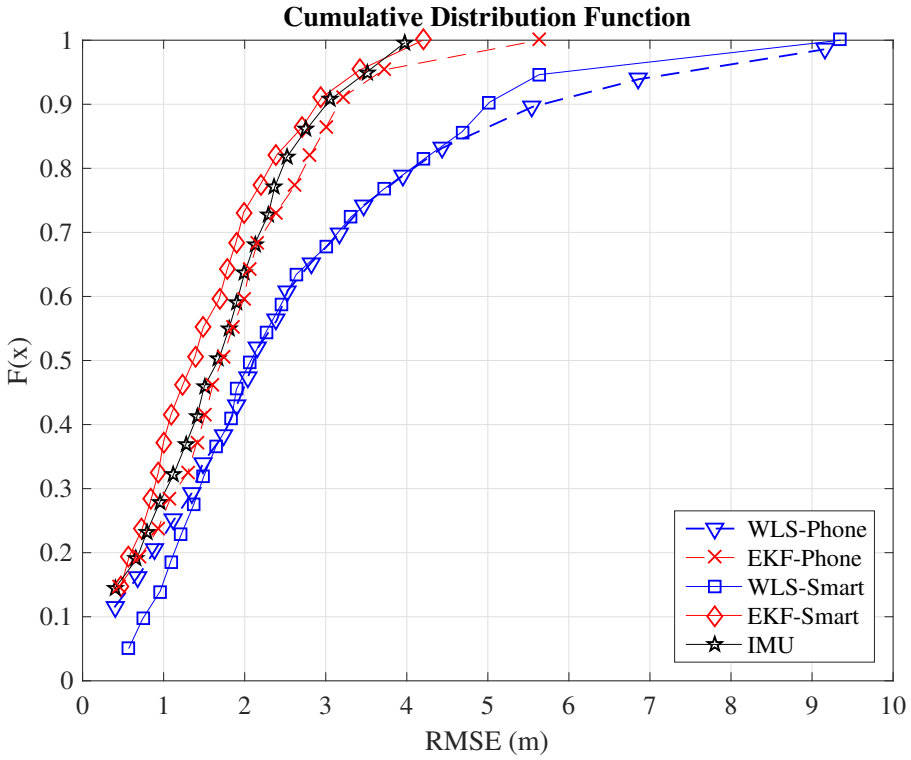

Figure 6.11: CDF of the positioning estimation error in Path 3.

6.7 Conclusions

In this chapter, we aimed to develop an indoor positioning system that can be applied to mass market applications. For this reason, we have selected a smartphone and a smartwatch as the devices that the user will carry in order to obtain his/her position. The designed system combines the inertial measurements of the smartphone placed in the pocket of the user with the RSS measurements from a WiFi network obtained by the smartphone and the smartwatch.

On the one hand, the position estimation based on the inertial measurements follows a step length and heading estimation approach that uses the pitch angle of the thigh to detect steps and the amplitude of the thigh pitch to estimate the step length. The inertial measurements are obtained from a commercial smartphone with an embedded low cost IMU. The designed PDR system is able to adapt to small changes in the measurement rate of the inertial sensors.

On the other hand, the position estimation based on the RSS of the WiFi network is computed using a GMM that combines the measurements of the two receivers to obtain an enhanced distance estimation. We also analyze the challenges of using an external WiFi network designed for communication purposes and without any control over the network configuration. We have demonstrated how the use of a smartwatch ameliorates these issues improving the overall accuracy of the system. The combination of the inertial and RSS measurements has been done using an extended Kalman filter with a constant velocity kinematic model. The system has been experimentally validated in a scenario with an area of $6000\,\mathrm{m}^2$, and the results show that the use of two RSS receivers in conjunction with the inertial measurement of a smartphone placed in the pocket of the user can improve the accuracy of the position estimation up to 56%.

Chapter 7

Conclusions and Future work

This PhD dissertation has explored the design of indoor positioning systems from an experimental perspective by studying IPS that can be implemented with the current commercial technologies. Moreover, we focus on the design of IPS that can be easily scaled to mass market applications by employing network based positioning systems and widely used wireless networks like the WiFi networks or the wireless sensor networks, which play a key role in the context of the internet of the things and its applications to smart cities and smart buildings.

First, we have considered an hybrid case combining the inertial measurements from a hip mounted inertial measurement unit with the RSS measurements from a wireless sensor network. Particularly, we designed two methods for exploiting the statistics of the RSS measurements in order to extend in time the short term accuracy of the inertial sensors. Afterwards, we continue the study of indoor positioning systems based on WSN by extending the problem to the multiple receiver case. We deployed multiple receivers on the body of the user and took advantage of the different attenuations suffered due to the effect of the human body on the wireless signals in order to estimate the position, velocity and heading of the user without the need of using inertial sensors. Finally, with the aim of applying our designs to mass market applications, we moved to a WiFI network and commercial devices, smartphones and smartwatches. The smartphone cooperates with the smartwatch in order to circumvent the problems detected in third party WiFi networks. Specifically, we design an hybrid indoor positioning system that combines the inertial measurements from a smartphone placed in the pocket of the user with the RSS measurements received from the smartphone and the smartwatch. In the following, we draw the conclusions of this thesis and some open issues to be addressed as future work.

7.1 Conclusions

After motivating this PhD thesis and giving an overview of the state of the art, in Chapter 3 we have introduced some of the key topics that have been used throughout this dissertation. Specifically, we have revisited the concepts of Bayesian estimation paying special attention to the analytical solution provided by the Kalman filter and specially the suboptimal solution provided by the extended Kalman filter which has been used in every indoor positioning system designed in this work.

Chapter 4 is devoted to the study of hybrid indoor positioning systems combining the RSS measurements from wireless sensor networks with the inertial measurements from a low cost inertial measurement unit. More precisely, we focus our attention to the statistical characteristics of the RSS measurements and how these can be used to configure the measurement noise covariance matrix of the EKF. To do so, we designed two novel methods that automatically configure the noise covariance matrix at every step of the filter: *i*) the power threshold covariance matrix tuning; and *ii*) the distance statistics covariance matrix tuning. On one hand, the PT-CMT method is a simple solution that considers two degrees of reliability in the measurements. It is designed for indoor areas with many small rooms (e.g. houses or offices). On the other hand, the DS-CMT takes into account a wider range of reliabilities in the position measurements. This method is specially designed for indoor open areas (e.g. large halls, museums, university classrooms).

The system has been experimentally validated in two different representative indoor scenarios with different densities of nodes and the proposed enhancements in the EKF reduce the positioning RMSE with respect to a regular EKF up to 40% in the scenarios tested. As a result, the proposed system is kept simple in terms of computational complexity, the accuracy is around the meter in terms of RMSE and also kept in the long term. In summary, we show that it is possible to design simple EKF based solutions that efficiently combine observations with different degrees of reliability.

Chapter 5 extends the study of indoor positioning systems based on WSN to the multiple receiver case. The huge variability of the indoor wireless channel produces inaccurate distance estimations. Moreover, if the user carries the mobile WSN node attached to the body, the attenuation of the human body introduces errors in the distance estimation. To circumvent this problem, we employed multiple receivers in order to introduce diversity as far as the attenuation of the human body affects each receiver in a different way. Then, we exploit the diversity of receivers to enhance the distance estimations and consequently the position estimations. We employ a machine learning pipeline to classify the data into groups of similar statistical patterns and then we apply a linear regression method to estimate the distance to the anchor nodes. Similarly, neural networks are employed to

estimate the velocity and heading of the user based on the RSS data.

Contrarily to most of the pedestrian tracking systems in the literature, the designed system avoids the use of inertial sensors and, accordingly, does not suffer from temporal drifts and hence its positioning accuracy is time invariant. Moreover, the computational complexity of the system is small compared to the systems using inertial sensors as there is no need to employ an additional Kalman filter to estimate the orientation of the IMU or to employ high sampling rates which drastically drains the battery of the WSN nodes. The system has been experimentally validated in different scenarios including a flat, a university classroom and a long corridor, achieving in all cases a positioning accuracy around 1 meter.

Chapter 6 covers the analysis of indoor positioning systems based on smartphones. The popularization of the smartphones in the last years converted the smartphone into the perfect device for mass market IPS. The different technologies integrated in nowadays commercial smartphones, as for example the WiFi and bluetooth radios or the inertial sensors allow the implementation of hybrid systems using a single device. In this chapter, we design an hybrid IPS that combines RSS measurements from a WiFi network with inertial measurements from a smartphone placed in the pocket of the user. First, we detailed the problems produced when an IPS is applied to a WiFi network without any control of the network by the IPS designer. Then, we apply the ideas of multiple receivers to the smartphone positioning problem by introducing a smartwatch. We design a method for combining the RSS measurements of the smartphone and smartwatch based on Gaussian mixture models. This method is designed with the aim of circumvent the main problems originated by the lack of control over the WiFi network. Finally, the combination of the inertial and RSS measurements has been done using an extended Kalman filter with a constant velocity kinematic model. The system has been experimentally validated in an scenario with an area of $6000\,\mathrm{m}^2$, and the results show that the use of two RSS receivers in conjunction with the inertial measurements of a smartphone placed in the pocket of the user can improve the accuracy in position estimation up to 56%. The result is an hybrid positioning system that can be implemented in nowadays commercial smartphones and smartwatches, thus it is suitable for mass market applications.

This Ph.D. thesis has explored the universe of indoor positioning systems for pedestrians and it has contributed with three novel IPS that have been experimentally evaluated in order to show the accuracy obtained in real scenarios. Before ending the conclusions of the work, let us emphasize the importance of indoor positioning systems due to its unlimited applications that go from the guidance of visual impaired users to the guidance of emergency agents or the development of assisted living systems for the care of elderly people. Fortunately, there is still much work to be done and we identify some of those

open issues in the next section.

7.2 Future Work

The work presented in this PhD dissertation can be extended as follows:

- To consider the use of the map information and reformulate the problems to take advantage of it.
- To extend the indoor positioning problem to the cooperative problem where different users cooperate between them to increase the localization accuracy.
- To characterize the computational complexity of the systems and measure the duration of the battery powered devices employed in the designed IPS.
- Finally, to increase the number of scenarios and number of users that perform the experimental validation in order to see the behavior of the systems over a large set of different scenarios and users.

As for the specific problems addressed in each chapter, in Chapter 4 some of the possibilities are:

- To take into account that the x,y components of the position measurements are correlated and reformulate the covariance matrix tuning methods.
- To analyze the statistics of the inertial measurements and to design methods for the automatic configuration of the parameters of the noise covariance matrix of the EKF that are related to the inertial measurements.
- To analyze the multiple receiver architectures introduced in Chapter 5 and Chapter 6 and design new covariance matrix tuning methods for these architectures.

In Chapter 5 we consider the following extensions:

- To modify the number of multiple receivers employed and determine the optimum number of receivers and the optimum position of the receivers on the body of the user.
- To model, if possible the path loss model of each receiver taking into account the attenuation of the human body.

- To extend the study to the multiple transmitter case where groups of anchors are deployed in a specific geometric distribution and act as a single anchor node.

Last but not least, the research lines that continue the work in Chapter 6 are:

- To track the position of the smartwatch using the inertial sensors and use the relative position of both receivers in the estimation of the distances and angles to the anchor nodes.
- To integrate in the system other sources of RSS measurements available in nowadays commercial smartphones such as Bluetooth or LTE.
- Finally, to extend the experimental validation to multiple different smartphones and smartwatches.

Bibliography

[1] "Indoor location in retail: Where is the money?," *ABI Research: Location Technologies Market Research*, 2015.

[2] Andy Harter, Andy Hopper, Pete Steggles, Andy Ward, and Paul Webster, "The anatomy of a context-aware application," in *Proceedings of the 5th Annual ACM/IEEE International Conference on Mobile Computing and Networking*, New York, NY, USA, 1999, MobiCom '99, pp. 59–68, ACM.

[3] Nissanka B. Priyantha, Anit Chakraborty, and Hari Balakrishnan, "The cricket location-support system," in *Proceedings of the 6th Annual International Conference on Mobile Computing and Networking*, New York, NY, USA, 2000, MobiCom '00, pp. 32–43, ACM.

[4] S. Gezici, Zhi Tian, G. B. Giannakis, H. Kobayashi, A. F. Molisch, H. V. Poor, and Z. Sahinoglu, "Localization via ultra-wideband radios: a look at positioning aspects for future sensor networks," *IEEE Signal Processing Magazine*, vol. 22, no. 4, pp. 70–84, July 2005.

[5] Abdulrahman Alarifi, AbdulMalik Al-Salman, Mansour Alsaleh, Ahmad Alnafessah, Suheer Al-Hadhrami, Mai A. Al-Ammar, and Hend S. Al-Khalifa, "Ultra wideband indoor positioning technologies: Analysis and recent advances," *Sensors*, vol. 16, no. 5, pp. 707, 2016.

[6] D. Niculescu and Badri Nath, "Ad hoc positioning system (aps) using aoa," in *IEEE INFOCOM 2003. Twenty-second Annual Joint Conference of the IEEE Computer and Communications Societies (IEEE Cat. No.03CH37428)*, March 2003, vol. 3, pp. 1734–1743 vol.3.

[7] V. Pierlot and M. Van Droogenbroeck, "A new three object triangulation algorithm for mobile robot positioning," *IEEE Transactions on Robotics*, vol. 30, no. 3, pp. 566–577, June 2014.

[8] N. Patwari, J.N. Ash, S. Kyperountas, III Hero, A.O., R.L. Moses, and N.S. Correal, "Locating the nodes: cooperative localization in wireless sensor networks," *Signal Processing Magazine, IEEE*, vol. 22, no. 4, pp. 54 – 69, july 2005.

[9] Xinrong Li, "Collaborative localization with received-signal strength in wireless sensor networks," *Vehicular Technology, IEEE Transactions on*, vol. 56, no. 6, pp. 3807–3817, 2007.

[10] J. Yang and Y. Chen, "Indoor localization using improved rss-based lateration methods," in *GLOBECOM 2009 - 2009 IEEE Global Telecommunications Conference*, Nov 2009, pp. 1–6.

[11] A. Zanella, "Best practice in rss measurements and ranging," *IEEE Communications Surveys Tutorials*, vol. 18, no. 4, pp. 2662–2686, Fourthquarter 2016.

[12] N. Patwari, A. O. Hero, M. Perkins, N. S. Correal, and R. J. O'Dea, "Relative location estimation in wireless sensor networks," *IEEE Transactions on Signal Processing*, vol. 51, no. 8, pp. 2137–2148, Aug 2003.

[13] A. Harter and A. Hopper, "A distributed location system for the active office," *IEEE Network*, vol. 8, no. 1, pp. 62–70, Jan 1994.

[14] M. Bolic, M. Rostamian, and P. M. Djuric, "Proximity detection with rfid: A step toward the internet of things," *IEEE Pervasive Computing*, vol. 14, no. 2, pp. 70–76, Apr 2015.

[15] N. Bulusu, J. Heidemann, and D. Estrin, "Gps-less low-cost outdoor localization for very small devices," *IEEE Personal Communications*, vol. 7, no. 5, pp. 28–34, Oct 2000.

[16] P. Bahl and V. N. Padmanabhan, "Radar: an in-building rf-based user location and tracking system," in *Proceedings IEEE INFOCOM 2000. Conference on Computer Communications. Nineteenth Annual Joint Conference of the IEEE Computer and Communications Societies (Cat. No.00CH37064)*, 2000, vol. 2, pp. 775–784 vol.2.

[17] D. Han, S. Jung, M. Lee, and G. Yoon, "Building a practical wi-fi-based indoor navigation system," *IEEE Pervasive Computing*, vol. 13, no. 2, pp. 72–79, Apr 2014.

[18] Galo Nuño Barrau and José M. Páz-Borrallo, "A new location estimation system for wireless networks based on linear discriminant functions and hidden markov models," *EURASIP J. Appl. Signal Process.*, vol. 2006, pp. 159–159, Jan. 2006.

[19] Moustafa Youssef and Ashok Agrawala, "The horus wlan location determination system," in *Proceedings of the 3rd International Conference on Mobile Systems, Applications, and Services*, New York, NY, USA, 2005, MobiSys '05, pp. 205–218, ACM.

[20] E. Foxlin, "Pedestrian tracking with shoe-mounted inertial sensors," *Computer Graphics and Applications, IEEE*, vol. 25, no. 6, pp. 38 –46, nov.-dec. 2005.

[21] A.R. Jiménez, F. Seco, J.C. Prieto, and J. Guevara, "Indoor pedestrian navigation using an ins/ekf framework for yaw drift reduction and a foot-mounted imu," in *Positioning Navigation and Communication (WPNC), 2010 7th Workshop on*, march 2010, pp. 135 –143.

[22] F. Zampella, M. Khider, P. Robertson, and A. Jiménez, "Unscented kalman filter and magnetic angular rate update (maru) for an improved pedestrian dead-reckoning," in *Proceedings of the 2012 IEEE/ION Position, Location and Navigation Symposium*, April 2012, pp. 129–139.

[23] Estefania Munoz Diaz, "Inertial pocket navigation system: unaided 3D positioning," *Sensors*, vol. 15, pp. 9156–9178, 2015.

[24] Wonho Kang and Youngnam Han, "SmartPDR: smartphone-based pedestrian dead reckoning for indoor localization," *IEEE Sensors Journal*, vol. 15, no. 5, 2015.

[25] A.R. Jimenez, F. Seco, C. Prieto, and J. Guevara, "A comparison of pedestrian dead-reckoning algorithms using a low-cost mems imu," in *Intelligent Signal Processing, 2009. WISP 2009. IEEE International Symposium on*, aug. 2009, pp. 37 –42.

[26] M. Angermann and P. Robertson, "Footslam: Pedestrian simultaneous localization and mapping without exteroceptive sensors ;hitchhiking on human perception and cognition," *Proceedings of the IEEE*, vol. 100, no. Special Centennial Issue, pp. 1840–1848, 2012.

[27] Maria Garcia Puyol, Martin Frassl, and Patrick Robertson, *Collaborative Mapping for Pedestrian Navigation in Security Applications*, pp. 49–60, Springer Berlin Heidelberg, Berlin, Heidelberg, 2012.

[28] S. Kaiser and E. M. Diaz, "Pocketslam based on the principle of the footslam algorithm," in *2015 International Conference on Location and GNSS (ICL-GNSS)*, June 2015, pp. 1–5.

[29] Korbinian Frank, Bernhard Krach, Noel Catterall, and Patrick Robertson, "Development and evaluation of a combined wlan & inertial indoor pedestrian positioning system," *ION GNSS*, 2009.

[30] J. Schmid, T. Gadeke, W. Stork, and K.D. Muller-Glaser, "On the fusion of inertial data for signal strength localization," in *Positioning Navigation and Communication (WPNC), 2011 8th Workshop on*, april 2011, pp. 7 –12.

[31] P. Tarrio, J.A. Besada, and J.R. Casar, "Fusion of rss and inertial measurements for calibration-free indoor pedestrian tracking," in *Information Fusion (FUSION), 2013 16th International Conference on*, July 2013, pp. 1458–1464.

[32] A. R. Jimenez, F. Seco Granja, J. C. Prieto Honorato, and J. I. Guevara Rosas, "Accurate pedestrian indoor navigation by tightly coupling foot-mounted imu and rfid measurements," *IEEE Transactions on Instrumentation and Measurement*, vol. 61, no. 1, pp. 178–189, Jan 2012.

[33] Frédéric Evennou and François Marx, "Advanced integration of wifi and inertial navigation systems for indoor mobile positioning," *EURASIP J. Appl. Signal Process.*, vol. 2006, pp. 164–164, Jan. 2006.

[34] Oliver Woodman and Robert Harle, "Pedestrian localisation for indoor environments," in *Proceedings of the 10th International Conference on Ubiquitous Computing*, New York, NY, USA, 2008, UbiComp '08, pp. 114–123, ACM.

[35] Hui Wang, H. Lenz, A. Szabo, J. Bamberger, and U.D. Hanebeck, "Wlan-based pedestrian tracking using particle filters and low-cost mems sensors," in *Positioning, Navigation and Communication, 2007. WPNC '07. 4th Workshop on*, March 2007, pp. 1–7.

[36] L. Klingbeil and T. Wark, "A wireless sensor network for real-time indoor localisation and motion monitoring," in *Information Processing in Sensor Networks, 2008. IPSN '08. International Conference on*, april 2008, pp. 39 –50.

[37] Thomas Stockx, Brent Hecht, and Johannes Schöning, "Subwayps: Towards smartphone positioning in underground public transportation systems," in *Proceedings of the 22Nd ACM SIGSPATIAL International Conference on Advances in Geographic Information Systems*, New York, NY, USA, 2014, SIGSPATIAL '14, pp. 93–102, ACM.

[38] Ling Pei, Jingbin Liu, Robert Guinness, Yuwei Chen, Heidi Kuusniemi, and Ruizhi Chen, "Using ls-svm based motion recognition for smartphone indoor wireless positioning," *Sensors*, vol. 12, no. 5, pp. 6155–6175, 2012.

[39] R Faragher and R Harle, "Smartslam–an efficient smartphone indoor positioning system exploiting machine learning and opportunistic sensing," in *ION GNSS*, 2013, vol. 13, pp. 1–14.

[40] Ramsey M Faragher and Robert K Harle, "Towards an efficient, intelligent, opportunistic smartphone indoor positioning system," *Navigation*, vol. 62, no. 1, pp. 55–72, 2015.

[41] Jingbin Liu, Ruizhi Chen, Ling Pei, Robert Guinness, and Heidi Kuusniemi, "A hybrid smartphone indoor positioning solution for mobile lbs," *Sensors*, vol. 12, no. 12, pp. 17208–17233, 2012.

[42] V. Radu and M. K. Marina, "Himloc: Indoor smartphone localization via activity aware pedestrian dead reckoning with selective crowdsourced wifi fingerprinting," in *Indoor Positioning and Indoor Navigation (IPIN), 2013 International Conference on*, Oct 2013, pp. 1–10.

[43] T. Moder, K. Wisiol, P. Hafner, and M. Wieser, "Smartphone-based indoor positioning utilizing motion recognition," in *Indoor Positioning and Indoor Navigation (IPIN), 2015 International Conference on*, Oct 2015, pp. 1–8.

[44] Zhenghua Chen, Han Zou, Hao Jiang, Qingchang Zhu, Yeng Chai Soh, and Lihua Xie, "Fusion of wifi, smartphone sensors and landmarks using the kalman filter for indoor localization," *Sensors*, vol. 15, no. 1, pp. 715–732, 2015.

[45] Y. Li, P. Zhang, H. Lan, Y. Zhuang, X. Niu, and N. El-Sheimy, "A modularized real-time indoor navigation algorithm on smartphones," in *Indoor Positioning and Indoor Navigation (IPIN), 2015 International Conference on*, Oct 2015, pp. 1–7.

[46] Hui Liu, H. Darabi, P. Banerjee, and Jing Liu, "Survey of wireless indoor positioning techniques and systems," *Systems, Man, and Cybernetics, Part C: Applications and Reviews, IEEE Transactions on*, vol. 37, no. 6, pp. 1067–1080, 2007.

[47] A. Boukerche, H.A.B. Oliveira, E.F. Nakamura, and A.A.F. Loureiro, "Localization systems for wireless sensor networks," *Wireless Communications, IEEE*, vol. 14, no. 6, pp. 6 –12, december 2007.

[48] Yuan Shen and M.Z. Win, "Fundamental limits of wideband localization; part i: A general framework," *Information Theory, IEEE Transactions on*, vol. 56, no. 10, pp. 4956–4980, 2010.

[49] Yuan Shen, H. Wymeersch, and M.Z. Win, "Fundamental limits of wideband localization; part ii: Cooperative networks," *Information Theory, IEEE Transactions on*, vol. 56, no. 10, pp. 4981–5000, 2010.

[50] Shikha Singh and Arun Aggarwal, "Article: Survey on localization techniques of rfid for iot," *International Journal of Computer Applications*, vol. 137, no. 12, pp. 23–27, March 2016, Published by Foundation of Computer Science (FCS), NY, USA.

[51] M. Bouet and A. L. dos Santos, "Rfid tags: Positioning principles and localization techniques," in *2008 1st IFIP Wireless Days*, Nov 2008, pp. 1–5.

[52] Junyi Zhou and Jing Shi, "Rfid localization algorithms and applications—a review," *Journal of Intelligent Manufacturing*, vol. 20, no. 6, pp. 695, 2008.

[53] A.K.M. Mahtab Hossain and Wee-Seng Soh, "A survey of calibration-free indoor positioning systems," *Computer Communications*, vol. 66, pp. 1 – 13, 2015.

[54] Chao-Lin Wu, Li-Chen Fu, and Feng-Li Lian, "Wlan location determination in e-home via support vector classification," in *IEEE International Conference on Networking, Sensing and Control, 2004*, 2004, vol. 2, pp. 1026–1031 Vol.2.

[55] D. Madigan, E. Einahrawy, R. P. Martin, W. H. Ju, P. Krishnan, and A. S. Krishnakumar, "Bayesian indoor positioning systems," in *Proceedings IEEE 24th Annual Joint Conference of the IEEE Computer and Communications Societies.*, March 2005, vol. 2, pp. 1217–1227 vol. 2.

[56] Piotr Mirowski, Philip Whiting, Harald Steck, Ravishankar Palaniappan, Michael MacDonald, Detlef Hartmann, and TinKam Ho, "Probability kernel regression for wifi localisation," *J. Locat. Based Serv.*, vol. 6, no. 2, pp. 81–100, June 2012.

[57] Jaewoo Chung, Matt Donahoe, Chris Schmandt, Ig-Jae Kim, Pedram Razavai, and Micaela Wiseman, "Indoor location sensing using geo-magnetism," in *Proceedings of the 9th International Conference on Mobile Systems, Applications, and Services*, New York, NY, USA, 2011, MobiSys '11, pp. 141–154, ACM.

[58] B. Li, T. Gallagher, A. G. Dempster, and C. Rizos, "How feasible is the use of magnetic field alone for indoor positioning?," in *2012 International Conference on Indoor Positioning and Indoor Navigation (IPIN)*, Nov 2012, pp. 1–9.

[59] S. He and S. H. G. Chan, "Wi-fi fingerprint-based indoor positioning: Recent advances and comparisons," *IEEE Communications Surveys Tutorials*, vol. 18, no. 1, pp. 466–490, Firstquarter 2016.

[60] R. Harle, "A survey of indoor inertial positioning systems for pedestrians," *Communications Surveys Tutorials, IEEE*, vol. 15, no. 3, pp. 1281–1293, 2013.

[61] Mark Pedley, "Tilt sensing using a three-axis accelerometer," *Freescale Semiconductor Application Note*, pp. 2012–2013, 2013.

[62] Oliver J. Woodman, "An introduction to inertial navigation," Tech. Rep., University of Cambridge. Computer Laboratory, August 2007, UCAM-CL-TR-696 ISSN 1476-2986.

[63] D. Titterton, J.L. Weston, and Institution of Electrical Engineers, *Strapdown Inertial Navigation Technology*, Electromagnetics and Radar Series. Institution of Engineering and Technology, 2004.

[64] Sujatha Rajagopal, "Personal dead reckoning system with shoe mounted inertial sensors," 2008.

[65] Johann Borenstein, Lauro Ojeda, and Surat Kwanmuang, "Heuristic reduction of gyro drift in imu-based personnel tracking systems," 2009, vol. 7306, pp. 73061H–73061H–11.

[66] Q. Ladetto, "On foot navigation: continuous step calibration using both complementary recursive prediction and adaptive kalman filtering," in *ION GPS/GNSS, 2000 Proceedings of*, sep. 2000, pp. 1735–1740.

[67] S. Beauregard, "A helmet-mounted pedestrian dead reckoning system," in *3rd International Forum on Applied Wearable Computing 2006*, March 2006, pp. 1–11.

[68] Seon-Woo Lee and K. Mase, "Recognition of walking behaviors for pedestrian navigation," in *Control Applications, 2001. (CCA '01). Proceedings of the 2001 IEEE International Conference on*, 2001, pp. 1152–1155.

[69] R.W. Levi and T. Judd, "Dead reckoning navigational system using accelerometer to measure foot impacts," Dec. 10 1996, US Patent 5,583,776.

[70] Harvey Weinberg, "Using the adxl202 in pedometer and personal navigation applications," *Analog Devices AN-602 application note*, vol. 2, no. 2, pp. 1–6, 2002.

[71] H. Durrant-Whyte and T. Bailey, "Simultaneous localization and mapping: part i," *IEEE Robotics Automation Magazine*, vol. 13, no. 2, pp. 99–110, June 2006.

[72] Tim Bailey and Hugh Durrant-Whyte, "Simultaneous localization and mapping (slam): Part ii," *IEEE Robotics & Automation Magazine*, vol. 13, no. 3, pp. 108–117, 2006.

[73] Jeffrey Hightower and Gaetano Borriello, "Location systems for ubiquitous computing," *Computer*, vol. 34, no. 8, pp. 57–66, Aug. 2001.

[74] K. Pahlavan, Xinrong Li, and J. P. Makela, "Indoor geolocation science and technology," *IEEE Communications Magazine*, vol. 40, no. 2, pp. 112–118, Feb 2002.

[75] Y. Gu, A. Lo, and I. Niemegeers, "A survey of indoor positioning systems for wireless personal networks," *IEEE Communications Surveys Tutorials*, vol. 11, no. 1, pp. 13–32, First 2009.

[76] Halgurd S. Maghdid, Ihsan Alshahib Lami, Kayhan Zrar Ghafoor, and Jaime Lloret, "Seamless outdoors-indoors localization solutions on smartphones: Implementation and challenges," *ACM Comput. Surv.*, vol. 48, no. 4, pp. 53:1–53:34, Feb. 2016.

[77] Jianga Shang, Xuke Hu, Fuqiang Gu, Di Wang, and Shengsheng Yu, "Improvement schemes for indoor mobile location estimation: A survey," *Mathematical Problems in Engineering*, vol. 2015, 2015.

[78] D. Dardari, P. Closas, and P. M. Djuri?, "Indoor tracking: Theory, methods, and technologies," *IEEE Transactions on Vehicular Technology*, vol. 64, no. 4, pp. 1263–1278, April 2015.

[79] Simo Särkkä, *Bayesian Filtering and Smoothing*, Cambridge University Press, New York, NY, USA, 2013.

[80] Stephan Sand, Armin Dammann, and Christian Mensing, *Positioning in Wireless Communications Systems*, Wiley Publishing, 1st edition, 2014.

[81] M.S. Arulampalam, S. Maskell, N. Gordon, and T. Clapp, "A tutorial on particle filters for online nonlinear/non-gaussian bayesian tracking," *Signal Processing, IEEE Transactions on*, vol. 50, no. 2, pp. 174 –188, feb 2002.

[82] Kalman R. E., "A new approach to linear filtering and prediction problem," *Journal of Basic Engineering Transactions*, vol. 82, no. 1, pp. 34–45, 1960.

[83] Greg Welch and Gary Bishop, "An introduction to the kalman filter," Tech. Rep., Chapel Hill, NC, USA, 1995.

[84] S. Kay, *Fundamentals of Statistical Signal Processing: Estimation Theory*, Number v. 2 in Prentice Hall signal processing series. Prentice Hall, 2001.

[85] H. Wymeersch, J. Lien, and M.Z. Win, "Cooperative localization in wireless networks," *Proceedings of the IEEE*, vol. 97, no. 2, pp. 427 –450, feb. 2009.

[86] Paula Tarrío, Ana M. Bernardos, and José R. Casar, "Weighted least squares techniques for improved received signal strength based localization," *Sensors*, vol. 11, no. 9, pp. 8569–8592, 2011.

[87] D. Gusenbauer, C. Isert, and J. Krösche, "Self-contained indoor positioning on off-the-shelf mobile devices," in *Indoor Positioning and Indoor Navigation (IPIN), 2010 International Conference on*, Sept 2010, pp. 1–9.

[88] M.H. Afzal, V. Renaudin, and G. Lachapelle, "Magnetic field based heading estimation for pedestrian navigation environments," in *Indoor Positioning and Indoor Navigation (IPIN), 2011 International Conference on*, sept. 2011, pp. 1 –10.

[89] L. Klingbeil, R. Reiner, M. Romanovas, M. Traechtler, and Y. Manoli, "Multi-modal sensor data and information fusion for localization in indoor environments," in *Positioning Navigation and Communication (WPNC), 2010 7th Workshop on*, march 2010, pp. 187 –192.

[90] Lei Fang, P.J. Antsaklis, L.A. Montestruque, M.B. McMickell, M. Lemmon, Yashan Sun, Hui Fang, I. Koutroulis, M. Haenggi, Min Xie, and Xiaojuan Xie, "Design of a wireless assisted pedestrian dead reckoning system - the navmote experience," *Instrumentation and Measurement, IEEE Transactions on*, vol. 54, no. 6, pp. 2342 – 2358, dec. 2005.

[91] Edwin L. Crow and Kunio Shimizu, *Lognormal Distributions: Theory and Applications*, Statistics: A Series of Textbooks and Monographs. Taylor & Francis, 1987.

[92] "Crossbow Iris: 2.4 ghz wireless sensor network module," `http://www.memsic.com/userfiles/files/Datasheets/WSN/IRIS_Datasheet.pdf`.

[93] "ATMEGA1281: 8-bit atmel microcontroller," `http://www.atmel.com/Images/Atmel-2549-8-bit-AVR-Microcontroller-ATmega640-1280-1281-2560-2561_datasheet.pdf`.

[94] "RF230: Low power 2.4 ghz transceiver for zigbee," `http://www.atmel.com/Images/doc5131.pdf`.

[95] "ADXL345: Digital accelerometer," `http://www.analog.com/static/imported-files/data_sheets/ADXL345.pdf`.

[96] "HMC5883L: Digital magnetometer," `http://www51.honeywell.com/aero/common/documents/myaerospacecatalog-documents/Defense_Brochures-documents/HMC5883L_3-Axis_Digital_Compass_IC.pdf`.

[97] "ITG-3200: Digital gyroscope," `http://invensense.com/mems/gyro/itg3200.html`.

[98] Trevor Hastie, Robert Tibshirani, and Jerome Friedman, *The Elements of Statistical Learning: Data Mining, Inference and Prediction*, Springer, 233 Spring Street, New York, NY 10013, USA, 2nd edition, 2009.

[99] Christopher M. Bishop, *Pattern Recognition and Machine Learning*, Springer Science+Business Media, 233 Spring Street, New York, NY 10013, USA, 1st edition, 2006.

[100] Ryan Rifkin and Aldebaro Klautau, "In defense of one-vs-all classification," *Journal of Machine Learning Research*, vol. 5, pp. 101–141, 2004.

[101] S Schmitt, S. Adler, and M Kyas, "The effects of human body shadowing in rf-based indoor localization," in *Indoor Positioning and Indoor Navigation (IPIN), 2014 International Conference on*, 2014.

[102] A. Correa, M. Barcelo, A. Morell, and J. Lopez Vicario, "Distance-based tuning of the ekf for indoor positioning in wsns," in *Signal Processing Conference (EUSIPCO), 2014 Proceedings of the 22nd European*, Sept 2014, pp. 1512–1516.

[103] "Zolertia Z1: low-power wireless sensor network module," `http://zolertia.sourceforge.net/wiki/images/e/e8/Z1_RevC_Datasheet.pdf`.

[104] "MSP430: mixed signal microcontroller," `http://www.ti.com/lit/ds/symlink/msp430f2131.pdf`.

[105] "CC2420: 2.4 ghz ieee 802.15.4 compliant rf transceiver," `http://www.ti.com/lit/ds/symlink/cc2420.pdf`.

[106] A Correa, M. Barcelo, A Morell, and J. Lopez Vicario, "Enhanced inertial-aided indoor tracking system for wireless sensor networks: A review," *Sensors Journal, IEEE*, vol. 14, no. 9, pp. 2921–2929, Sept 2014.

[107] E. Munoz Diaz, F. de Ponte Müller, A. R. Jiménez, and F. Zampella, "Evaluation of ahrs algorithms for inertial personal localization in industrial environments," in *Industrial Technology (ICIT), 2015 IEEE International Conference on*, March 2015, pp. 3412–3417.

[108] E. Munoz Diaz and A. L. M. Gonzalez, "Step detector and step length estimator for an inertial pocket navigation system," in *Indoor Positioning and Indoor Navigation (IPIN), 2014 International Conference on*, Oct 2014, pp. 105–110.

[109] D. B. Rubin A. P. Dempster, N. M. Laird, "Maximum likelihood from incomplete data via the em algorithm," *Journal of the Royal Statistical Society. Series B (Methodological)*, vol. 39, no. 1, pp. 1–38, 1977.